AN ALTERNATIVE METHOD FOR PILLAR STABILITY ANALYSIS BASED ON MACHINE LEARNING ASSISTED GEOMECHANICAL SIMULATIONS

A THESIS SUBMITTED TO
THE GRADUATE SCHOOL OF NATURAL AND APPLIED SCIENCES
OF
MIDDLE EAST TECHNICAL UNIVERSITY

BY

DİLAN DUMAN

IN PARTIAL FULFILLMENT OF THE REQUIREMENTS
FOR
THE DEGREE OF MASTER OF SCIENCE
IN
MINING ENGINEERING

AUGUST 2023

Approval of the thesis:

AN ALTERNATIVE METHOD FOR PILLAR STABILITY ANALYSIS BASED ON MACHINE LEARNING ASSISTED GEOMECHANICAL SIMULATIONS

submitted by **Dilan Duman** in partial fulfillment of the requirements for the degree of **Master of Science** i**n Mining Engineering, Middle East Technical University** by,

Prof. Dr. Halil Kalıpçılar
Dean, Graduate School of **Natural and Applied Sciences** _____

Prof. Dr. N. Emre Altun
Head of the Department, **Mining Engineering** _____

Asst. Prof. Dr. Ahmet Güneş Yardımcı
Supervisor, **Mining Engineering, METU** _____

Examining Committee Members:

Prof. Dr. Bahtiyar Ünver
Mining Eng, Hacettepe University _____

Asst. Prof. Dr. Ahmet Güneş Yardımcı
Mining Eng, METU _____

Assoc. Prof. Dr. Mustafa Erkayaoğlu
Mining Eng, METU _____

Date: 28.08.2023

I hereby declare that all information in this document has been obtained and presented in accordance with academic rules and ethical conduct. I also declare that, as required by these rules and conduct, I have fully cited and referenced all material and results that are not original to this work.

Name Last name : Dilan Duman

Signature :

ABSTRACT

AN ALTERNATIVE METHOD FOR PILLAR STABILITY ANALYSIS BASED ON MACHINE LEARNING ASSISTED GEOMECHANICAL SIMULATIONS

Duman, Dilan
Master of Science, Mining Engineering
Supervisor: Asst. Prof. Dr. Ahmet Güneş YARDIMCI

August 2023, 124 pages

Coal reserves remain to be one of the major sources to provide the global energy demand. Weak rock characteristics make instability a vital concern in terms of occupational health and safety in coal operations. As a support element, pillar is a critical structure in an underground mine plan. Although various methodologies have been developed for designing a geotechnically stable pillar, structural and geological variations may be misleading. This study makes use of a 2D plane-strain based numerical modeling scheme to investigate the effects of variations in geomechanical properties, field stress ratio, coal seam angle, and mine depth. Numerical outputs like horizontal and vertical displacements, yielded element thicknesses, percentage of yielding in pillars, and maximum principal stress in abutments will be used to establish correlations between the control variables. The aforementioned variables are acquired through finite element analysis and documented. Furthermore, the yielded span percentages are computed and recorded for each individual pillar encompassed within the analysis. Through this approach, a comprehensive database is established. Besides the conventional statistical methods, a supervised machine learning model was trained using the database and an alternative method for analysis of stability in underground mine pillars is proposed. The study outputs have potential

to provide a safe and user-friendly scheme for inexperienced technical staff assisting the conventional design methods.

Keywords: Coal Mining, Pillar Stability, Abutment Pressure, Numerical Analysis

ÖZ

TOPUK DURAYLILIK ANALİZİ İÇİN JEOMEKANİK SİMÜLASYON DESTEKLİ MAKİNE ÖĞRENİMİNE DAYALI ALTERNATİF BIR YÖNTEM

Duman, Dilan
Yüksek Lisans, Maden Mühendisliği
Tez Yöneticisi: Dr. Öğr. Üyesi Ahmet Güneş YARDIMCI

Ağustos 2023, 124 sayfa

Kömür rezervleri, küresel enerji talebini karşılamak için temel kaynaklardan biri olmaya devam etmektedir. Zayıf kaya özellikleri, kömür operasyonlarında iş sağlığı güvenliği açısından duraysızlığı endişe kaynağı haline getirmektedir. Yeraltı madenciliğinde topuk, kritik bir destek elemanıdır. Jeoteknik olarak dayanıklı bir topuğun tasarımı için çeşitli yöntemler geliştirilmiş olmasına rağmen, yapısal ve jeolojik varyasyonlar yanıltıcı olabilir. Bu çalışma, jeomekanik özellikler, arazi gerilimleri, kömür damarı açısı ve maden derinliğindeki değişimlerin etkilerini araştırmak için iki boyutlu düzlemsel deformasyon tabanlı sayısal modelleme yönteminden yararlanmaktadır. Kontrol değişkenleri arasında korelasyonlar kurmak için yatay yer değiştirmeler, yenilen eleman kalınlıkları, topuklardaki yenilme yüzdeleri ve dayanak noktalarındaki en yüksek asal gerilmeler gibi sayısal çıktılar kullanılacaktır. Bu değişkenler, sonlu elemanlar analizi yoluyla elde edilir ve belgelenir. Ayrıca, analiz kapsamındaki her bir topuk için elde edilen yenilme yüzdeleri hesaplanır ve kaydedilir. Bu yaklaşımla kapsamlı bir veri tabanı oluşturulur. Geleneksel istatistiki yöntemlerin yanı sıra, veri tabanı kullanılarak denetimli/güdümlü bir makine öğrenmesi modeli eğitilmiş ve yeraltı madeni topuklarındaki duraylılık analizi için alternatif bir yöntemi önerilmiştir. Çalışmanın çıktıları, geleneksel tasarım yöntemlerine yardımcı olmak adına deneyimsiz teknik

personel için güvenli ve kullanıcı dostu bir tasarım planı sunma potansiyeline sahiptir.

Anahtar Kelimeler: Kömür Madenciliği, Topuk Duraylılığı, Dayanak Noktası Gerilmesi, Sayısal Analiz

To my mom,

ACKNOWLEDGMENTS

For his valuable contribution and guidance in determining the thesis topic, elaborating its scope, interpreting the results, and full support throughout this study, I would like to express my endless thanks to my thesis advisor, Assist. Prof. Dr. Ahmet Güneş Yardımcı.

I would also like to thank Assoc. Prof. Dr. Onur Gölbaşı for his encouragements.

I wish to express sincere gratitude to the General Manager of the General Directorate of Energy Affairs for the Republic of Türkiye, Ministry of Energy and Natural Resources, Dr. Ömer Erdem, for his patience.

I extend my gratitude to my thesis defense committee members, Prof. Dr. Bahtiyar Ünver and Assoc. Prof. Dr. Mustafa Erkayaoğlu, for making my defense a remarkable experience, and for their valuable feedback and recommendations.

Lastly, I would like to express special thanks to my mother, Güldal Duman and my friends for their invaluable support and guidance throughout my endeavors. Their contributions have been crucial to my success at every level.

TABLE OF CONTENTS

LIST OF TABLES

LIST OF FIGURES

LIST OF ABBREVIATIONS

ILO	The International Labour Organization
ANN	Artificial Neural Network
USA	The United States of America
IEA	The International Energy Agency
GDP	Gross Domestic Product
Mt	Million tons
SCCL	Singareni Collieries Company Limited
LTCC	Longwall Top-Coal Caving
TTK	Türkiye Taşkömürü Kurumu (National Hard Coal Enterprise)
ALPS	The Analysis of Longwall Pillar Stability
ARMPS	The Analysis of Retreat Mining Pillar Stability
AMSS	The Analysis of Multiple Seam Stability
UCS	Uniaxial Compressive Strength
RQD	Rock Quality Designation
RSR	Rock Structure Rating
RMR	Rock Mass Rating
Q	Quality Index
SRF	Stress Reduction Factor
GSI	Geological Strength Index
RMQR	Rock Mass Quality Rating

DD	Degradation Degree
DSN	Discontinuity Set Number
DS	Discontinuity Spacing
GWSC	The Seepage Condition of Groundwater
GWAC	The Water Absorption Characteristics of Rocks
DC	Discontinuity Condition
ARMR	Anisotropic Rock Mass Rating
FEM	Finite Element Method
FDM	Finite Difference Method
BEM	Boundary Element Method
DEM	Distinct Element Method
DDA	Discontinuous Deformation Analysis
FDEM	Finite-/Discrete-Element Modelling
SVC	Support Vector Machine Classification
2D	The Two Dimensional
MP	The Material Property
RSData	RocScience Data Software
CSA	Coal Seam Angle
RS2	RocScience2 Software

LIST OF SYMBOLS

Wo	the widths of the opening
W_p	the widths of the pillar
L_p	the length of the pillar
P	the load on the pillar
γ	the weight of the unit volume of the rock
h	the depth of the mine
σ	the stress on the pillar
θ	the inclination of the coal seam
μ	The Poisson's ratio
ν	The Poisson's ratio of mass rock
σ_v	the vertical stress
g	the specific gravity
S_p	The pillar strength
σ_1	major principal stress
w	the width of pillar
h	the height of working
l	the pillar length
H	coal seam depth
φ	acute angle of the corners of the coal pillar
φ	Internal Friction Angle

m	meter
J_n	joint set number
J_r	roughness number
J_a	alteration number
J_w	water reduction factor
D	the disturbance factor; owing to blasting and stress relaxation
J_{wice} , J_w	water reduction factor
W	neuron weight
b	block of neuron
k	field stress ratio
E	Modulus of Elasticity
c	Cohesion
°	degree
R	The coefficient of correlation
R^2	The coefficient of determination
ε	Major principal strain

CHAPTER 1

INTRODUCTION

Coal consumption has been rising due to the expansion of industrial use and population growth in the developing countries. In 2022, a new record has been set long after the previous peak in 2013 by an increase of 1.2% (International Energy Agency, 2022). The total coal consumption in the world exceeded 8.2 billion tons in 2022, while it was 7.9 billion tons in 2021 (IEA, 2021). Since the industrial revolution, energy demand has been a significant topic in global politics. Bulk amounts of reserves made coal a key input to meet the energy requirements in civil and military purpose manufacturing industries (Yılmaz & Koyuncu, 2020). Advances in the mining technology and strata geomechanics improved the production rate of the reserves. Despite no other energy source has still taken down the advantages of coal, environmental pollution keeps being a controversial issue among societies due to greenhouse gases like carbon dioxide, and methane emitted by burning coal. Regarding 29 tons of carbon dioxide is emitted by exploiting each ton of underground coal reserves, the rise in the coal consumption increases the carbon footprint by 8.7 billion tons from coal mining alone (Ivanova et al., 2022).

Governments have been collaborating with international organizations to enforce the clean coal technologies world-wide. Investigation of human-related effects on the climate change and climatic effects of coal energy have triggered the initial attempts for developing carbon-free energy policies. In 2015, 196 parties agreed on the deal to act after 2020 for preventing the climate change under the roof of the United Nations Framework Convention on Climate Change (Cahill-Webb, 2018). Each became a side of the Paris Agreement, which entered into force in November 2016. This agreement intends to reduce the greenhouse gas emissions down to zero by 2050 (IEA, 2021b). Despite all the measures, fossil fuels like coal and oil still have the

highest share among the energy sources in the world (IEA, 2021a). The increasing demand for electricity is the main reason for the growing coal production. Thermal power plants hold the majority of the coal demand. Another common use is the heating of residential spaces. In Türkiye, the industrial use has the highest share in coal consumption, and it is followed by the housing, trade, and service sectors.

Similar to the other fossil fuels, coal is projected to be replaced with renewable energy sources. However, unstable global politics have unexpectedly increased the importance of coal resources in the recent years. During the Russia-Ukraine war in 2022, energy export restrictions enforced by Russia to the European countries have increased the demand for domestic coal reserves. The coal mines previously returned to cold storage in Europe have started production, and coal replaced the Russian gas. This sudden change increases the potential coal mining problems in terms of occupational health and safety. Most accidents in underground coal mines are caused by geomechanical problems like pillar failure, roof collapse at the roadways, surface subsidence, and face instability.

This research focuses on the geomechanical aspects of underground coal mining. Specifically, the study proposes an auxiliary tool to analyze the pillar stability and performance under various conditions. The literature involves numerous studies on the empirical and numerical assessment of pillar stability. However, they are valid only under specific conditions in terms of the rock mass quality, the pillar geometry, the structural conditions, the depth and the in-situ stresses. This study aims to propose a unified methodology to serve in the preliminary analysis of pillar stability in underground coal mines. Geomechanical simulations were used to test the pillar performance under various conditions by parametric analyses. The mechanical indicators were obtained to create a database, which can provide a useful understanding on the pillar performance in different cases. The developed framework involves the empirical methods for identification of the rock mass quality. The database was initially presented using conventional charts and tables to assess the suitable pillar design by comparing the similar conditions. Later a machine learning-based model was created to offer a user-friendly tool to make use of the

numerical simulation outputs. Although the geomechanical models are capable of analyzing the rock mass behaviors in a realistic manner, they rely on complex mechanical relationships. High computational sources and long periods of time are required for model creation and interpretation. The aim of this research is to make the geomechanical data viable to non-experienced users by saving the modelling/computation time and preventing any potential modelling mistakes.

1.1 Research Motivation and Problem Statement

The main motivation of this study is to prevent underground coal mine accidents related to pillar failure. In underground coal mines, roof control is essential as the strata is weak and tends to yield immediately after the excavation. Rock mechanics principles are commonly employed to determine the suitable support configuration; however, the cheapest alternative is always the natural support, which is composed of unmined coal pillars. Pillars are an essential part of coal mine layout whether the longwall mining or room and pillar mining method is used. Therefore, assessment of the pillar stability is vital for a sustainable production. Empirical pillar design methods are commonly used but they are only valid under certain circumstances that cover a limited range of values of the design parameters. In addition, they rely on case histories, and they are extremely costly and difficult to update. Alternatively, numerical models are used to simulate the coal pillars with parametric studies to test the mechanical behavior under different conditions. However, the numerical models require an extensive knowledge in geomechanics to prepare, run, and interpret the model results. For complex problems and depending on the numerical method, the model may require high computational resources. Even with powerful hardware, the run time may reach up to days, which makes it not suitable for quick analyses. Also, interpretation of the model results needs skilled experts with a background in mechanics, mathematics, and geosciences. This study proposes an improved methodology to make the numerical model results viable for any operator with basic skills.

1.2 Objectives and Scope of the Study

This study aims to offer an easy and reliable tool for pillar stability assessment in underground coal mines. The pillar performance is intended to be evaluated with elastoplastic finite element models by monitoring the yielded span regarding various mining depth, field stress ratio, material properties, seam dip, and pillar width. A trained statistical model is intended to replace the conventional tables and 2D plots for the interpretation of numerical model outputs. The study objectives are summarized in the list below:

1. To develop a tool for pillar design that is easy to use and suitable for non-experts in geomechanical simulations.
2. To assess the performance of various pillar dimensions, with different geomechanical characteristics, coal seam dip and in-situ stress ratio.
3. To run numerical simulations with parametric analyses for creating a reliable database involving the mechanical indicators of pillar performance.
4. To compare the conventional tables and 2D plots with a machine learning based model to express and interpret the numerical model results.

1.3 Research Methodology

The research methodology is shown in Figure 1.1 which are the stages covered in designing and implementing the study. The following steps were accommodated to reach the research objectives:

1. Identification of the representative underground coal mine models
2. Determination of the geomechanical and geometrical properties to come up with a unified methodology for the preliminary assessment of pillar performance
3. Determining the suitable numerical simulation method to analyze the underground pillar stability

4. Monitoring the mechanical indicators of coal pillar performance from the numerical simulations
5. Interpreting the data obtained from numerical modeling based on conventional tables and 2D plots to examine the relationship between parameters
6. Determining the drawbacks of the conventional data presentation methods and why they lack in a clear presentation of numerical model results.
7. Interpreting the data obtained from numerical models using a non-linear model trained by artificial neural networks.

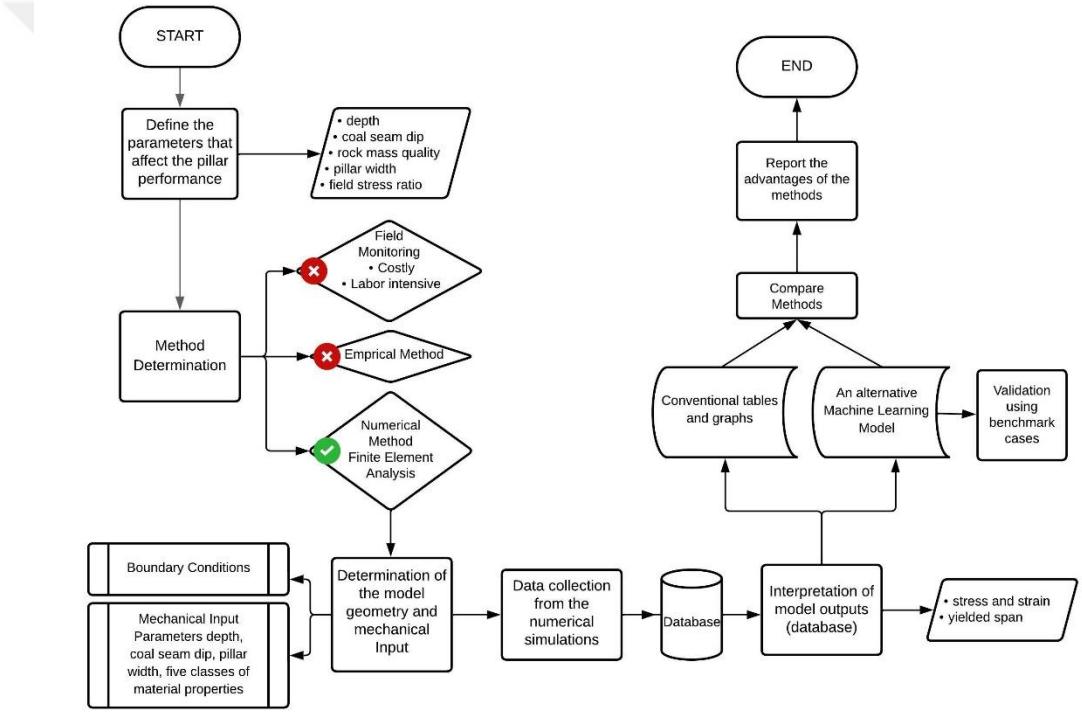

Figure 1.1 The methodology of the thesis

1.4 Contributions to Literature

This study contributes to the literature by offering a unified pillar design tool for the preliminary stability analysis. Unlike the empirical methods, the model can be easily updated by training with the outputs of additional simulations. New variables and

different intervals for the existing ones can be adopted into the model. The proposed method can also improve the model by including the field observations and case histories. Lastly, the current study is a novelty as it makes the reliable outputs of complex geomechanical simulations viable to non-experts. Alternative pillar designs can be quickly investigated considering various geomechanical aspects. Long-computational times and exhaustive model preparation stages will be eliminated.

1.5 Structure of the Thesis

This dissertation demonstrates a comprehensive approach to the complexities and challenges associated with underground coal mining. A specific emphasis on the critical factors of strata control and pillar stability was placed. Chapter 1 presents an overview of the global coal scenario, highlighting the paramount importance of maintaining stable conditions below ground to ensure the safety and productivity of coal mining activities.

In Chapter 2, the study covers a literature review analyzing various aspects such as economic mineral deposits of sedimentary origin, coal mining techniques, strata control methodologies, rock mass quality classifications, and the use of numerical simulation and machine learning in geomechanics.

In Chapter 3, several key factors that are taken into consideration in the assessment of stability risks in underground mining operations, were explained. This includes the attributes of the existing models and provides guidance on their analysis, comprehensive details regarding the model geometry, input parameters, numerical analysis, and corresponding graphical representations. The second part of the chapter delves into the application of machine learning techniques in conjunction with data analysis. This section aims to shed light on the inherent limitations and drawbacks of empirical systems and offers the use of numerical simulations as an additional tool to enhance the results.

Chapter 4 introduces an innovative approach for analyzing the stability of pillars in different scenarios. It utilizes a database of mechanical indicators derived from numerical investigations and employs an artificial neural network (ANN) model as an alternative method to provide a user-friendly interface for obtaining accurate simulation results. The ANN model was validated by comparing it to various cases simulated in FEM. The chapter also compares and discusses the recommendations and performance of hypothetical cases based on traditional empirical methods, numerical analysis, and the ANN model. Furthermore, it identifies the primary factors persuading pillar stability and addresses any uncertainties and restrictions faced during the study.

The final chapter provides a summary of the main results derived from the study. It offers suggestions for designing stable pillars in underground coal mines, drawing upon the consequences of study. Furthermore, the chapter highlights potential avenues for future research and advancements in the field with the consequences of the research.

CHAPTER 2

LITERATURE REVIEW

This section introduces the background and a review of the current knowledge about pillar stability in underground coal mines. The literature research covers the coal mining methods, strata control, empirical rock mass quality classifications, and the numerical analysis methods.

2.1 Coal Mining

As a fossil fuel, coal is a non-renewable energy source that originates from organic materials like vegetation. Coal formation is often called as bedding and the deposit itself can also be named as a ‘seam’. During the formation different exposure time to pressure and heat determines the coal type. Four of the main coal types are peat, brown coal, black coal, and anthracite. Peat originates from organic materials. Brown coal is a woody material formed deeper than the peat (Simeons, 1978). Brown coal covers lignite, sub-bituminous and bituminous coal with low water content. Lignite is popular for heating and generating power. Sub-bituminous coal is brittle and known as black lignite. Low volatile bituminous coal is classified under the brown coal and known as steam coal, which is used for generating electricity. Medium (coking coal) and high (gas coal) volatile bituminous coals are classified as black coal (Pohl, 2011). While coking coal is used in steel industry, gas coal is suitable for liquid fuel production. Anthracite is a rare coal type that is resistant and glossy black. It is often used for heating. Graphite is a kind of anthracite, which is a high-ranking coal type.

In Türkiye, coal had the second highest share in electricity generation, with 31% in 2021 as seen in Figure 2.1. Coal is mainly demanded by the industry with 71% and housing, trade, and service sectors with 29%. Türkiye is planning to expand the share of domestic reserves in its consumption to support the national economy.

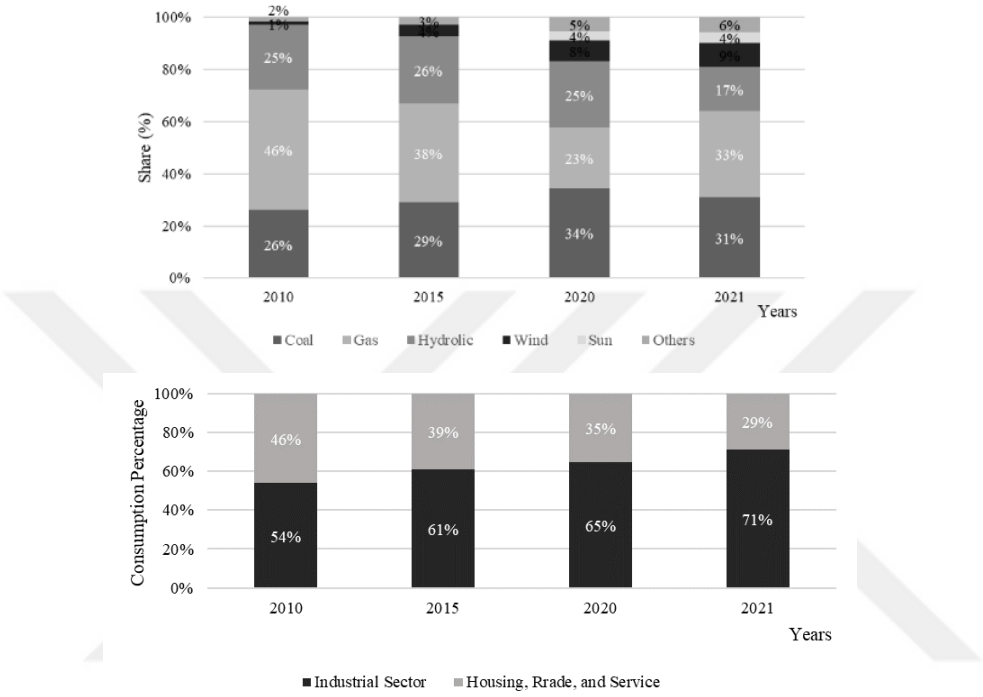

Figure 2.1 Share of energy sources for electricity generation and coal consumption by sectors in Türkiye (Ministry of Energy and Natural Resources, 2023)

Coal mining has been carried out using both surface and underground mining methods. For deep reserves, underground mining is unavoidable considering the cost of recovering the thick overburden layer. For shallow or outcropping deposits, surface mining is typically employed as the primary extraction method.

Surface mining entails the utilization of explosives to fragment both ore and overburden material into smaller pieces, which are subsequently transported to the stockpile with a variety of materials handling equipment such as draglines, shovels, and trucks. For hard rocks, the conventional drilling and blasting cycle is a common strategy to fragment the rock mass. However, for weak rocks mechanical excavation

is a viable alternative to avoid the risks of blasting. Commonly, the open-pit, open-cast and strip-mining methods are used for surface coal mining. Compared to the open-pit mining where the waste is managed by haulage to the waste dump, the waste is disposed to the previous production regions in open-cast and strip mines. Surface mining is indeed a safer and more productive option. However, as the shallow reserves deplete, the number of underground coal mines operated by room and pillar and longwall methods will continue to increase in the near future.

The room and pillar mining is a widely-used method for coal deposits with a flat and tabular shape. This method is implemented by excavating rooms within the seam, while pillars provide support to the roof. Where the geotechnical considerations allow, coal recovery techniques may be considered at the later stages. The mining cycle of a room and pillar operation has five stages. These stages include undercutting, face drilling, blasting, loading, and roof bolting (Peng, S. S., 1978). Initially, slots are created, and boreholes are drilled, followed by the actual blasting, and then coal is transported to the surface. Finally, to ensure the stability of the pillars during the recovery process, the use of bolts is integral to reinforce them. This process is executed with precision to ensure optimal productivity and safety measures are in place. Figure 2.2 presents a typical layout of the room and pillar mining technique.

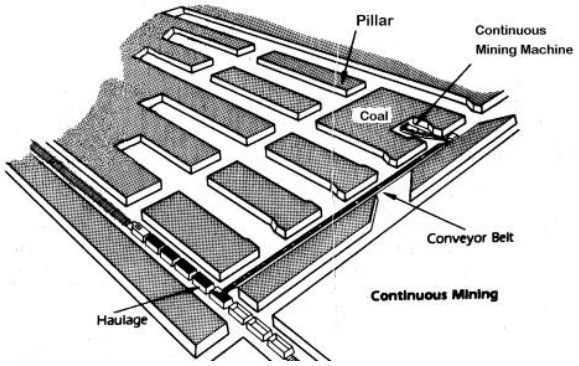

Figure 2.2 Layout of a typical room and pillar coal mine (Energy Information Administration, 1995)

Despite the method has a broad history going back to the ancient times, production in modern means has been ongoing in the Upper Silesian Coal Basin (USCB) since the 18th and 19th centuries, and it is the deepest case in the world that uses room and pillar mining method (Waclawik et al., 2016).

Longwall mining has been identified as a highly efficient method for extracting coal that have a flat-lying deposit. Compared to room and pillar mining, longwall mining is a continuous process that yields higher productivity rates. This makes it favorable for maximizing the output while minimizing the operational costs (Stefanko, 1983). The face is the production region where coal is excavated with mechanical shearers. The shields are mainly employed as the roof support through the panels (Karacan, 2009). Figure 2.3 illustrates a diagram of a typical longwall operation.

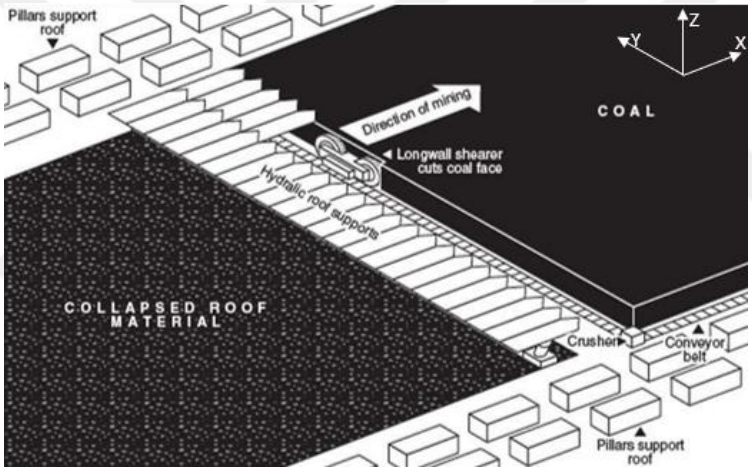

Figure 2.3 A typical longwall operation (Coal Mining, 2015)

The longwall method is suitable for extraction of multiple coal seams. For thick seams, it is modified in the form of 'Longwall top-coal caving (LTCC)', which is widely used by the mainstream coal producers like China and Australia. Ömerler underground coal mine is a local example from Kütahya, Türkiye where the thick coal seam was divided into two parts, to produce the lower part by excavation and the upper part by caving (Le et al., 2018).

In selection of an underground mining method, it is essential to consider the geological features of the ore and waste minerals. Different mining methods are

required for different geological and structural conditions. For instance, the room and pillar mining and the longwall mining methods are suitable for flat dipping, tabular, narrow, and moderately deep deposits. However, selective mining is not possible. Careful consideration of these methods will ensure the safe and efficient extraction of minerals from underground operation.

2.2 Underground Coal Mine Strata Control

Depth, shape, and geometry of the mining excavations, in-situ stress state in the area, geotechnical features, discontinuities, and seismic loads on the rock mass have been classified as various causes influencing the stability of underground excavations (Salmi & Sellers, 2022). Roof fall, rib spalling, and coal bursts induced by fault slip, footwall swelling are major types of instability events that can occur in coal mines related to geomechanical problems causing fatalities and economic harm. Brown coal and hard coal have characteristic instability problems that cause many mine accidents each year around the world. In China, %53 of coal seams is reported to have weak coal characteristics (Zhu et al., 2022). Under such circumstances, through the longwall face, coal tends to decompose easily. Therefore, roof collapse and support instability problems can be observed. Moreover, thick coal seams may pose several unique geotechnical difficulties. These problems cause mining and mechanization problems. One of the solutions is production with the multi-seam technique, which cuts the deposit in sequences, produces safe working place, and provides easier recovery in underground mines; on the other hand, this technique may reduce productivity, increase the cost and may cause some strata control problems related to operation running at the same time on the upper and lower seams. Strata control is essential for productivity and safety.

The mining industry has been addressing the geotechnical challenges and developing strategies and innovative solutions to enhance the productivity. These solutions focus on the establishment of a sustainable production environment. Among these techniques are the roof and wall support systems, anchoring, backfill materials, and

underground support systems. These techniques are employed to prevent the collapse of mine openings and mitigate undesired deformations. Additionally, multi-seam mining techniques, which involve the simultaneous extraction of multiple coal seams, can potentially increase production, and optimize resource utilization in underground mines (McArdle, 2016). However, the instability risks associated with each method also need to be carefully managed.

Surface subsidence causes remarkable fractures on the topography. Every step of longwall operation causes deformations above the ground. Subsidence covers the lateral extents of the underground production and converges through the center of the excavation (Peng & Chiang, 1984). The ground movement is not caused by only the induced loads, but many other mechanical effects govern the process. Subsidence also determines the future of mining activities in the region by changing the structure of floor and roof strata (Galvin, 2016).

Coal mines have a remarkable history of accidents around the globe. On July 24, 2002, in a coal mine operated by Quecreek Mining Company in Somerset County, USA, 9 miners were stuck in a one-meter-high area, 73 meters below the ground, due to the collapse of the wall of an abandoned mine next to it. All miners were rescued after four days (Frank, 2002). On August 6, 2007, 6 miners were stranded due to the collapse at the Crandall Canyon Coal Mine in Huntington, Utah, USA Between 1950 and 2017, as a geological disaster due to ground collapse in China, 446 workers died in mine accidents (Noraishah Ismail et al., 2021). In 1960, in an accident in the Coalbrook Coal mine in South Africa, half of the 1000 miners working 900 meters below the ground could leave the underground using the inclined shaft, while 435 miners could not reach the escape routes closed because of the collapse. The cause of this incident was the reduction of pillar width and depth in an attempt to achieve higher coal production since 1952. These modifications decreased the load-bearing capacity of the pillars, initiating the collapse, which eventually led to the collapse of all pillars in the 3 km² area.(Van der Merwe, 2006).

Coal mines in Türkiye have more fatalities per million tons of produced coal than China considering all mine accidents between 2000 and 2008 (Spada & Burgherr, 2016). Between 1941 and 2003, 3,094 deaths were recorded due to underground coal mine accidents in Türkiye (Kucuker, 2006). On February 6, 2011, and February 10, 2011, two slopes slided in the Çöllolar open pit coal mine in the Afşin district of Kahramanmaraş city, Türkiye and eleven miners lost their lives. National Hard Coal Enterprise (TTK) announced that between 1994 and 2003, coal mining accidents caused by roof failure accounted for 49% of the 164 reported deaths in Türkiye (Kucuker, 2006). Additionally, there were 16,002 accidents related to roof falls in hard coal underground mines at Karadon Hard Coal Enterprise between 2000 and 2014 (Erdogan et al., 2019). To avoid mine accidents due to irrelevant pillar design, various methods have been developed. The following section covers the common methods for pillar design and stability analysis.

2.2.1 Background of Pillar Stability Assessment

The pillar is an unmined portion of the rock mass that supports the roof. To determine the safe pillar design, various approaches were developed such as the analytical solutions, empirical equations, and numerical simulations (Bieniawski, 1984). Mark (2006) states that the initial attempts of the pillar stability research are the empirical pillar strength equations of Salamon and Munro (1967), Obert and Duvall (1967), Holland and Gaddy (1973), and Bieniawski (1984); the analytic solutions of Wilson (1972; 1981) and the numerical models of Peng (1986). Later, the remarkable study outcomes from ‘the analysis of longwall pillar stability (ALPS)’, ‘the analysis of retreat mining stability (ARMPS)’ and ‘the analysis of multiple seam stability (AMSS)’ pillar design methods were employed in many underground coal mines in the USA. ALPS has an extensive database containing pillar parameters. It was considered as a novel pillar design method which is valid for only square pillars (Mark & Agioutantis, 2019).

Bieniawski (1977) conducted field measurements and derived findings indicating that for a cube shape, the strength of the pillar diminishes as the pillar size increases and this trend ends up as soon as a critical dimension is attained.

Putri (2020) employs empirical coal pillar strength formulas including Obert-Duvall (1967), Holland (1967), Holland-Gaddy (1956), Salamon-Munro (1967), and Bieniawski (1983) for Airlaya's coal seam. It was observed that Bieniawski's equation provides the highest accuracy in terms of the pillar strength. Consequently, the study recommends the Bieniawski and Obert-Duvall equations to calculate the pillar strength.

The pillar should bear to the driving stresses caused by the depth of the seam, field loadings, and excavation. Commonly, the pillar design stages include the estimation of the induced loads pillar strength, and calculation of the safety factor (Mark, 2006). One of the most widely used method for calculation of the pillar loads is the 'tributary area theory' (Ghasemi & Shahriar, 2012) as seen in Figure 2.4.

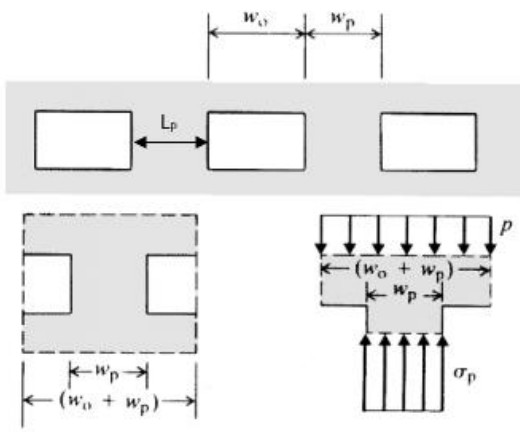

Figure 2.4 The idea of loading pillars using the tributary area concept (Brady & Brown, 2004)

It provides a basic scheme for the estimation of the load. The concept relies on the assumption that the pillars and openings are aligned. The structural integrity of the surrounding opening is dependent on the load-bearing capacity of the pillar, which is equal to half of the width of the rock formation. While 'P' in the equation (1)

represents the load on the pillar, the width of the opening and pillar are shown by 'W_o' and 'W_p' and the length of the pillar is 'L_p'. '**γ**' is the weight of the unit volume of the rock mass and 'h' is the depth of the mine. The stress on the pillar is 'σ_P' in equation (2) and (3) is used for inclined coal seams, where inclination is denoted by 'θ'. Also, 'μ' is the Poisson's ratio and the vertical stress 'σ_v' is equal to 'γgh' (g is the gravitational acceleration).

$$P = (L_P + W_O) * (W_P + W_O) * \sigma_V \quad (1)$$

$$\sigma_P = \frac{(L_P + W_O) * (W_P + W_O) * \sigma_V}{(L_P * W_P)} \quad (2)$$

For inclined coal seams;

$$\sigma_P = \frac{(L_P + W_O) * (W_P + W_O) * \sigma_V}{(L_P * W_P)} * \left(cos\theta + (\mu * sin\theta)\right) \quad (3)$$

Lack of any prediction about the load distribution can be mentioned to be the limitation of this method. Stresses concentrate more on the outer extents of a pillar opposite to the prediction of the tributary area theory (Mark & Chase, 1997). In fact, the failure initiates on the pillar face, which makes it the most critical region.

Frith and Reed (2019) studied on the pillar design for underground coal mines. They claimed that the prediction of the tributary area is accurate, but the strength of the pillars is lower than the calculated. Overestimation of the pillar strength could lead to mistakes in the design where the field loadings are unique. Also, Frith & Reed (2018) claimed a novel approach to coal pillar design in underground mining, which focused on the concept of reinforcement rather than suspension. To test the feasibility of the method, they analyzed failed pillars from publications such as Coalbrook disaster in 1960. They used the Tributary Area Theory for the design. However, they state that empirical methods offer suggestions for the appropriate factor of safety regardless of how accurate the equations are.

To improve the pillar design methodology, various studies have been performed and the major ones are listed in Table 2.1. The key parameters remaining in most of the approaches are the coal strength, width, and height ratio.

Table 2.1 Pillar design empirical formulas (Ram et al., 2022)

Source	**Formula**	**Remarks**
Bieniawski (1992)	$S_p=\sigma_1(0.64+0.36(w/h))$	Least width, w = 23 m; height of working, h = 4 m; in situ coal strength, σ_1= 10 MPa; pillar length, l = 33 m
Mark and Chase (1997)	$S_p=\sigma_1(0.64+0.54(w/h)-0.18(w^2/lh))$	
Obert & Duvall (1967)	$S_p=\sigma_1(0.778+0.222\ (w/h))$	
Salamon & Munro (1967)	$S_p=7.2(w^{0.46}/h^{0.66})$	
Sheorey (1992)	$S_p=0.27kh^{-0.36}+\{[(H/250)+1]*[(w/h)-1]\}$	Effective width, w = 27 m; depth of cover, H = 850 m; height of working, h = 4 m; uniaxial compressive strength (UCS) of intact rock, k = 14 MPa
Van der Merwe & Mathey (2013)	$S_p=5.47(w^{0.8}/h)$	
Maleki (1992)	$S_p=32[1-exp(-0.339w/h)$ (in confinement control) $S_p=26[1-exp(-0.264w/h)$ (in structural control)	

Table 2.1 (continued)

Das et al. (2019)	$S_{incline} = \{1-[1-(\cos\theta)^{2.4}(\sin\varphi)^{0.8}]$ $*(H/(w/h))^{0.04}\}S_{flat}$	Dip of the coal seam, θ=12; acute angle of the corners of the coal pillar, $\varphi = 70°$; S_{flat} is the pillar strength as per Sheorey (1992)

Coal pillar design in mines where coal burst risk exists was studied by X. Li & Chai (2019). Their classification system for coal pillars states that as the width of the pillars decrease, the stress distribution changes, and it affects their stability by increasing the risk of coal burst. The study is useful to adjust the pillar width considering the field conditions. However, more information on what should trigger the adjustment, and its potential consequences should be covered in more detail.

Kang et al. (2023) focused on ground control with static, empirical, dynamic, informational, systematic, and scientific designs. For deep coal mines, they created a better scheme to categorize rocks near coal mine roads by using accurate measurements of geological and geotechnical factors and evaluating with the machine learning to classify the geological condition. Their study suggests ground support patterns and the influencing parameters have been emphasized.

Mark and Agioutantis (2019) investigated the history of coal pillar design methods used in US underground coal mining. These methods have helped to make ground control safer, to decrease the number of pillar failures, and to prevent longwall tailgate blockages. They also mention that choosing the right program can be difficult and that different programs may produce different results. To solve this problem, a new framework called the analysis of coal pillar stability (ACPS) was introduced. This integrates existing methods into a single system, making the design process easier, more accurate, and more user-friendly.

Tewari et al. (2018) investigated the safe crown pillar design for mining the steeply dipping coal seams. Crown pillar dimensioning is difficult and depends on experience and extraction methods. Research on steeply dipping coal seams is

limited, but this study used simulation and empirical analysis to identify the best size, taking into account the safety factors, stability, and the roof strata. Analyses show that the roof stability can be maintained even if the thickness of the crown pillar is reduced. The results obtained from numerical modeling show a strong correlation with the findings from the empirical analysis. A systematic approach can help determine the ideal crown pillar size.

Recently, numerical models are used to check the empirical relations for designing pillars in complex and unique conditions. Nguyen et al. (2022) presents a FLAC3D model in their study involving a rock mass and mine workings to explore the effect of various coal pillar dimensions. Factors affecting coal pillar geometry are examined, including their impact on stress in inclined rock layers. The study also determines the extent of plastic deformation around auxiliary mine workings. Coal pillar size is linked to support type, and research suggests a width of 10 m to 15 m for coal pillars to ensure both ideal mining conditions and safety.

Das et al. (2023) addresses significant geotechnical challenges when mining beneath highly stressed coal seams. Issues such as strain burst, side spalling, roof collapse, and irregular caving are common in this scenario. The research focuses on designing appropriate underground structures such as optimum rib pillars and support systems to mitigate these challenges. This is achieved by evaluating factors like energy build-up, strain burst potential, stress conditions, and opening stability. A safety factor based on energy considerations was developed and incorporated into numerical models to identify areas prone to yielding. These numerical simulation finding were supported by field investigations and monitoring data from geotechnical instruments.

Le and Dao (2023) aimed to anticipate potential geomechanical problems in underground coal mining. They investigated the roof strata and outlined the mechanisms that lead to roadway instability under various structural conditions. The researchers employed a numerical code to evaluate the stability both in coal pillars and roadways under different roof conditions. The technical recommendations offered in this article may be considered under similar geological settings.

2.2.2 Empirical Rock Mass Quality Evaluation

Empirical methods constitute the preliminary stage of the stability analysis for surface and underground rock structures. Rock mass classification systems provide a basis for the underground opening design based on the expert opinion and geomechanical facts (Sheng et al., 2022). It is a common practice to establish connections between the support configuration, the opening dimension, and the rock mass quality. Historically, the initial attempts of rock mass classification systems are Terzaghi's Rock Load (1946), Deere's RQD (1964), Wickham and colleagues' Rock Structure Rating (RSR) (1972), Bieniawski's Rock Mass Rating (RMR) (1973), and Barton's Q-System (1974).

Bieniawski's Rock Mass Rating (RMR) is widely used in mining and civil engineering projects. The system uses five basic parameters involving the uniaxial compressive strength, RQD, groundwater condition, discontinuity spacing and condition (Sheng et al., 2022b). The RMR system utilizes score ranges to evaluate factors like the point load strength index and uniaxial compressive strength. This results in an overall score and corresponding rock mass quality class. Additionally, the rock mass quality classes are assigned geomechanical properties such as cohesion and internal friction angle.

The RMR system is useful for determining the average stand-up time, and the required support configuration based on the rock mass quality. It is commonly used in designing tunnels, slopes, foundations, and mines. It is especially useful for hard coal mines and is often considered as a starting point for more advanced geomechanical analyses. Although the system had its last major revision in 1989, it had some minor fixes in 2014 (Azarafza et al., 2020).

The Q-tunneling index is another method for rock determining the rock mass quality and support systems. It was developed based on many case studies as stated by Barton et al. (1974). Q-system took its last form in 2014 (Azarafza et al., 2020). The system covers six basic parameters, which are RQD, stress reduction factor (SRF), joint set number (J_n), joint roughness number (J_r), joint alteration number (J_a) and

groundwater factor (J_w). Each of these inputs are assigned with a score interval on the logarithmic scale. The Q score ranges between 0.001, expressing the poor-quality rock to 1000, indicating the good quality rock. Q-system is the most common empirical tool used in tunnel design and construction (Osgoui, 2007). The proposed chart correlates the rock mass quality score with the recommended support configurations with design details. Unlike the RMR, Q-system involves a stress reduction factor to cover the field loads.

Geological Strength Index (GSI) is another recent system that characterizes the rock mass quality regarding the structure and joint condition (Hoek et al., 2000). The GSI rating was set between 0-100, while 10 stands for poor rock characteristics and 100 indicates the high-quality rock mass. This system was subsequently incorporated into the Hoek & Brown empirical failure criterion to compute the rock mass failure.

It is possible to convert RMR, Q, and GSI scores into each other. Although direct conversion is not recommended by the authors of any of these systems, the practical reasons may favor using these empirical equations. The equations presented above depend on the estimation of the geotechnical strength index (GSI) using Bieniawski's rock mass rating (RMR), as outlined in (Brown & Hoek, 1988). Subsequently, equation (10) shows the direct conversion of GSI if RMR > 25, on the other hand, it is not applied to rock masses categorized as weak with a RMR below 18 (Cui et al., 2022),

$$GSI = RMR - 5 \tag{10}$$

The determination of the Geotechnical Strength Index (GSI) of jointed rocks is carried out by assessing the surface quality and interlocking of rock pieces. The characteristics of rock, including its surface conditions and composition, play a crucial role in determining its GSI score. For instance, a modification of the conventional GSI scheme for the weak rock mass. In this method, the geomechanical parameters of the rock mass can be determined from the intact rock properties.

The commonly used rock mass classification systems have experienced several modifications that conforms better with specific purposes. For instance, the RMR

system was modified specifically for use in coal mines, which is called as M-RMR. Such attempts are made by revisiting the parameter types, ranges and adapting the expert view.

Rock Mass Quality Rating (RMQR) is a recent rock classification method modified from the RMR concept. Its fundamental parameters involve the geomechanical properties of intact rock. The system offers a potential for not only quantitative but also qualitative assessment. Similar to the common methods, RMQR considers the discontinuity properties. The overall rock quality score is determined from six basic parameters. The degradation degree (DD), discontinuity set number (DSN), discontinuity spacing (DS), the seepage condition of groundwater (GWSC), the water absorption characteristics (GWAC), and discontinuity condition (DC) are related to alteration and weathering of intact rock due to water and pressure effects with time (Aydan et al., 2014). Also, the parameter of discontinuity condition is divided into three sub-classes as aperture or separation, infilling, and roughness. This rating system is viable for the assessment of instability problems where stress-induced yielding is the case (Aydan et al., 2015). The concept also proposes empirical formulas for supporting systems.

Another recent trend is to use the machine learning algorithms and the fuzzy logic to improve the common weaknesses of the rock mass classification systems. For instance, the fuzzy RMR system is a modified rock quality prediction method for weak rock-slope stability. It is based on the basic RMR system. Uncertainties are recovered by the Fuzzy Logic to reveal the relationship between the safe overall slope angle and the slope height (Yardimci & Karpuz, 2017).

Anisotropic Rock Mass Rating (ARMR), developed for classifying anisotropic rock masses, is a new rock mass classification system. Its basic parameters are the anisotropy strength index, uniaxial compressive strength of intact rock, degree of structure anisotropy, corrected rock quality designation (RQD), condition of anisotropy surfaces, and groundwater conditions. To be able to discriminate two

anisotropic rock masses from different degrees of structural anisotropy is the purpose of this rating system (Saroglou et al., 2019).

2.2.3 Numerical Simulations in Pillar Stability Assessment

For constructing a rock structure, it is essential to determine the parameters related to material, geometry, and boundary conditions, such as the geomechanical factors, structural condition, and the force field. The load interaction of geological materials commonly exhibits a nonlinear trend, and information about the in-situ conditions is limited. Under these circumstances, taking advantage of the computational mechanics, parametric studies help to test the stability and performance of an underground excavation well before it is implemented. Various numerical methods have been developed to reduce the computational cost and increase the accuracy of the simulation.

To mimic the reaction of a solid under stress, it is essential to thoroughly characterize its stress-deformation path. The rock strength and the load curve are mostly dependent on the geomechanical properties, which are the Young's Modulus, Poisson's ratio, cohesion, internal friction angle, and tensile strength. Laboratory and in-situ testing can be performed to characterize the elastoplastic material model that effectively simulates the rock mass. In the absence of analytical methods or field scale trial works, numerical analyses provide a cost-efficient and precise alternative.

A numerical method is expected to fit the nature of the material that is modeled. Continuum and discontinuum methods are used considering the structural condition of the rock. Finite element method (FEM), Finite difference method (FDM), Boundary element method (BEM), Distinct element method (DEM), Discontinuous deformation analysis (DDA), hybrid methods such as finite-/discrete-element modelling (FDEM) (Havaej et al., 2014) are some sample numerical methods. Two-dimensional plane strain analysis is embraced commonly for continuum and discontinuum models where it is possible (Barbero & Barla, 2010).

However, if three-dimensional loading conditions exist and they are critical for the overall model behavior, a three-dimensional numerical code can be considered.

In underground mining, the in-situ stress distribution is manipulated by the excavation. Induced stresses cause damage around the openings and even may initiate violent failures at extreme depths. The damage in the rock mass can be traced from the fractures. Assuming the rock mass as a continuum, finite element method (FEM) is commonly used to simulate the induced stresses around the excavation. FEM mostly relies on a small deformation formulation to simulate the initial sequences of the ultimate failure (Vlachopoulos & Vazaios, 2018). It calculates the stress and displacement of the model body. The force equilibrium and deformations are calculated for every element using the mathematical material models (Eberhardt et al., 2004).

Chen and Stimpson (1997) show the finite element analysis model configuration that the finite element meshes on the pillar of a Potash mine. The orientation and size of meshes are determined regarding the expected cracks features. In the sample model, a uniformly distributed load at the top of the pillar is employed to simulate the overburden pressure. The model provided the stress concentrations on the pillar, including the induced loads.

FEM requires setting the boundary conditions to increase the simulation accuracy. The force interactions with the rest of the rock mass, external loads on the surface due to construction and heavy equipment and also dynamic loads are involved in the boundary conditions.

FEM is widely used in the simulation of mining activities. For instance, Jaiswal and Shrivastva (2009) examined the stress-strain distribution in an underground coal mine pillar using FEM models. They concluded that a hybrid model of the finite and boundary element methods gives the most accurate solution for higher coal pillar recovery.

Numerical simulations were used for improving safety and productivity in the Taldinskaya-Zapadnaya-2 multi seam coal operation in Russia. Longwall method

poses strata instability risks in the close vicinity of the production region. The mine layout was modified considering the stress concentrations on the abutment that were extracted from the numerical simulations (Sidorenko et al., 2021).

The pillar dimensions at the borders of the Svea Nord coal mine were investigated with FEM models to assess the potential of shifting to room and pillar mining instead of the current longwall operation. The simulations pointed out that the pillar width should be between 25 and 35 m around the border of the previous workings, to continue with the room and pillar mining (Shabanimashcool & Li, 2013).

CHAPTER 3

NUMERICAL ANALYSIS OF PILLAR PERFORMANCE IN A TYPICAL UNDERGROUND COAL MINE WITH PARAMETRIC STUDIES

This section presents the numerical analyses that investigate the effects of the pillar width, depth, in-situ stress ratio and the geomechanical properties on the stability of coal pillars in a typical underground mine. Even though in-situ measurements offer the most accurate understanding of the pillar performance, testing for different rock mass qualities requires expensive and time-consuming field works. On the other hand, geomechanical simulations can easily produce the computational models of various scenarios and provide the mechanical indicators in great detail. This way, parametric analyses can be used to develop an auxiliary methodology for pillar design covering various mining conditions. The following topics start by presenting the numerical study, which covers the model geometry, model input parameters and parametric analyses. Later, a machine learning model based on the computational model outputs are explained to propose an auxiliary pillar design scheme.

3.1 The Model Geometry and The Boundary Conditions

The modelling started by determination of a representative underground coal production layout. In room and pillar mining and in longwall mining around the main roads, the mine layout is frequently composed of a series of excavations and pillars, which are unexcavated portions of the coal seam. Considering a 2D plane strain based numerical code is intended to be used for the computational study, a critical cross-section was determined inside a rectangular external boundary that is 304 m in height and 400 m in width. The coal seam thickness was set to 4 m and four different seam depths were studied for 100 m, 200 m, 300 m and 400 m below the surface.

The width and height of the footwall and the thickness of the coal seam was kept fixed.

While different pillar widths were simulated between 4 m and 16 m with 4 m increments, the opening widths were kept as 4 m inside the coal seam. When the pillar width was 4 m, the total width of the production region was found to be 84 m and 9 pillars fitted into the seam. The mid-pillar was used to align the production region at the center of the model external boundaries. The location of the coal bed is kept the same in all the models. The distance between the top of the coal seam and the bottom of the external boundary was set to 200 m for all the models. A sample model view is shown in Figure 3.1.

For the boundary conditions, only the left and right bottom corners were set completely fixed in the model's external boundary. In other words, the model was restricted both on x and y dimensions with triangular fixes. The right and left walls of the model were fixed only in x-dimensions with rollers. Finally, the surface was kept free to move in any direction.

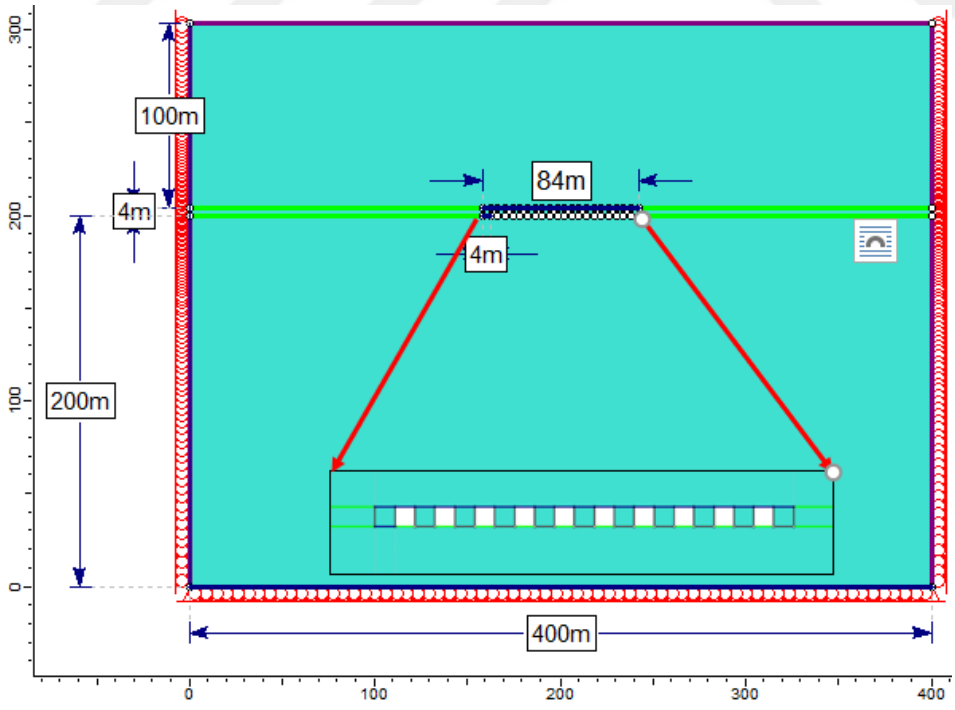

Figure 3.1 A sample model geometry used in the study

The model was computed with Rocscience RS2 software, which is a 2D finite element code. The model geometry was discretized and meshed with graded and six nodded triangles that concentrate around the coal seam. A sample finite element mesh can be seen in Figure 3.2.

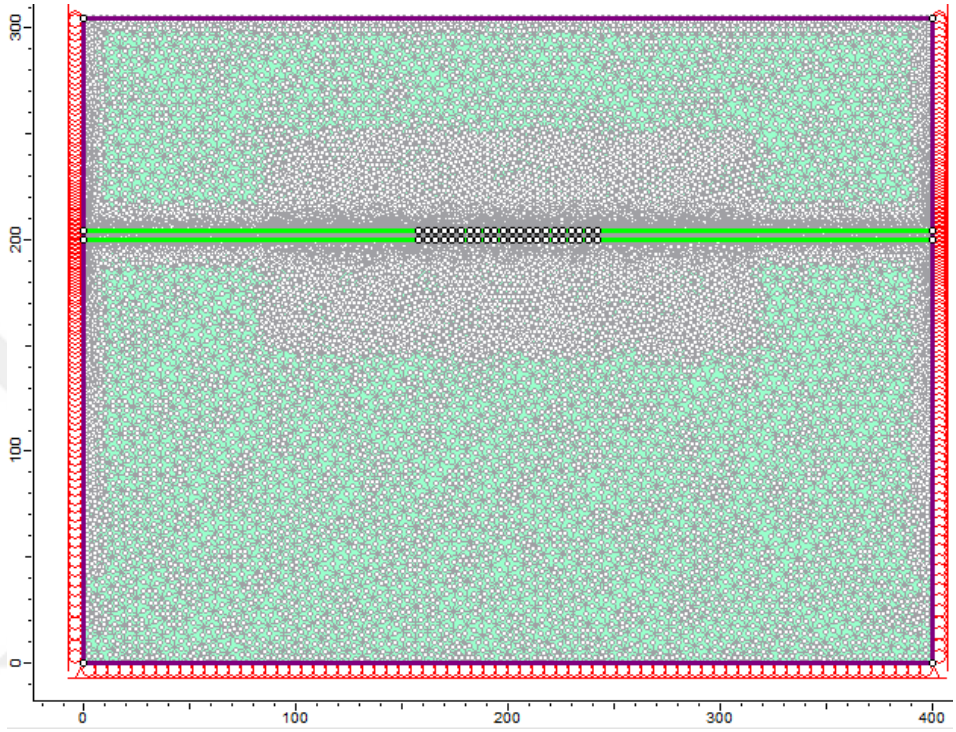

Figure 3.2 A sample model with the finite element mesh

3.2 Material Input Parameters

The material properties are necessary in numerical modeling to define the elastoplastic behavior of rock units. Because the aim of this study is to develop a methodology for pillar stability analysis, various geomechanical conditions were represented under five overall classes named MP_1, MP_2, MP_3, MP_4, and MP_5. The rock mass quality was mainly determined according to the RMR system of Bieniawski (1989). MP_1 stands for the highest quality rock mass whereas the mechanical properties sequentially degrade for MP_2, MP_3, MP_4, and MP_5.

For five different material classes, the calculated rock mass parameters can be seen in Table 3.1.

Table 3.1 Rock mass properties used in the numerical models

Parameters	MP_1	MP_2	MP_3	MP_4	MP_5
GSI	95	85	65	35	20
Rock Mass Quality based on RMR	Very Good	Good	Fair	Poor	Very Poor
Modulus of Elasticity[a], E (MPa)	8364	3212	2400	1645	669
Poisson's Ratio, ν	0.25	0.25	0.25	0.25	0.25
Uniaxial Compressive Strength[b], UCS (MPa)	49.2	8.0	4.0	2.2	1.0
Tensile Strength[c], T (MPa)	2.1	1.0	0.5	0.3	0.1
Cohesion, c (MPa)	10.2	2.1	1.3	0.8	0.4
Internal Friction Angle, φ (°)	45	35	25	20	15
Unit Weight, γ (MN/m^3)	0.02	0.02	0.02	0.02	0.02
Dilation Angle[d] (°)	5	4	3	2	2

The rock mass quality in terms of RMR score was used to calculate the elastic and plastic parameters such as modulus of elasticity, cohesion, and internal friction angle. For the field scale parameters, the interpretation table of RMR matching the rock mass quality with the mechanical properties (Bieniawski, 1989), the Hoek and Brown criterion (Hoek & Brown, 2019) and Hoek and Diedrichs (Hoek & Diederichs, 2006) recommendations were used.

As a first step, the representative RMR scores were determined for each material class and the GSI scores were calculated with equation (10). This section aims to provide a comprehensive explanation of the underlying assumptions and adjustments made for the parameters indicated in lowercase in Table 3.1.

a = The Generalised Hoek & Diedrichs method was employed to compute the elastic modulus for the rock masses of MP_1 and MP_2. The rest of the classes ranging from fair to very poor were determined from the recommendations of Hoek et al. (2002).

The elastic modulus defines the stiffness of the rock mass. There are various empirical relationships to estimate the elastic modulus for the rock mass based on other rock properties. Some of them are seen in Table 3.2.

Table 3.2 Equations for estimation of rock mass modulus

Formula	Author
E_{rm}=2RMR-100 (RMR>50)	Bieniawski (1978)
$E_{rm}=10^{(RMR-10)/40}$ (RMR<50)	Laginha Serafim & Paulino Pereira (1983)
$\frac{E_{rm}}{E}=0.02+\frac{1-D/2}{1+e(\frac{60+15D-GSI}{11})}$	Hoek & Diederichs (2006)
$E_{rm} = (\sigma c/100)^{0.5} \times 10^{(GSI-10/40)}$	Hoek & Brown (1997)
$E_{rm} = 0.1(RMR/10)^3$	Read et al. (1999)

b = Uniaxial compressive strength was calculated from Mohr-Coulomb failure criterion as shown in equation (11), where c is the cohesion and φ is the internal friction angle) (Hoek et al., 2002).

$$UCS = 2ctan\left(45 + \frac{90 - 2\phi}{2}\right) \quad (11)$$

c = While there is no confinement ($\sigma_3 = 0$), the tensile strength, T was computed from the Griffith theory using equation (12) (Griffith, 1921)

$$UCS = 8T_o \quad (12)$$

d = The dilation angle was calculated by dividing the internal friction angle by a factor of 10.

When coal undergoes deformation, it exhibits a plastic behavior, which results in irreversible deformation and the inability to recover its original shape. Due to this,

the coal does not expand much during cutting or deformation, leading to a low dilation angle. However, the dilation angle only controls the post failure behavior.

To determine the cohesion and friction angle values of the rock mass, mainly the RMR interpretation table was used. Furthermore, a thorough literature survey was carried out to ensure if the geomechanical parameters are consistent with the anticipated quality of the rock mass.

Hoek and Brown (1997) present a comprehensive range for the uniaxial compressive strength of coal, which is valuable for preliminary design purposes. Based on the data provided, it is evident that the strength of intact coal falls within the medium-strong range, with a value ranging from 25 to 50 MPa. Notably, typical properties for very poor-quality rock mass are provided in the 'Post-Failure Behavior' part. The values of cohesion, 0.55 MPa and internal friction angle, 24° are instrumental in supporting empirical solutions and numerical results.

Through literature research, it has been determined that the cohesion and internal friction angle values are consistent with the RMR system. An example of this can be seen in Li et al. (2021), where coal cohesion was found to be 0.5 MPa and the internal friction angle was 22°. These values serve as confirmation for the classification of the rock mass as "very poor" in this thesis.

The study conducted by Liu et al. (2020) includes elastic modulus (2.43 GPa), compressive strength (4.08-4.20 MPa) and tensile strength (0.34-0.35 MPa) for the mechanical properties of coal within the stratigraphic column. These values hold significance for the numerical similarities exhibited by the MP_3 values that have been examined in the present research.

The cohesion (1.5 MPa) and the internal friction angle (26°) of the Sunjiagou coal mine, determined from the geological data from Sun et al. (2020), are close to the values used in this thesis.

Putri (2020) presents coal rock mass properties for Air Laya mine with friction angle 11.8° and cohesion 0.34 MPa for very poor coal classification. The values demonstrate resemblance to the values presented in this study.

Coal specimens from China have weaker strength compared to those from South Africa, USA, and India with the minimum and maximum UCS being 1.37 MPa and 65.56 MPa (Kang et al., 2023).

For the material constitutive relation, elastic-perfectly plastic model was used due to its computational advantages. In this case, the peak and residual values of tensile strength, cohesion, and internal friction angle were kept equal to each other. Although the geomaterials are well known to show a softening behavior in the post failure region, for the current study the post failure stage is not significant, which helps to reduce the computational cost.

RS2 is a numerical code that performs two-dimensional finite element analyses on geological materials. RS2 generates finite element meshes within the model. To model, external boundaries must first defined and the material properties must be specified. Subsequently, the material type and properties need to be established and allocated between the model boundaries. The meshing phase can be finalized subsequently. After completing the model, users are required to execute the simulation to compute stress and displacement at the nodal points of the model's mesh. It relies on a small deformation code, which may result in convergence problems for the weak rock mass properties. This is because the complete failure sequence cannot be modeled with this formulation but only the initiation could be detected. Thus, the force equilibrium cannot be achieved due to the plastic deformations or the body motion. This behavior can be attributed to certain types of rock quality classes, such as MP_4 and MP_5, which are relatively weaker and may experience extremely high displacements. However, non-convergence points out the failure of the pillar and the model result can be still useful to develop the proposed methodology.

3.3 Parametric Analysis of Pillar Stability

To accurately cover the pillar performance under various geological and geomechanical conditions in underground coal mines, the numerical model settings and the geometry must be defined thoroughly. The input parameter intervals need to be limited due to computational restrictions. By analyzing the simulation results regarding the changes in stress, displacement, and yielded span through numerical simulation, a valuable insight can be obtained about the pillar stability.

This study investigates the changes in factors such as coal seam depth, coal seam dip, the pillar width, the geomechanical properties of the rock mass, and the field stress ratio to develop an auxiliary tool for pillar stability that relies on the powerful numerical simulation background.

A comprehensive dataset comprising 8280 mechanical outputs of stress, yielded span and displacement was recorded from a total of 276 models. A detailed account of how the data being generated is presented below.

In the preliminary stage of the numerical study, a total of 240 mechanical models were generated with a 4 m thick coal seam. These models were encompassing all the combinations of the model input parameters. The depth of the seam covered all of the 100, 200, 300, and 400 m. In addition, the inclination of the coal bed was studied at four different degrees, which were 0°, 5°, 10°, and 15°. In addition, three different field stress ratios; 0.5, 1 and 1.5, and five different material properties, were simulated. Table 3.3 gives the intervals of the model input parameters.

Table 3.3 Input parameter intervals used in the numerical simulations

Field Stress Ratio, k	0.5	1	1.5		
Depth, (m)	100	200	300	400	
Pillar Width, (m)	4	8	12	16	
Coal Seam Angle, (°)	0	5	10	15	
Material Property	MP_1	MP_2	MP_3	MP_4	MP_5

After running all the combinations of input parameters for 4 m pillar width, the rest of the pillar widths were simulated for a smaller input set to reduce the computational cost. The data trends obtained from the initial analyses were used to complete the model results with reduced input intervals. These models were covering only 200 and 300 m of seam depth, 0° and 5° for seam inclination and only the hydrostatic stress conditions. For three other pillar widths, which were 8, 12, and 16 m, a total of thirty-six models were run and analyzed.

Thirty-one mechanical readings were recorded from each model. Some of these readings are the horizontal displacement in meter for the left-most, center and the right-most pillars, the distance between the wall of the left-most and right-most openings, distance of the peak value of the major principal stress (σ_1) in the left and right abutments, and the yielded span of the pillars and abutments. Figure 3.3 presents a representative view of the query points within the prototype of the simulated underground coal mine working.

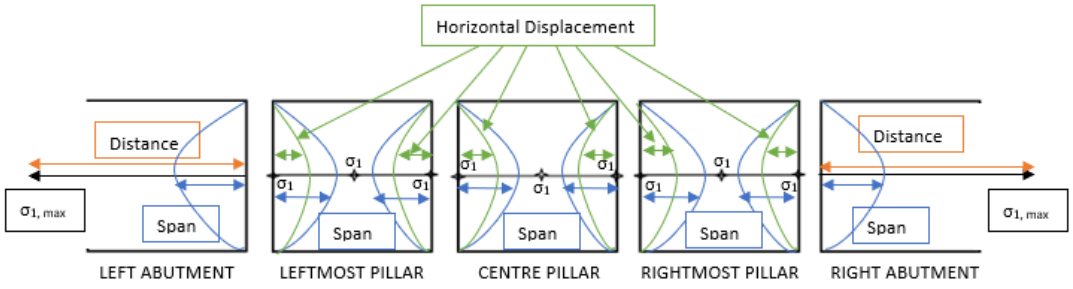

Figure 3.3 An exhibition of points of measurements

Table 3.4 shows the locations of each of the thirty-one mechanical records taken from the numerical models to create a database. In the next section, measurements are mentioned in detail.

Table 3.4 The identified locations for mechanical measurements

LEFTMOST PILLAR	Horizontal Displacement (m)	Left Wall
		Right Wall
	Major principal stress (MPa)	Left Wall
		Centre Node
		Right Wall
	Yielded Span (m)	Left Wall
		Right Wall
	Yielded Span (%)	calculated
CENTRE PILLAR	Horizontal Displacement (m)	Left Wall
		Right Wall
	Major principal stress (MPa)	Left Wall
		Centre Node
		Right Wall
	Yielded Span (m)	Left Wall
		Right Wall
	Yielded Span (%)	calculated
RIGHTMOST PILLAR	Horizontal Displacement (m)	Left Wall
		Right Wall
	Major principal stress (MPa)	Left Wall
		Centre Node
		Right Wall
	Yielded Span (m)	Left Wall
		Right Wall
	Yielded Span (%)	calculated
LEFT ABUTMENT	Major principal stress (MPa)	
	The extent of the peak value of σ_1 in the left abutment	From Right Wall
	Yielded Span (m)	Right Wall

Table 3.4 (continued)

	Major principal stress (MPa)	
RIGHT ABUTMENT	The extent of the peak value of σ_1 in the left abutment	From Left Wall
	Yielded Span (m)	Left Wall
SOLUTION STATUS		Converge or Non-Converge

3.4 Interpretation of Numerical Model Outputs

Upon completion of numerical analysis with finite element analysis, it is critical to obtain precise measurements to accurately interpret the pillars. Measurements were taken from the numerical models to analyze the pillar stability and abutment conditions. The process for measuring the locations of stress and the methodology employed are consistent across all pillars. The measurements were recorded as a database in the form of an Excel sheets. A sample sheet for the leftmost pillar is included Table 3.5, which is identical for all pillars.

Table 3.5 Spreadsheet for leftmost pillar

						LEFT PILLAR							
						Horizontal Displacement		**Major Principal Stress, σ_1**			**Yield Elements Thickness**		**Span (%)**
No	Material Property	Depth	Pillar Width	Coal Seam Dip	K	Left Wall	Right Wall	Left Wall	Centre Node	Right Wall	Left Wall	Right Wall	Total
1	…												
2	…												
3	…												
…	…												
…	…												

A comprehensive spreadsheet was compiled including the various model features alongside their corresponding data for both the pillars and abutments. The measurement points and processes are consistent across all pillars. For example, the leftmost pillar's measurement points and a sample interpretation are shown in Figure 3.4.

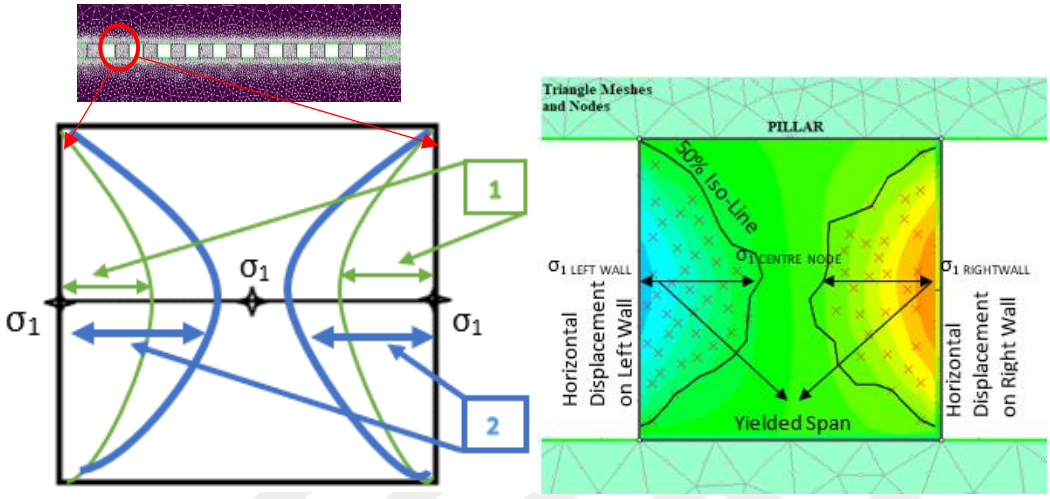

Figure 3.4 An illustration of the measurement points and a sample FEM model for the leftmost pillar

Once the models have been created and run, a query line was set from the midpoint of the pillar, extending from wall to wall regarding the location of the pillar. As illustrated in

Figure 3.4, a query was used to assess ‘Sigma 1’, the major principal stress. This measurement was taken from the point that aligns with the midpoint of the left and right walls of the pillars and the central region of the pillar.

The horizontal displacements are represented with number 1 in Figure 3.4. The horizontal displacements were acquired from the left and right walls. Then the 50% iso-line for the yielded elements as represented by number 2 on

Figure 3.4 was drawn using the tool and if at all possible, the yielded span on the left and right were noted. To determine the percent of yielded span, the yielded lengths were summed up and s divided by the total pillar width. This process was repeated

for the leftmost, rightmost, and center pillars. The horizontal displacement and the yielded span were measured in meters, while the stress unit was recorded in MPa. It is vital to approach these measurements with care and precision.

When analyzing the left and right abutments, three key factors were considered: the maximum principal stress in MPa, the extent of peak stress on the abutment, and the span of the yielded elements in meters as seen in Figure 3.5.

Uniformity in measurement points and processes were maintained across all left abutments. To illustrate, the measurement points and model interpretation for the left abutment are presented below.

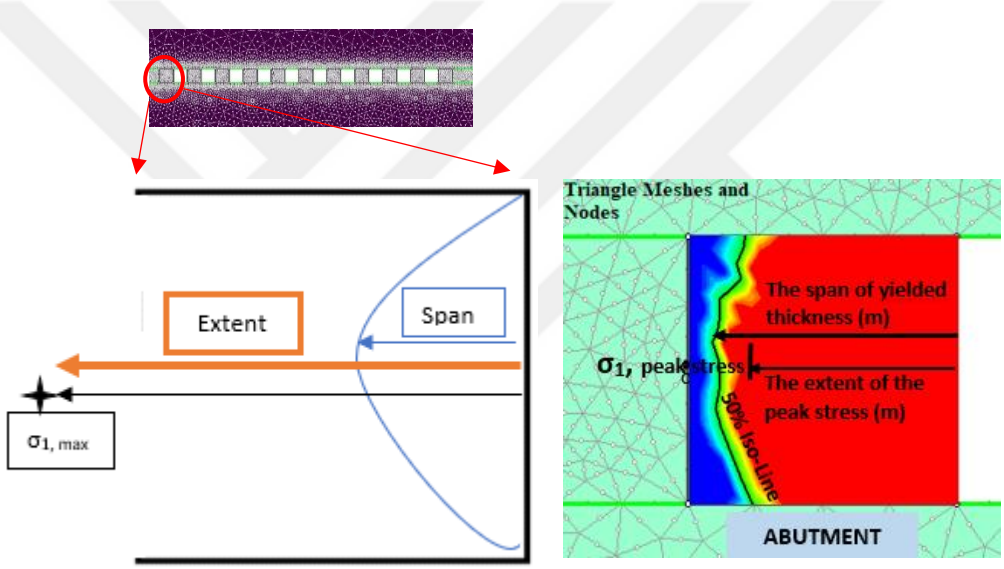

Figure 3.5 An illustration of the measurement points and FEM model result of a sample left abutment

Table 3.6 Spreadsheet for abutments

						LEFT/RIGHT ABUTMENT		
No	Material Property	Depth	Pillar Width	Coal Seam Dip	K	**Peak Stress**	**The extent**	**Span (m)**
1	…							
2	…							
…	…							

Also, a database was created specifically for abutments as seen in Table 3.6. For both abutments, headers of spreadsheet were similar.

For the measurements on the abutments, to attain the location of the peak value of the σ_1 throughout the wall, the query was extended on the midpoint. The maximum stress value was obtained from the "Solid Total Stress" component of RS2. Second, it was essential to maintain an accurate record of the extent the peak stress value on the abutment. To measure the span for the left abutment, the distance was measured from the right wall of the abutment using the "Yielded Elements" section of RS2. The maximum principal stress on the query was then selected and marked for the location. This measurement was based on the thickness of yielded elements. Subsequently, the 50% iso-line was drawn. The measurement of the yielded span was the distance between the opening wall and the 50% iso-line.

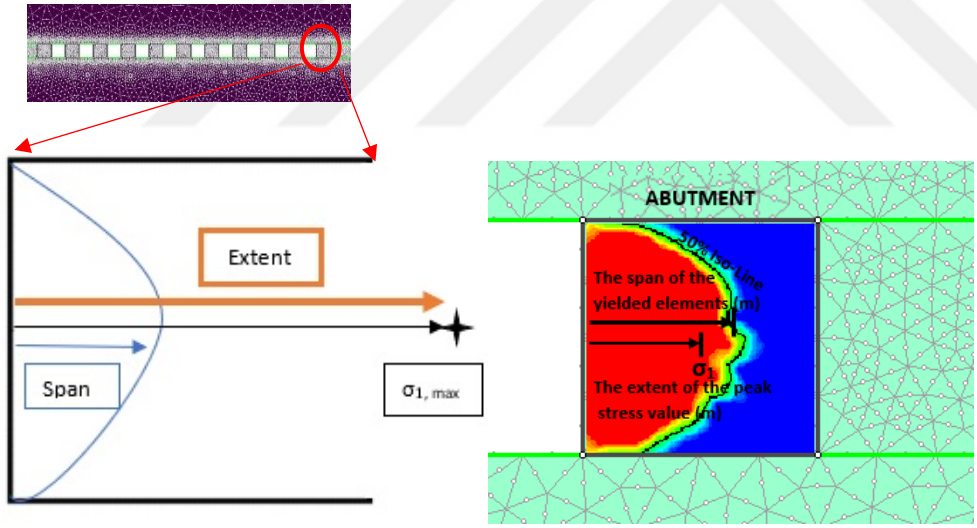

Figure 3.6 An illustration of the measurement points and FEM model result of a sample left abutment

The measurement points and processes seen in Figure 3.6 were consistent across all the models. An example of this was shown for the right abutments. It has the same measurements as the left abutment; however, a query was drawn symmetrical to the left one. It was then appropriate to select and mark the maximum principal stress on

the query. Also, the query was drawn from the left wall of the abutment to outside of it to determine the extent of the peak stress on the abutment. Finally, the distance between the opening wall and the peak stress can be measured to establish the extent of the peak stress value on the abutment. The yielded span was found by drawing the 50% iso-line and subsequently determining the distance between this line and the opening wall. This entire process was repeated for both the left and right abutments.

CHAPTER 4

RESULTS AND DISCUSSION

In this section, the outcomes of the mechanical simulations and the performance of the proposed pillar design tool for underground coal mines were discussed. The FEM model results were presented in conventional 2D plots. Effects of the mechanical, geological, and structural conditions on the pillar performance were explored through parametric analyses. The plastic models were interpreted by considering a percent of yielded span to determine the failure.

4.1 Evaluation of Pillar and Abutment Performance Based on the FEM Models

A dataset comprising 8280 mechanical readings from 276 models was used to plot the correlation between the geological, mechanical and structural conditions and the pillar performance. Complexity of large numbers of data with multi variable relationships makes conventional 2D plots impractical. Therefore, alternative data interpretation techniques were required.

4.1.1 FEM Model Results

FEM results for the pillars and abutments were presented in the form of 2D plots. The sample graphs for the left pillar and the left abutment under different depths were given in the context. The right abutment plots for various k ratios and all the other graphs given in appendices A to H.

The study allows for checking the changes of various parameters while any of the depth, k, pillar width and material property are kept constant. The line color in the

graphics indicate different coal seam dips. ‘CSD’ was used to refer to the coal seam dip and ‘MP’ represents the material property.

In the light of all the analyses, some results emerged. The content of the Appendices A, B and C are mentioned below. In the Appendices D and E, graphs indicate pillar mechanical performance when the field stress ratio is 1. The displacements were compared with respect to the coal seam angles of 0° and 5°, when the seam depths are 200 m and 300 m, respectively. Also, for these depth values, only MP_2, MP_3 and MP_4 were analyzed. In this case, the line colors represent different widths.

The graph points out that increasing the pillar width provides greater stability as the horizontal displacements reduce. For the pillar widths greater than 12 m, difference in the horizontal displacement regarding the material type becomes less noticeable. Conversely, a decrease in the geomechanical characteristics from MP_2 to MP_4 leads to an increase in the horizontal displacement. Another remark is that the pillars in a coal seam with 5° dip exhibit more horizontal displacements compared to those with a horizontal seam. Increasing horizontal displacements with the seam depth is also another finding.

Comparing the left pillar and the center pillar, the only discernible difference is that when the pillars are at the same depth and the pillar width is fixed, the horizontal displacement remains almost constant despite changes in the dip of the coal seam.

Also, the trend in the right-most pillar shows that when the models have the same depth and pillar width, the horizontal displacement value stays nearly the same regardless of the coal seam dip.

The second part of the analysis was on the abutment pressure. The extent of the peak stress value on the left abutment, peak stress and the yielded span were studied for different rock mass quality conditions, coal seam depth, and coal seam dip.

As can be seen from the plots, when the seam dip is 5° the peak stress value is closer to the wall of the opening compared to the horizontal models. Thus, the left abutment at 5° coal seam dip can be mentioned to bear a higher potential to face instabilities

compared to the horizontal seams. This may be related to the fact that the left abutment is deeper compared to the horizontal models. This concludes that comparing the models with 0° and 5° coal seam dip, a clear numerical difference can be observed from analyses.

The yielded span in both the left and right abutments shows a similar trend. When the rock mass quality decreases, the yielded span expands consistently in all the analyses. When the coal seam dip is 5°, it was noticed that the yielded span is greater. As much as the pillar width increases, the yielded span decreases. This is also the same trend when rock mass quality increases.

Appendices F, G, and H show the models which are in depth equal to 400, and k equals to 0.5, 1, and 1.5, respectively.

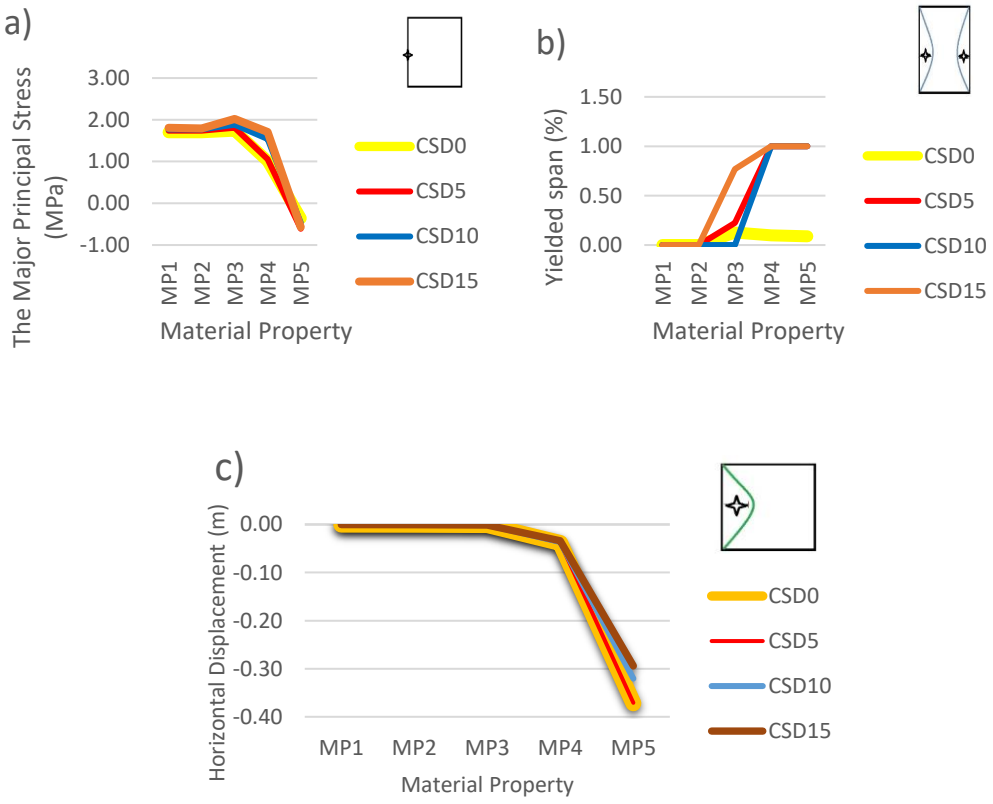

Figure 4.1 a) The major principal stress, b) yielded span, c) horizontal displacement vs. material properties for the left pillar

This section covers the interpretation of the models with 100 m depth is and 0.5 k. In Figure 4.1, the left pillar was demonstrated in three parts. (a) represents the relation between the major principal stresses, material properties and coal seam dips. An increase in the coal seam dip leads to an increase in major principal stress, while weakening of the material property also causes the major principal stress to increase. (b) shows that the percentage of the yielded span increases as the material property weakens. On the other hand, there is no totally yielded pillar in any material property for the horizontal coal seam. (c) demonstrates that horizontal displacement increases with the weakening of the material property. The minus sign indicates the direction of displacement.

Figure 4.2 focuses on both the left and right abutments. So, the relation of left and right abutments can be idealized. (a) shows the relation between the peak stresses, material properties and coal seam dips. The peak stress increases as the coal seam dip increases. As shown in (b), the peak stress point approaches the abutment as the rock weakens. Lastly, (c) shows that as the rock weakens, the thickness of the yielded elements increases on the abutments.

a)

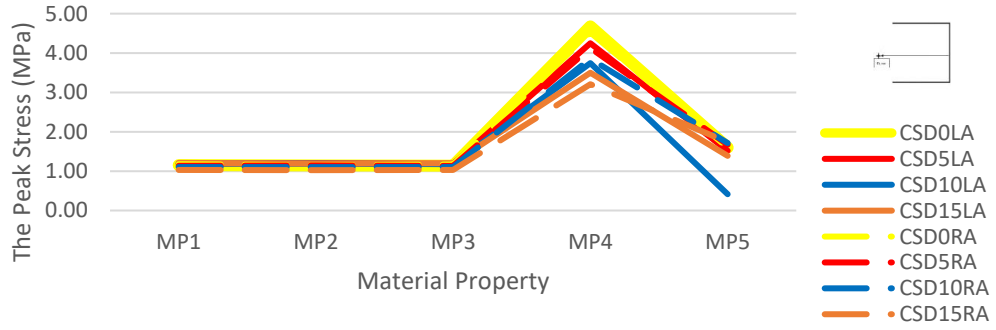

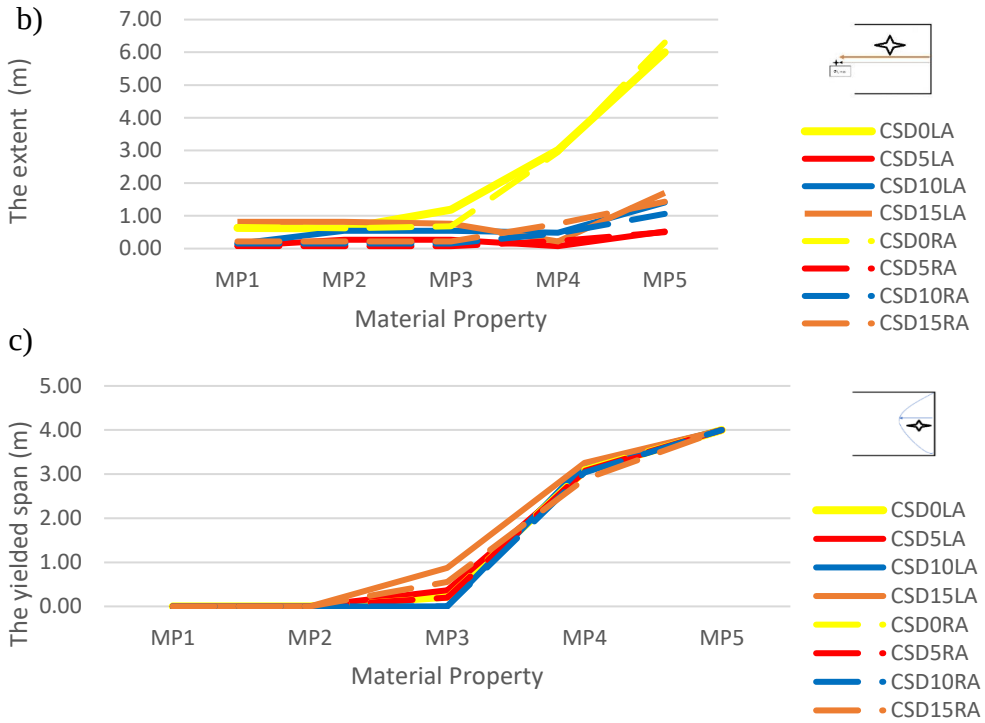

Figure 4.2 a) Peak Stress, b) The Extent of Peak Stress Value on The Abutment, c) The Span of the Yielded Elements vs. Material Properties for Left Abutment

Since the left abutment is at a lower depth than the right abutment according in the inclined seams, all measurements of left abutments are higher than the right abutment measurements. In this case, the analysis results for the left and right abutments are displayed together in the same graph to facilitate comparison. However, for the other analyses, distinct and clearer graphs have been generated for each of them. All other graphs related to this part can be seen in Appendix A.

This section covers the models when the depth is 100 m, the field stress ratio is 1 and pillar width is 4 m. In Figure 4.3, the model results of the left pillar are shown in three parts. (a) represents the relation between the major principal stresses, the material properties, and the coal seam dip. An increase in the seam dip leads to an increase in major principal stress, while weakening of the material property also causes the major principal stress to increase. (b) shows that the percentage of yielded span increases as the material property weakens. (c) demonstrates that horizontal

displacement increases with the weakening of the material property. The minus sign indicates the direction of displacement.

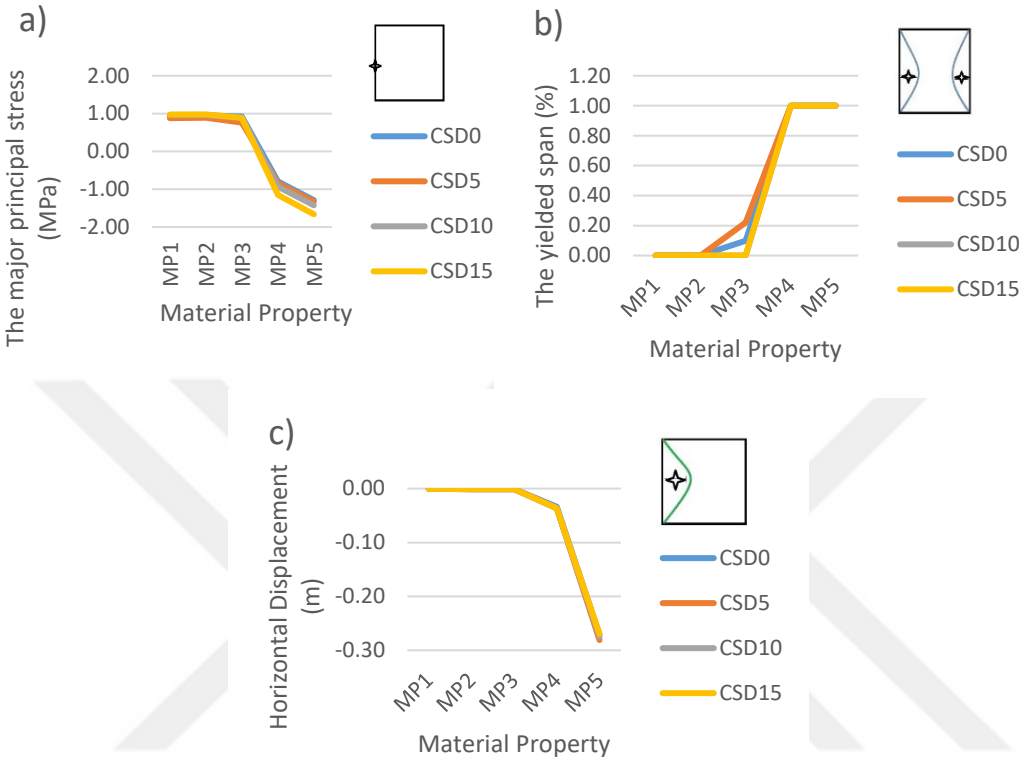

Figure 4.3 a) Major Principal Stress, b) Yielded Span, c) Horizontal Displacement vs. Material Properties for the Left Pillar

Figure 4.4 focuses on the left abutment from three different aspects. (a) shows the relation between the peak stresses, material properties and coal seam dips. The peak stress increases as the coal seam dip increases. As shown in (b), the peak stress point approaches the abutment as the rock weakens. Lastly, (c) shows that as the rock weakens, the thickness of the yielded elements increases for the left abutment.

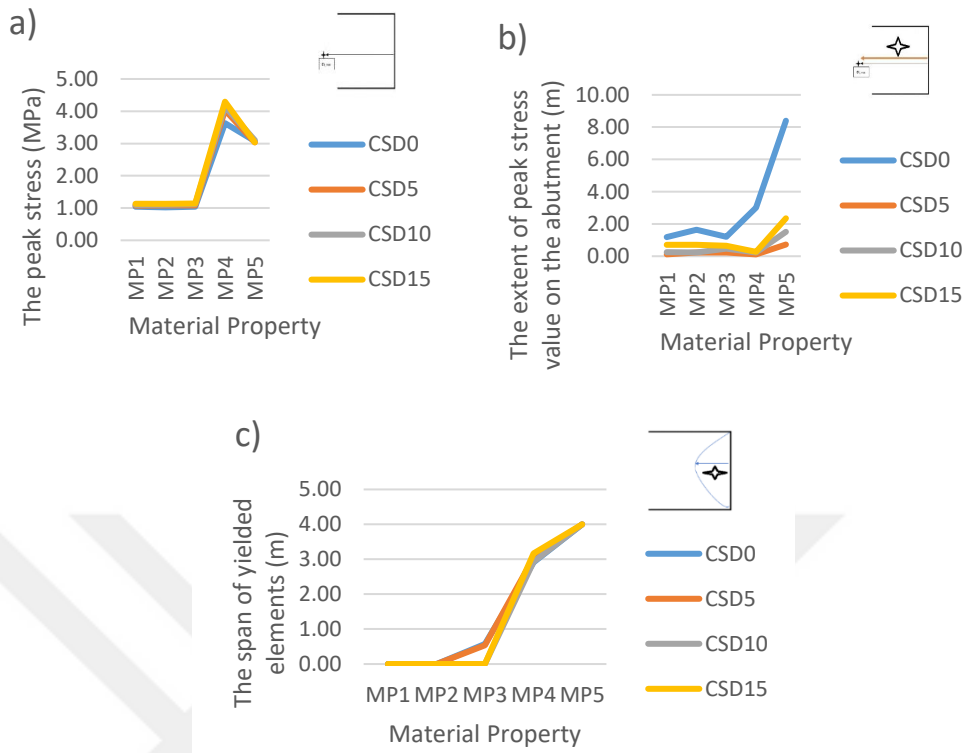

Figure 4.4 a) Peak Stress, b) The Extent of Peak Stress Value on The Abutment, c) The Span of the Yielded Elements vs. Material Properties for the Left Abutment

All other graphs related to this part are seen in Appendix B.

Figure 4.5, shows the model results for the left pillar when the seam depth is 100 m depth and k=1.5. (a) illustrates how the depth and coal seam dip corresponds to a rise in the major principal stress. Similarly, a decrease in material strength leads to an increase in the major principal stress. Moving on to (b), it becomes evident that as the material strength diminishes, the yielded span increases. Finally, (c) reveals that horizontal displacement grows in magnitude as the material strength weakens.

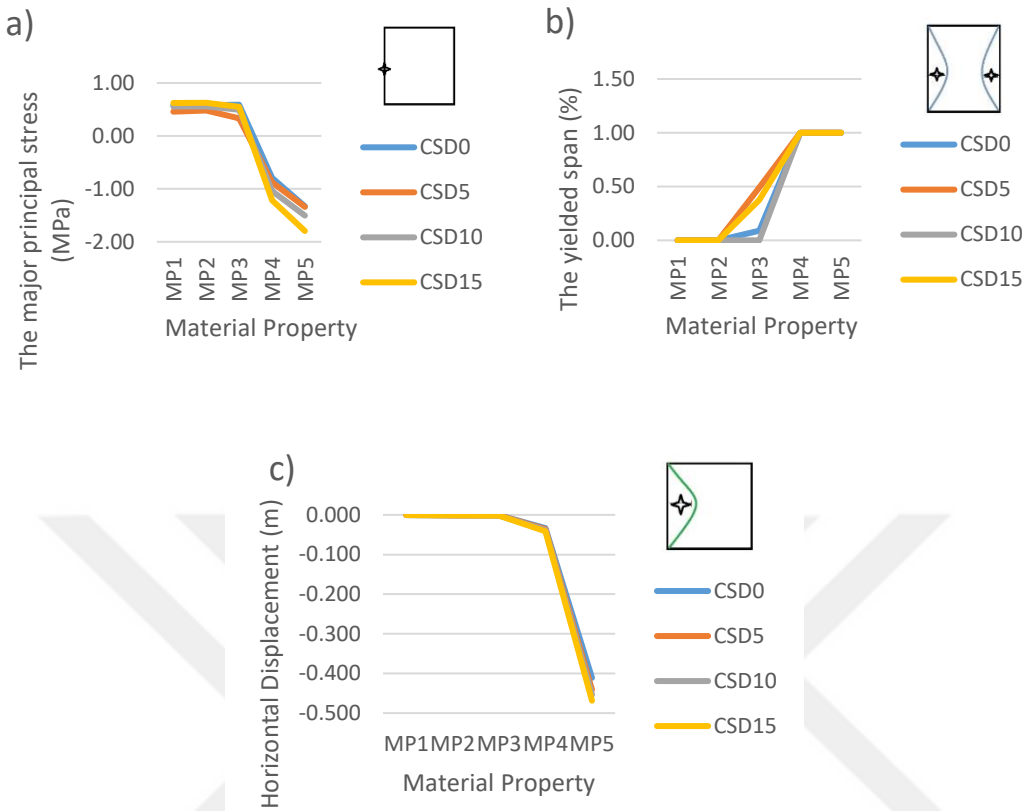

Figure 4.5 a) Major Principal Stress, b) Yielded Span, c) Horizontal Displacement vs. Material Properties for the Left Pillar

This part focuses on the left abutment from three different aspects. (a) illustrates the correlation between the peak stress, material characteristics, and coal seam angles, highlighting that peak stress rises with an increase in coal seam angle. As depicted in (b), the point of peak stress approaches closer to the abutment as the strength diminishes. Lastly, (c) demonstrates that as the strength decreases, the thickness of the yielded elements expands for the left abutment.

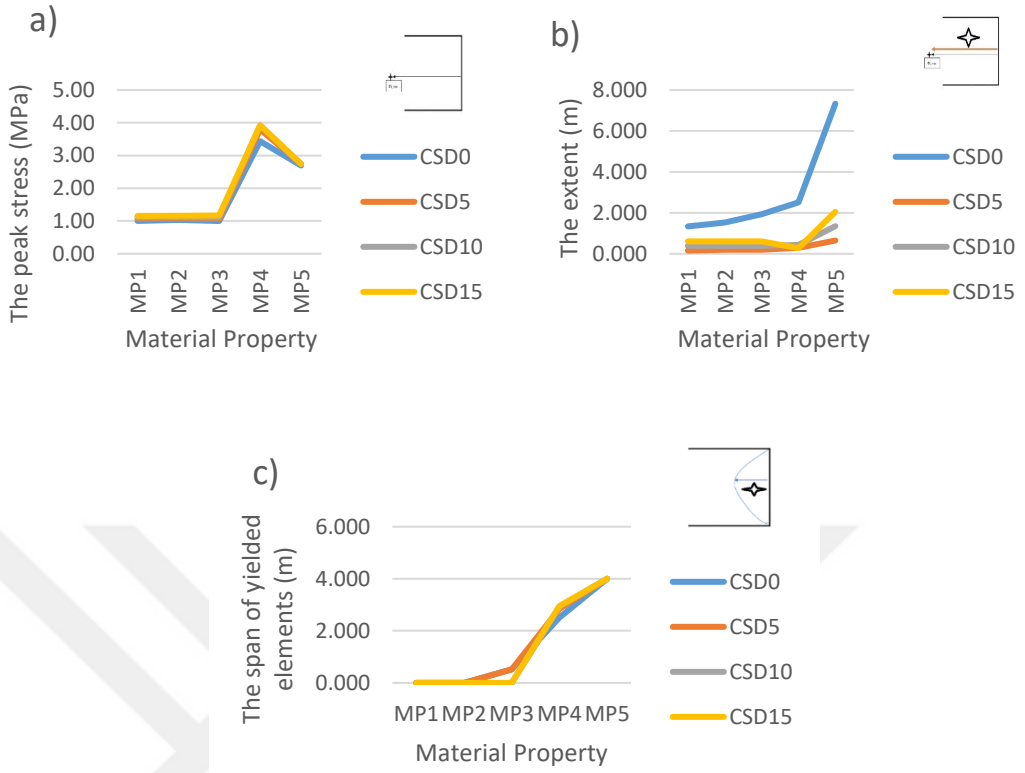

Figure 4.6 a) Peak Stress, b) The Extent of Peak Stress Value on The Abutment, c) The Span of the Yielded Elements vs. Material Properties for the Left Abutment

All other graphs related to this part can be seen in Appendix C.

4.1.2 FEM Results for various Depth and k Values when the Pillar Width=4m and The Seam is Horizontal

In the Figure 4.7, the graph depicts horizontal displacement, which changes based on the values of k and material properties as well as the depth for theleft pillar. The colors on the graph indicate different material properties, while the lines separate the depth zones and display the corresponding values. The horizontal axis shows three different k values, but only MP_1 displays a clear change. The minus sign denotes the direction of the displacement, and the graphs are evaluated accordingly. Specifically, when k is equal to 1, horizontal displacement decreases and remains lower compared to the other k values. As depth increases, horizontal displacement also increases.

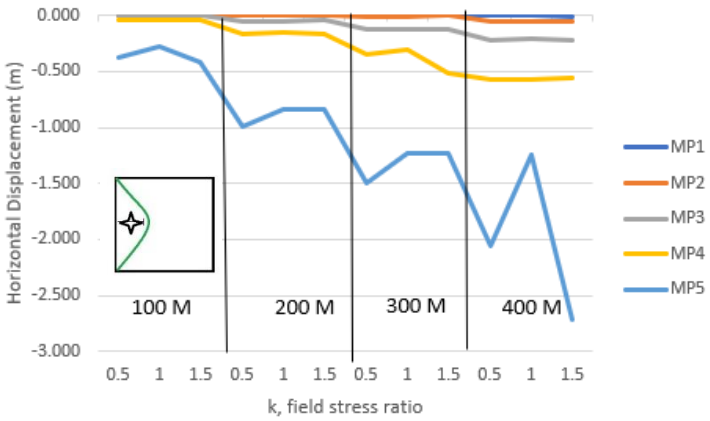

Figure 4.7 Horizontal Displacement for all material properties, depth and k values constant width and coal seam angle for Left Pillar

4.1.3 FEM Results in All Depths, Coal Seam Dips, and k Values for a Fixed Pillar Width of 4m

Using all 240 models with 4 m pillar width, the mechanical outputs can be plotted to carry out a visual sensitivity analysis of pillar stability. The sample plots are given to prove that the visual interpretation becomes more complex as the number of parameters increase. Figure 4.8 shows a graph of the horizontal displacement on the left pillar when the pillar width is 4 m. This includes the models with all 5 different rock mass properties. The depth is represented by four different colors while the k values are represented by different color tones. The coal bed inclinations are indicated by four different line styles corresponding to the four models studied at different angles. The data series are also coded such as '100MA0K0.5', which represents a 100 m seam depth, 0° seam dip, and a 0.5 k value.

Negative horizontal displacements show the direction of yielding. As the depth increases it was observed that the horizontal displacements also increase. When the depth and k values are fixed, the horizontal displacements of the 0° and 5° seam dip models are nearly identical. However, the horizontal displacement decreases as the dip of the coal seam increases as seen in the 10° and 15° models.

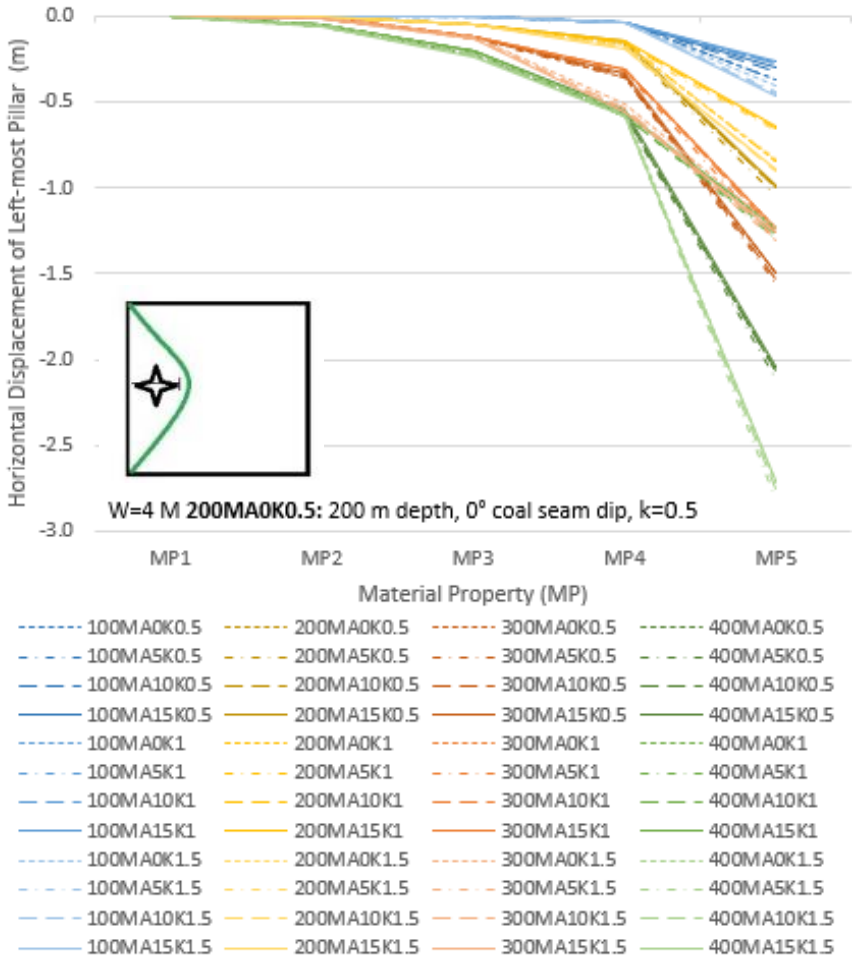

Figure 4.8 The overall plot showing the horizontal displacement at the left-most pillar

For a width of 4 m, the center and right-most pillars exhibit the same horizontal displacement trend as the left-most pillar.

Figure 4.9 shows the overall graph including all combinations of the input parameters to see their effect on the extent of the peak value of σ_1 in the left abutment. The legend is similar with the previous graphs.

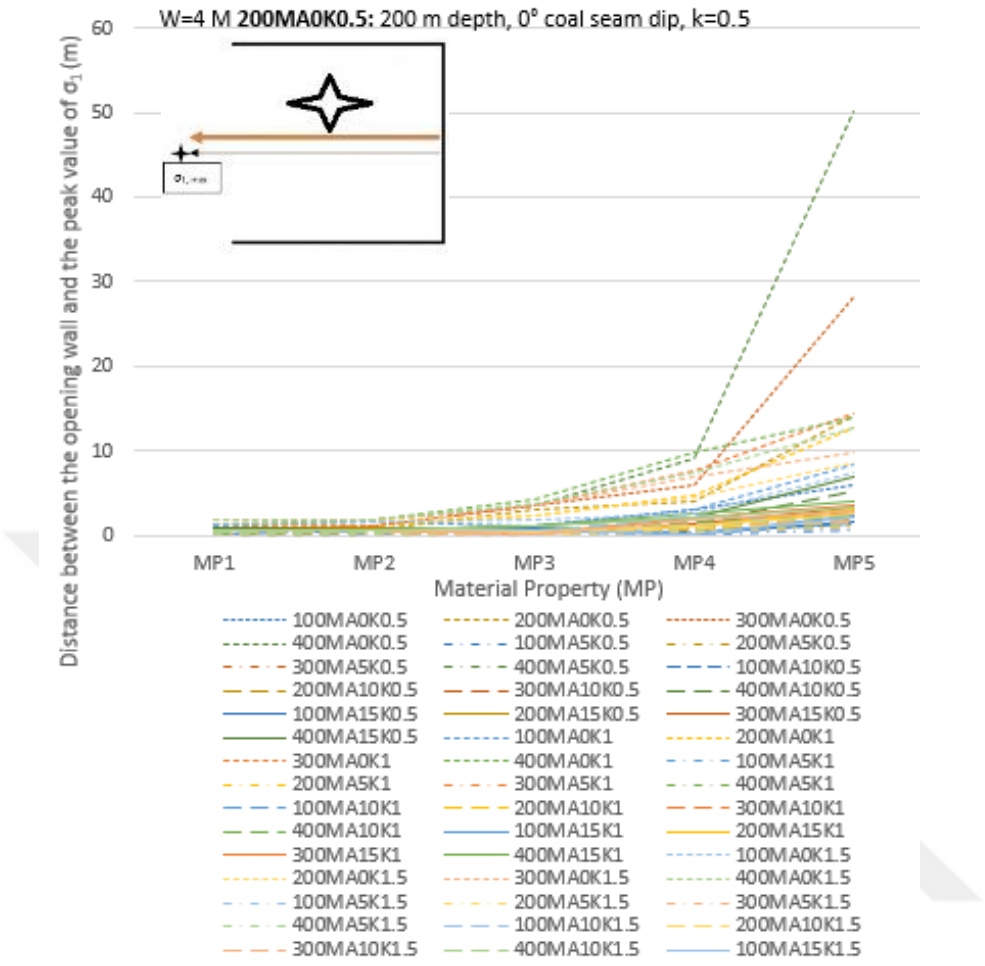

Figure 4.9 The overall graph showing the extent of the peak value of σ_1 in the left abutment

The models indicate that as the rock mass quality decrease, the risk of pillar instability increase. MP_5 is the weakest rock mass and the one which is most likely to give rise to instability. Based on the graph, the model that has the greatest distance between the left abutment wall and the peak value of σ_1 is the one that had MP_5 rock mass properties. This trend suggests that the more this distance, the more stable the left abutment.

If the k value decreases, the distance between the left abutment wall and the peak value of σ_1 decrease, which also degrades the pillar stability. However, checking for the distance based on the coal seam dip with constant depth and k value, the left abutment is in its highest stability condition at the horizontal seam condition. For

models with 5°, 10°, and 15° dips, the most stable left abutment were found when the seam dip is 15°. Nevertheless, as the seam dip increases, the pillar is expected to have more tendency to failure, causing the extent of the stress concentration at the abutment wall to decrease.

4.2 Machine Learning Based Pillar Stability Assessment

In this section, the results and discussions of the machine learning analysis are presented. The study focuses on the importance of using artificial neural networks (ANN) to predict pillar performance in geomechanics. Furthermore, the methodology of the proposed machine learning scheme for pillar performance analysis is explained, including the processes, input parameters, and outputs. Additionally, the machine learning-based pillar stability method is discussed, emphasizing the use of ANN models to account for biases observed during numerical modeling. Later, the proposed ANN model for the pillar design was tested comparing the ANN predictions with the mechanical indicators of hypothetical benchmark cases extracted from the FEM models. Overall, this section comprehensively summarizes the methodology and results of ANN-based pillar performance analysis.

4.2.1 Machine Learning Applications in Geomechanics

Machine learning algorithms have been employed more than ever to solve the geomechanics problems. Machine learning can be considered as an advanced statistical method that fits a mathematical model relying on the current data. The approach is viable to reveal the linear and non-linear trend of the data to make predictions within the input boundary conditions. The predictions can be reliable for the similar cases, but the model requires to be updated for different conditions.

Machine learning categories can be listed as supervised, unsupervised, semi-supervised, and reinforcement seen at Figure 4.10. Supervised and unsupervised methods are the most widely used types as seen in (Alamri, 2022). Supervised

learning is implemented by using the raw data to design the function (Wojtecki et al., 2022).

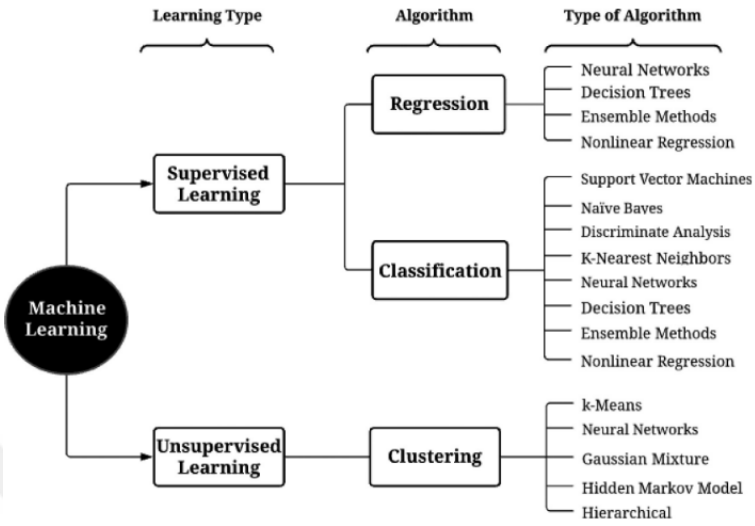

Figure 4.10 Commonly used machine learning types (Alamri, 2022)

Neural network, logistic regression model, support vector machine classification (SVC), and J48 are commonly used algorithms in earth sciences to examine the underground pillar stability (Zhou et al., 2019).

In neural network analysis the mathematical model aims to mimic the behavior of a human neuron. It produces functions to distinguish the differences of the training data set. A typical machine learning model makes use of training, validation, and test stages. The training stage assigns a numerical value of weight for every neuron and explores the data trend by generating mathematical functions for each path (Zhang et al., 2020). The trained model can be used for prediction from new inputs for similar conditions.

Wojtecki et al., (2021) uses different types of machine learning algorithms such as the artificial neural network, decision tree, random forest, and gradient boosting, for assessing the rockburst risk in one of the deep hard coal mines in the Upper Silesian Coal Basin, Poland. They found that neural network can detect all rockburst.

Soomro & Jilani (2020) use the ANN prediction for explosion or ignition in an underground coal mine. A database is used as input, including methane gas, coal dust, and carbon monoxide levels obtained from sensors from the mine. ANN was noted to be more reliable than other machine learning algorithms.

Goh and Zhang, (2012) determined the safety factor for avoiding instabilities due to overstressing in tunnels and caverns at deep underground workings. Numerical simulations require high computational resources and expertise for the safety factor analysis. Moreover, change in the geomechanical properties influence the failure mechanism. On behalf of preventing failure, the modest technique is settled with an artificial neural network approach. Rock mass quality scores and cavern dimensions were used as inputs to obtain the safety factor from ANN. ANN was successful to forecast the stability of caverns. They also proposed a chart relating the rock mass quality and the measurements from caverns with the safety factor.

(J. X. Li et al., 2023) evaluate each key input required for the Coal Mine Roof Rating (CMRR) calculation with machine learning analysis. They use several machine learning algorithms, such as random forest (RFR) and XGBoost (XGB), support vector machine (SV), and artificial neural network (ANN). They demonstrate that machine learning techniques are used to predict various geological and geotechnical parameters accurately, suggesting that machine learning is indeed good at prediction in their study. The automated predictions enhance efficiency and accuracy, which can be crucial in the field of mining for improving safety and design confidence.

4.2.2 The Proposed Machine Learning Scheme for The Pillar Performance Analysis

An artificial neural network is a mathematical model that can learn from data and make predictions for the similar conditions. In this study the feed-forward backpropagation technique was used to train the model to predict the pillar' mechanical performance. The method is popular in training a network to improve

the predictions over time. The backpropagation process is like a feedback loop, where the network learns from its mistakes and adjusts its internal parameters to get better results. Back-propagation neural networks find extensive use due to their simple background and being easy for implementation (Shan et al., 2022). To optimize this learning process, the Levenberg-Marquardt algorithm was utilized, which helps the network converge faster and more accurately (Deshpande et al., 2022).

Inside the network, there are units called neurons that process information. To make these neurons work effectively, we used the hyperbolic tangent sigmoid function (Javed et al., 2015). This function allows the network to handle a wide range of inputs and produce meaningful outputs.

Finally, the network's performance was tested using regression analysis. This method evaluates how well the network's predictions match the actual data. By continuously adjusting the internal parameters through backpropagation, minimization of the difference between the predicted and actual values were aimed. This also makes the network increasingly reliable in making predictions.

The regression plot provides the R value as a coefficient of correlation. R is often recognized as a factor showing the accuracy of the model. High values of R also indicate the success of the network's design and the quality of its training data. In regression plot, training, validation, and test stages hare included.

The elements and flow of an ANN were explained in a diagram as given in Figure 4.11. In this study, ten hidden layers were used for the models. Every neuron has a weight (W) and a block (b) for the hidden and output layers. This flow provides an output, which is created in a predictive manner.

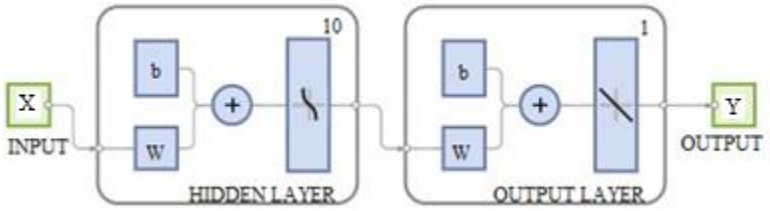

Figure 4.11 Scheme of a two-layer feedforward network with hidden and linear output neurons (Matlab, 2023)

In this study, a total of 276 numerical models were used to create a database involving the mechanical output that represent the pillar performance under different conditions such as the seam depth (H), the seam dip (CSA), the pillar width (W), the material property, and field stress ratio. Measurement points were explained in the previous section. Each model provided 31 measurements for the training database that was used in the machine learning model.

After 2D numerical modeling, 6 of 276 models were chosen randomly to test the accuracy of the ANN model. For five different locations indicating the pillar and abutment stability, (the left abutment, leftmost pillar, center pillar, rightmost pillar, and right abutment) the measurements of 270 models were grouped as inputs and targets. Then, the overall measurements database was used to train models for each location with the help of a neural net fitting tool. 70% of 270, 188 models were used for training and 15% of all models, 41 were used for validation; and the other 15%, 41 were used in the testing stage. After the training part, a network function and the regression plots were obtained.

Five different codes and regression plots were attained for the five different measurement locations. The list in Table 4.1 shows the inputs and outputs.

The simple schematics showing inputs and outputs used in the ANN analysis were also given in Figure 4.12 and Figure 4.13.

Table 4.1 The list of inputs and outputs of the ANN models

Nr.	For the leftmost, center, and rightmost pillars		For the left and right abutments	
	Prediction of the yielded span		Prediction of the extent of the peak stress value	
	Inputs	Outputs	Inputs	Outputs
1	Geomechanical properties (MP#)	The yielded span (%)	Geomechanical properties (MP#)	The extent of the peak stress value on the abutment (m)
2	Coal seam dip (°)		Coal seam dip (°)	
3	Depth (m)		Depth (m)	
4	In-situ stress ratio (k)		In-situ stress ratio (k)	
5	Pillar width (m)		Abutment width (m)	
6	Horizontal displacement (m)		The maximum principal stress (MPa)	
7	The major principal stress on left wall (MPa)		Span of the yielded elements (m)	
8	The major principal stress on center node (MPa)			
9	The major principal stress on right wall (MPa)			

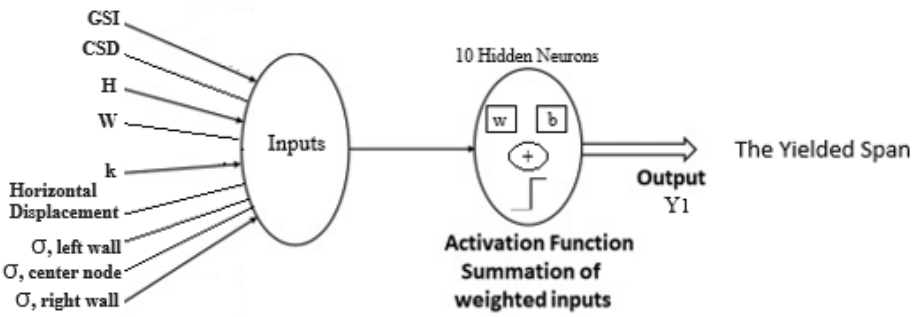

Figure 4.12 Schematic of the ANN model predicting the yielded span (%) on the leftmost, center and rightmost pillars

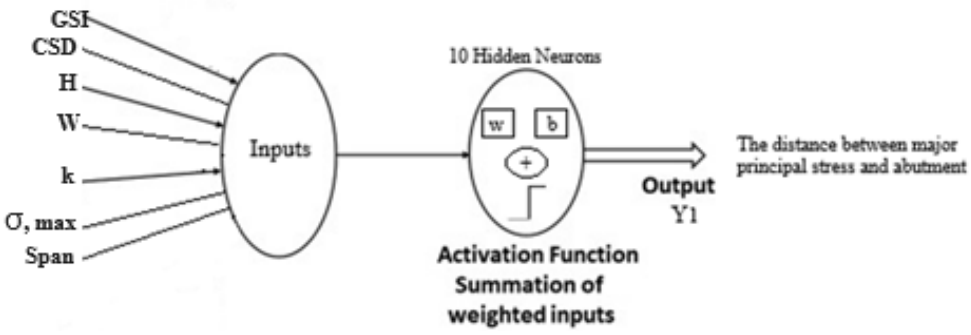

Figure 4.13 Schematic of the ANN model predicting the extent of the peak stress value on the left and right abutments

To make predictions, each model was tested using six benchmarks. The ANN model predicted the intended mechanical outputs for each of the 6 cases. In this process, the measurements obtained from the numerical modeling were compared with the ANN predictions. The regression analysis was used to determine the level of agreement between the two. Linear operating functions help to estimate the relationships between variances. The closer the correlation factor R is to 1, the stronger the positive relationship between variables. Conversely, the closer it is to 0, the stronger the negative relationship. The coefficient of determination, R, is an indicator of prediction success. This process is repeated for all five measurement sites, including the left and right abutment points, leftmost, center, and rightmost pillars.

4.2.3 The Machine Learning based Pillar Stability Method

This section presents the interpretation of numerical solutions using artificial neural networks (ANN). The ANN model undergoes training and testing, with its performance being compared to benchmark cases by utilizing model outputs. This suggests that the ANN model can effectively account for any biases observed during the numerical modelling process.

This study created a total of 8280 data points, and each measurement was analyzed using ANN prediction. Matlab was used to implement the training and testing stages.

In the training stage different inputs and targets were fed into the model for each measurement point.

After the data for the left abutment is loaded to the Matlab-ANN section, the image containing information about the number of hidden layers, the number of data used for training, validation and testing, entry points and results are given in Figure 4.14.

For abutments, totally eight parameters were measured from the numerical simulations. Seven of them were noted as inputs, depth, coal seam dip, pillar width, field stress ratio, rock mass material property, the major principal stress, and the yielded span. The ANN model provided the extent of the major principal stress as an output.

For pillars, depth, coal seam dip, pillar width, field stress ratio, rock mass material property, and horizontal displacement on the wall and the major principal stresses from three different places of the pillar, left wall, centre point, and right wall, were introduced as inputs. The output of the ANN model was the percent of the yielded span.

After training, a Matlab function and a regression plot were obtained to check the validity of the trained model. The coefficient of correlation (R) was close to 1 for all three regression graphs (training, validation, and test), indicating a low error and strong correlation between inputs and outputs.

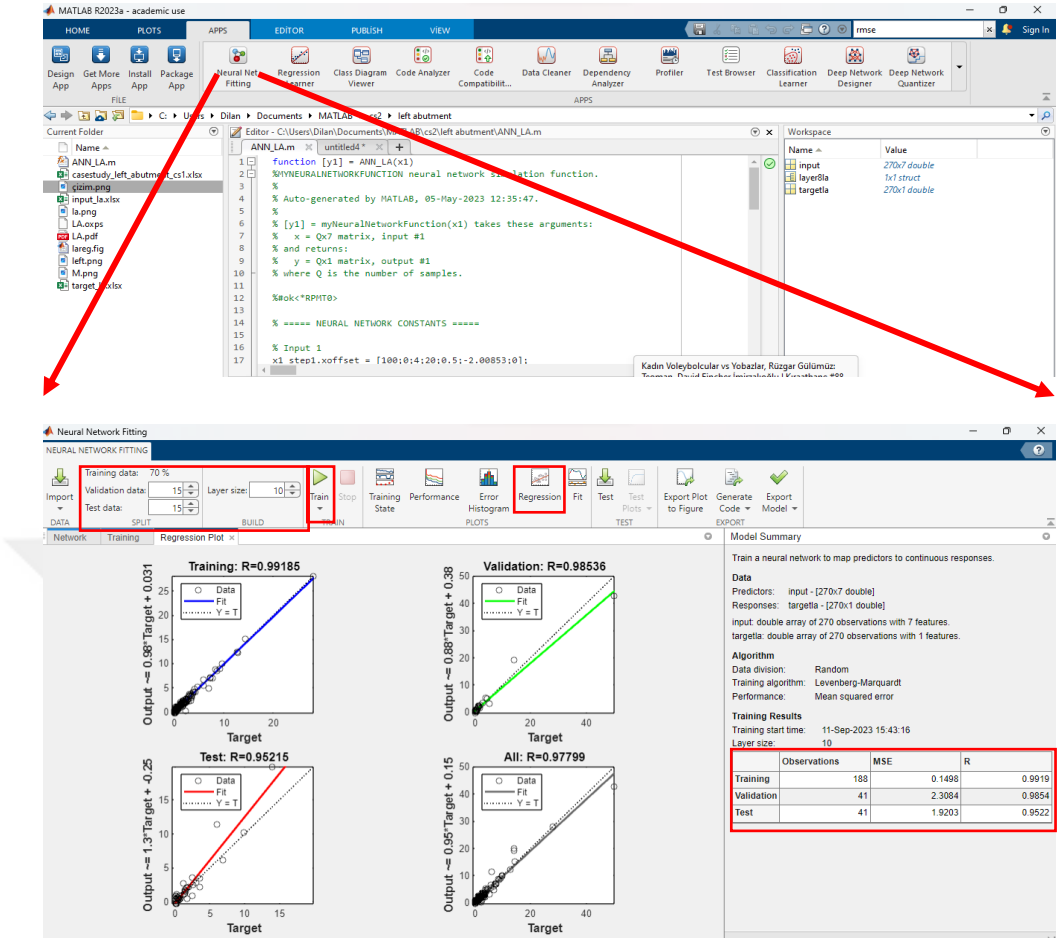

Figure 4.14 A sample view from the Matlab and ANN toolbox

Then, benchmark cases were designed and run to establish an additional stage for the validity of the models. The benchmark cases were designed to see whether the trained model can accurately and meaningfully make predictions for the intermediate conditions. After that, a regression graph giving the determination coefficient was created, and the results of numerical model and ANN prediction were compared. For dependable and accurate results, the determination coefficient (R) was aimed to be more than 90%. This signifies a high level of accuracy in the predictions made by the ANN. The generated model was intended to be utilized for prediction of various scenarios.

The first benchmark study was carried out on the left abutment. Inputs, target, and ANN prediction can be seen in Table 4.2.

Table 4.2 Inputs and outputs of the benchmark study in the left abutment

Inputs									Outputs	
Model Condition						Measurements			The extent of the peak stress value on the abutment (m)	
No	H (m)	CSD (°)	W (m)	GSI	k	σ_1 (MPa)	Yielded Span (m)		FEM Model	ANN Prediction
1	100	0	4	95	1	1.05	0.00		1.19	1.53
2	100	5	4	65	1	1.08	0.54		0.23	0.10
3	300	5	4	65	0.5	13.35	3.83		0.31	0.55
4	300	10	4	65	0.5	12.50	3.37		0.08	0.50
5	400	15	4	20	1.5	-2.09	4.00		3.26	3.36
6	200	0	16	35	1	2.11	3.18		3.57	3.44

The illustration of the left abutment and the form of measurements can be seen in Figure 4.15.

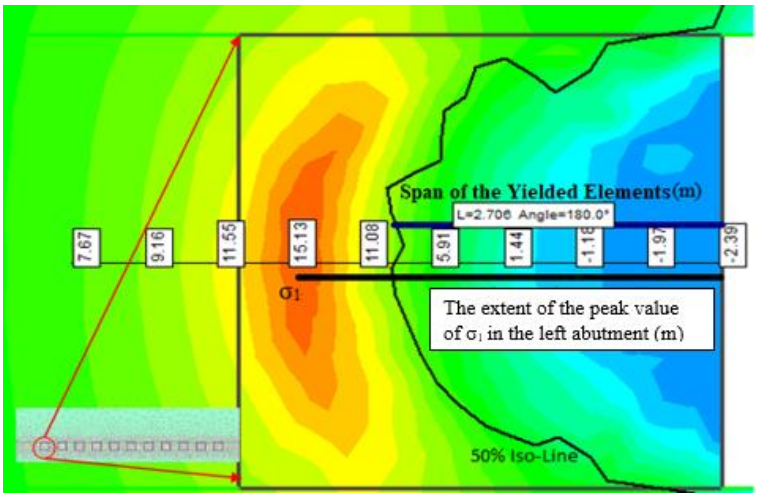

Figure 4.15 The illustration of the left abutment and a sample query line

After the training, a Matlab function and regression plot were obtained for the left abutment. The regression plot was given in Figure 4.16 and the function can be seen equation (13). The coefficient of correlation (R) proves the success of the uploaded data. For all three stages of, training, validation, and test, R is so close to 1 means acceptably low error, and it is understood that inputs and outputs are well related.

OUTPUT (THE EXTENT) of ANN_LA = [DEPTH; COALSEAM DIP;WIDTH;GSI;k; PEAK STRESS,σ_1;YIELDED SPAN]; (13)

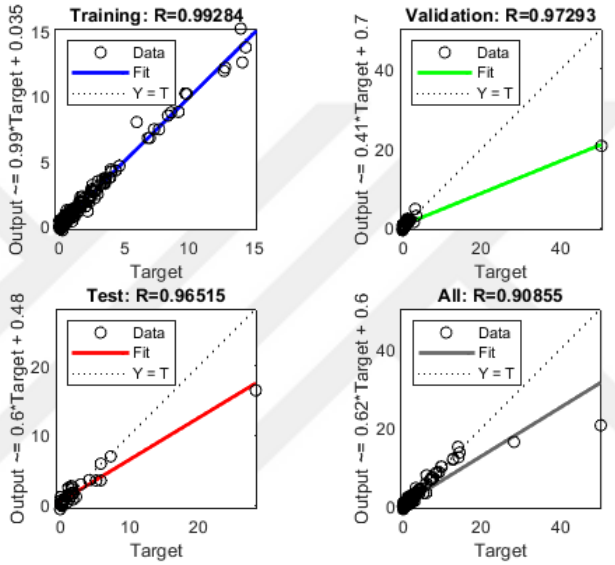

Figure 4.16 The correlation plots for the ANN model of the left abutment

After the neural net fitting, the Matlab script involving the trained machine was run with 6 different benchmark cases to test the ANN's prediction capability. Finally, the numerical model outputs and ANN predictions were compared using regression analysis, as in Figure 4.17.

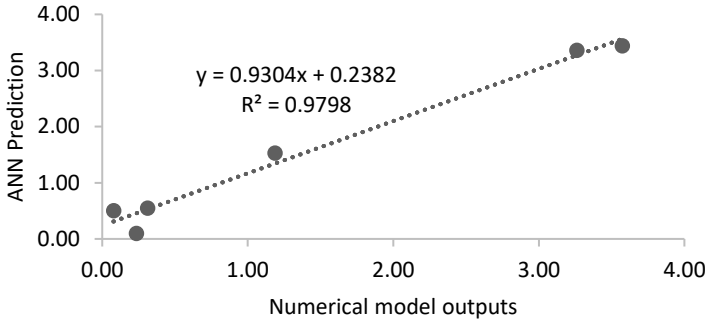

Figure 4.17 Correlation of the numerical simulation and ANN predictions on the left abutment

Based on the regression analysis, the results were correlated by 98% in predicting the numerical simulation outcomes. This suggests that the ANN model is useful for testing the intermediate cases, which were not included in the numerical simulation set.

Table 4.3 Hidden layers and R values for left abutment

Hidden Layer Number	R Value
7	0.82
8	0.97
9	0.95
10	0.94
11	0.76
12	0.76

A study was conducted specifically for the left abutment, with the goal of achieving a balanced fitting process that avoids overfitting. To accomplish this, 5 different hidden layer numbers were used in the analysis and the resulting R values were recorded in Table 4.3. Based on expert evaluation and common sense, the hidden layer number was selected as 10 and subsequent analyses were carried out accordingly.

The second benchmark study was the leftmost pillar. Inputs, target, and ANN prediction can be seen in Table 4.4.

Table 4.4 Inputs and outputs of the benchmark study in the leftmost pillar

Inputs										Outputs	
Model Condition						Horizontal Displacement (m)	Major Principal Stress, σ_1 (MPa)			The Yielded Span (%)	
No	H (m)	CSD (°)	W (m)	GSI	k	Left Wall	Left wall	Centre Node	Right Wall	FEM Model	ANN Prediction
1	100	0	4	95	1	0.00	0.95	1.78	1.17	0.00	-0.06
2	100	5	4	65	1	0.00	0.76	1.93	1.03	0.22	0.33
3	300	5	4	65	0.5	-0.13	-3.13	1.04	-2.53	1.00	0.93
4	300	10	4	65	0.5	-0.13	-2.81	1.30	-2.50	1.00	0.88
5	400	15	4	20	1.5	-2.70	-7.36	-6.83	-7.32	1.00	1.11
6	200	0	16	35	1	-0.02	-2.01	1.00	-2.06	0.41	0.43

The illustration of the leftmost pillar and the form of measurements can be seen in Figure 4.18.

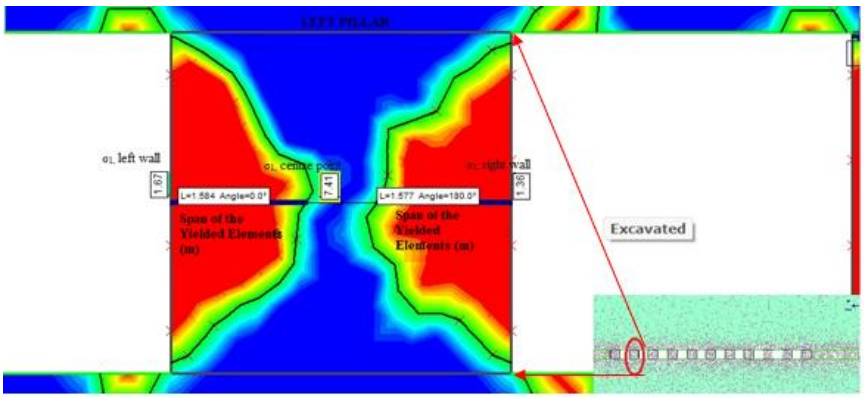

Figure 4.18 The illustration of the leftmost pillar and a sample query line

The regression plot is given in Figure 4.19. The coefficient of correlation (R) shows the success of the uploaded data.

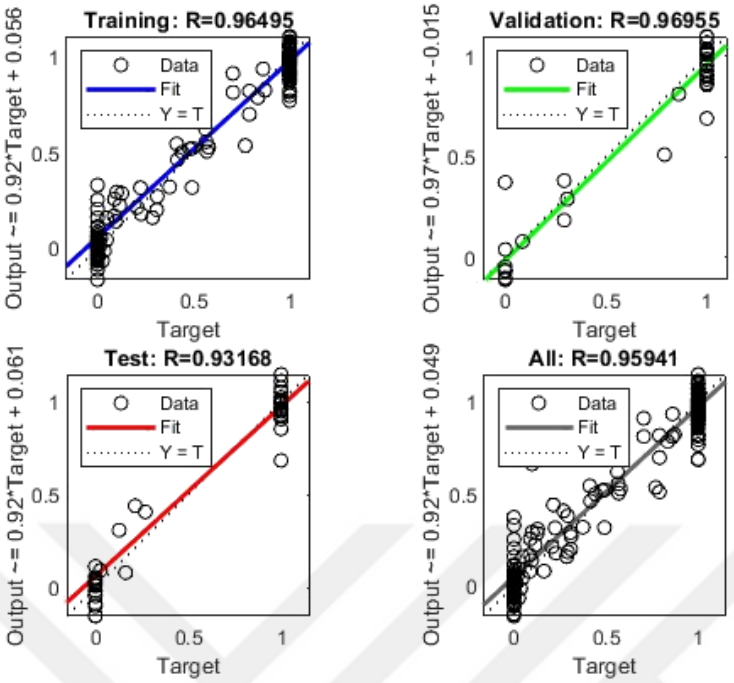

Figure 4.19 The regression plot of leftmost pillar data

For all three regression graphs, training, validation, and test, R is so close to 1 means acceptably low error. For instance, R equals to 96.5% for training part. It means that inputs and outputs are well related.

The trained machine obtained after the neural net fitting process was used for estimation in the six benchmark cases. The numerical simulation outputs and ANN predictions were then compared through regression analysis in Figure 4.20.

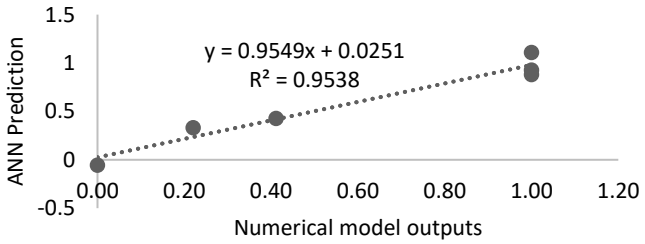

Figure 4.20 Correlation of the numerical model outputs and ANN predictions for

The correlation coefficient of 0.9538 points out the success of the prediction model. This indicates that the ANN model trained in Matlab can be used for prediction about the pillar stability.

The third benchmark study was carried out at the center pillar. Inputs, target, and ANN prediction can be seen in Table 4.5.

Table 4.5 Inputs and outputs of the benchmark study in the center pillar

Inputs										Outputs	
Model Condition						Horizontal Disp. (m)	Major Principal Stress, σ_1 (MPa)			The Yielded Span (%)	
No	H (m)	CSA (°)	W (m)	GSI	k	Left Wall	Left wall	Centre Node	Right Wall	FEM Model	ANN Pred.
1	100	0	4	95	1	0.00	1.34	2.05	1.34	0.00	-0.08
2	100	5	4	65	1	0.00	1.14	2.16	1.08	0.23	0.30
3	300	5	4	65	0.5	-0.17	-3.04	0.24	-3.09	1.00	0.87
4	300	10	4	65	0.5	-0.16	-3.00	1.21	-2.96	1.00	0.92
5	400	15	4	20	1.5	-2.84	-7.21	-6.51	-7.30	1.00	0.99
6	200	0	16	35	1	-0.02	-2.03	1.07	-2.01	0.40	0.33

The measurement points were given in Figure 4.21.

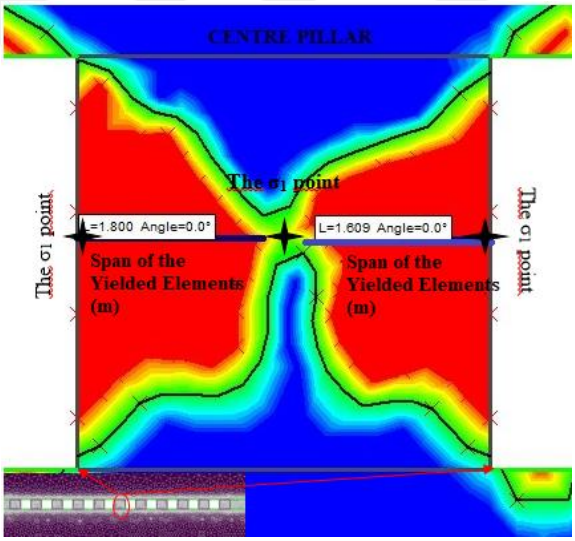

Figure 4.21 The illustration of the center pillar and a sample query

The regression plot was obtained as shown in Figure 4.22. The coefficient of correlation (R) was used to measure the accuracy of the prediction.

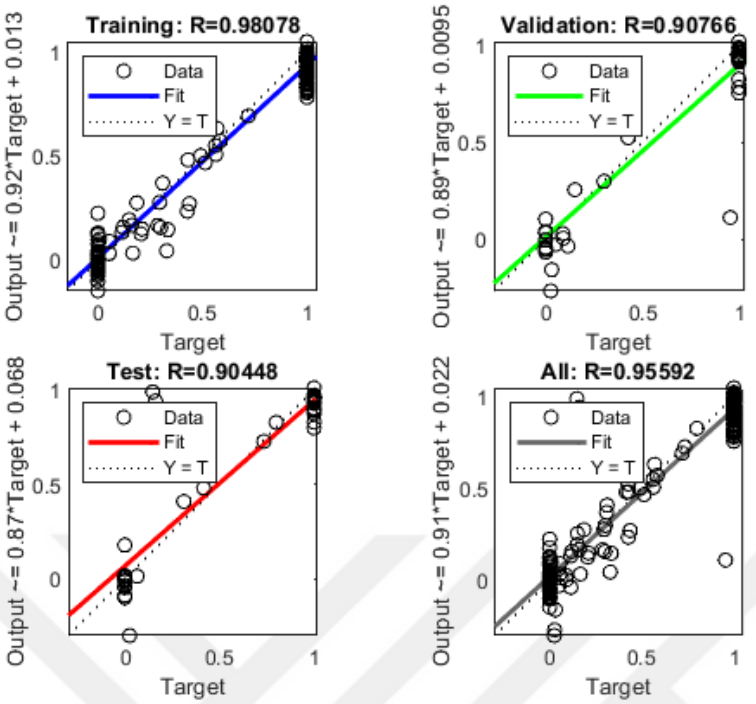

Figure 4.22 The correlation plot for the center pillar data

For all three regression graphs, training, validation, and test, R is so close to 1 means acceptably low error. For instance, R equals to 98.1% for training part. It means that inputs and outputs are well related.

Once the neural net fitting process is completed, the trained model was tested on six benchmark cases to check the quality of the ANN predictions. The results were then compared in Figure 4.23 for regression analysis between the targets and ANN predictions.

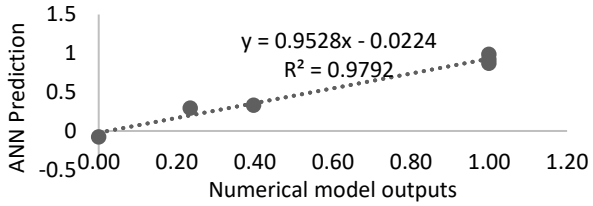

Figure 4.23 ANN prediction vs. numerical model outputs for center pillar

According to the regression analysis, the statistical results indicate a high level of correlation, with a 98% accuracy rate. This finding suggests that the artificial neural network (ANN) model has practical use and can be applied to additional scenarios with similar parameters.

The fourth benchmark study was carried out on the right most pillar. Inputs, target, and ANN prediction can be seen in Table 4.6.

Table 4.6 Inputs and outputs of the benchmark study in the rightmost pillar

Inputs										Outputs	
Model Condition						Horizontal Disp. (m)	Major Principal Stress, σ_1 (MPa)			The Yielded Span (%)	
No	H (m)	CSA (°)	W (m)	GSI	k	Left Wall	Left wall	Centre Node	Right Wall	FEM Model	ANN Pred.
1	100	0	4	95	1	0.00	1.17	1.79	0.95	0.00	-0.01
2	100	5	4	65	1	0.00	0.99	1.81	0.77	0.26	0.21
3	300	5	4	65	0.5	-0.08	-2.78	3.18	-3.02	1.00	1.08
4	300	10	4	65	0.5	-0.08	-2.01	-0.32	-2.72	1.00	0.99
5	400	15	4	20	1.5	-2.41	-7.02	-6.37	-7.02	1.00	0.98
6	200	0	16	35	1	-0.02	-1.95	1.00	-2.00	0.40	0.43

The measurement points were shown in the Figure 4.24.

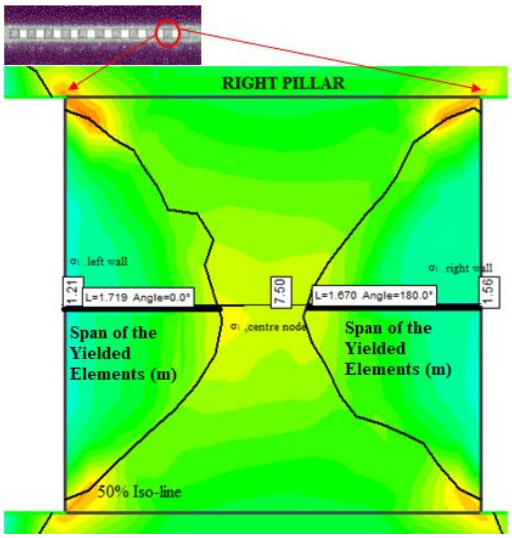

Figure 4.24 The illustration of the rightmost pillar and its measurements

It is important to carefully examine the regression plot in Figure 4.25. The coefficient of correlation (R) serves as a measured for evaluating the success of the uploaded data.

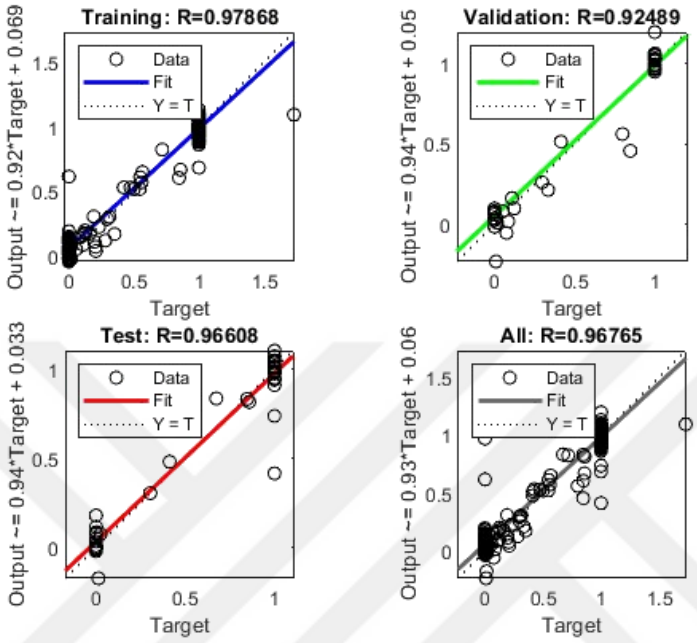

Figure 4.25 The regression plot of rightmost pillar data

The regression graphs for training, validation, and test show that the error rate is acceptably low with an R value close to 1. For example, the training has an R value of 97.9%, indicating a strong correlation between inputs and outputs.

After the neural net fitting the code is used to estimate ANN predictions for 6 different cases. Figure 4.26 compares the targets and ANN predictions for regression analysis.

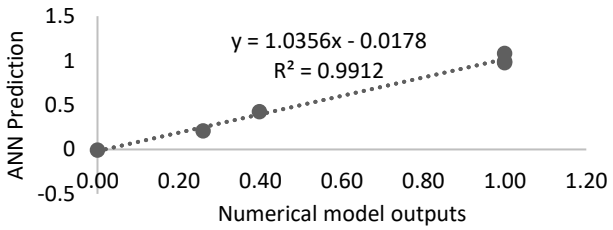

Figure 4.26 ANN prediction vs. numerical model outputs for rightmost pillar

The regression analysis points out a correlation of 0.9912, which means that 99% success was obtained on how specific the results were about the predictions. This indicates that ANN model was helpful for any other prediction.

The fifth benchmark study was on the right abutment. Inputs, target, and ANN prediction can be seen in Table 4.7.

Table 4.7 Inputs and outputs of the benchmark study in the right abutment

Inputs								Outputs	
Model Condition						Measurements		The extent of the peak stress value on the abutment (m)	
No	H (m)	CSA (°)	W (m)	GSI	k	Peak Stress (MPa)	Yielded Span (m)	FEM Model	ANN Prediction
1	200	5	12	85	1	1.48	0.24	0.17	0.44
2	200	0	8	65	1	2.33	1.79	1.68	1.84
3	300	5	8	65	1	4.99	2.46	0.22	0.36
4	200	5	16	65	1	1.71	1.77	0.18	0.39
5	300	5	16	35	1	4.25	4.18	0.35	0.93
6	200	15	4	65	1.5	7.17	2.39	0.65	0.55

The illustration of the right abutment and the form of measurements can be seen in Figure 4.27.

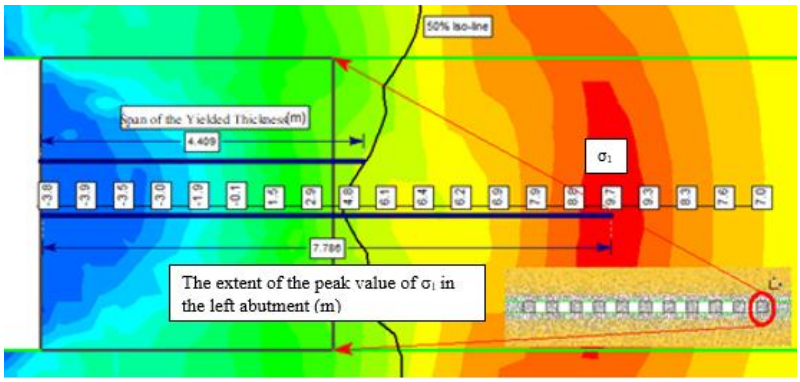

Figure 4.27 The illustration of the right abutment and a sample query

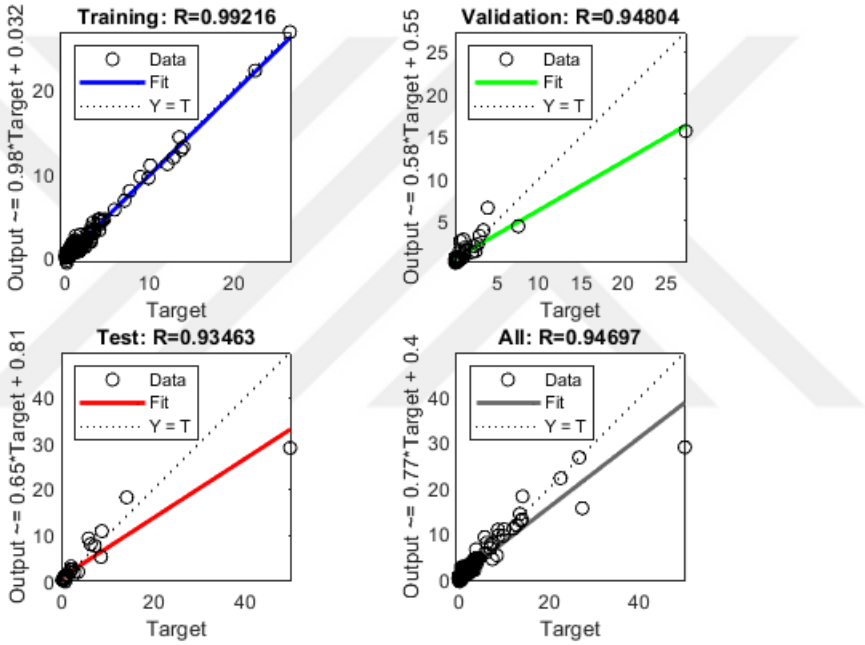

Figure 4.28 The regression plot of right abutment data

The regression plot was given in Figure 4.28. The coefficient of correlation (R) shows the success of the uploaded data. For all three regression graphs, training, validation, and test, R was so close to 1 means acceptably low error, and it was understood that inputs and outputs were well related.

Upon completion of the neural net fitting process, the resulting model as utilized to generate ANN predictions for six distinct cases. The targets and ANN predictions were subsequently subjected to regression analysis, as demonstrated in Figure 4.29.

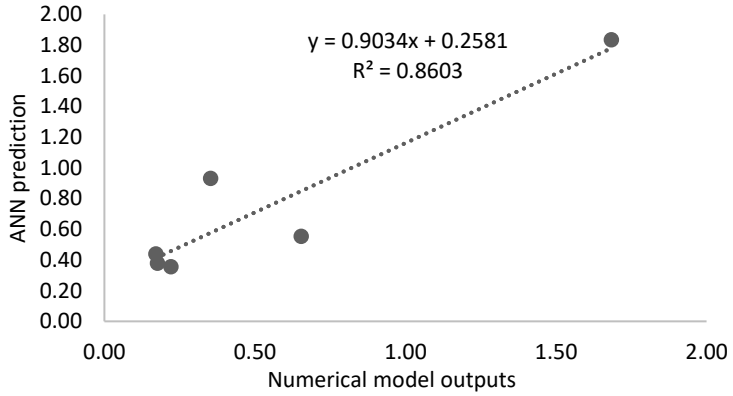

Figure 4.29 Correlation of the numerical model outputs and the ANN predictions at the right abutment

The correlation coefficient from the regression analysis was 0.8603, indicating an 86% success rate in predicting outcomes. This suggests that the ANN model can be used for predictions.

When comparing two data sets, the root-mean-square error determines the amount of error present. This is achieved by comparing predicted values with known or observed values. FEM model results and ANN prediction values were given to Matlab, which has the function of RMSE in it. Finally, RMSE values are appeared.

Table 4.8 RMSE values of measurement locations

Measurement Location	**RMSE**
Leftmost Pillars	0.09
Center Pillars	0.08
Rightmost Pillars	0.04
Left Abutments	0.26
Right Abutments	0.76

During this thesis, the RMSE values for FEM model results and ANN prediction values were examined using Matlab. The RMSE values for each measurement

location, such as left and right abutments and leftmost, center, and rightmost pillars, were evaluated and reported Table 4.8. The results show that the RMSE values generally indicate accurate results.

CHAPTER 5

CONCLUSIONS

In this research, pillar stability was examined using advanced computational and statistical techniques to propose an auxiliary tool for one of the geomechanical challenges in underground coal mining. By employing geomechanical modeling and machine learning, the factors influencing the pillar performance were investigated. Later, an auxiliary pillar design tool was proposed to enhance the interpretation of the numerical simulation results. The method was also aimed to be used for the safe pillar design.

The research motivation raised from the need to improve safety and efficiency in coal mining operations. Through a comprehensive review of historical coal mine accidents, various events were discovered related to the pillar instability. Although empirical and numerical methods have been developed for the assessment of pillar stability, these methods either require advanced mechanical and computational skills or they are restricted with the locally valid predictions. This study aims to make the results of the advanced and reliable numerical solutions available for mine design.

In the scope of the computational studies, 276 finite element models were created, to obtain a comprehensive data set consisting of 8,280 readings. For a typical underground coal mine layout, the model geometry and boundary conditions were prepared to reveal the pillar performance. Parametric analyses provided stress and percent of yielded span values to create pillar performance charts, which provides valuable insights about the pillar stability. Conventional 2D plots generated from the database were used to check the pillar performance under various geological, geomechanical and structural conditions. However, it was discovered that multiple variables and data series do not offer a user-friendly scheme for checking the numerical model results.

Therefore, a machine learning scheme was developed, which relies on the numerical simulation results. By leveraging the power of machine learning algorithms, the efficiency and accuracy of prediction for the intermediate conditions and the interpretation of complex numerical data are enhanced. Based on the benchmark tests, the ANN model has generated satisfactory outcomes. Therefore, the intermediate conditions, which are not covered in the numerical study can be accurately revealed relying on the proposed method.

The regression analyses point out that the predictions of the proposed ANN model correlate with the numerical simulations by 95.3% on average, and the error margin has remained well below 5%. These findings indicate a high level of accuracy and reliability. The ANN model was satisfactorily accurate in identifying the mechanical outputs of the pillar performance. In addition, various designs regarding the coal seam depth and coal seam dip can be tested to determine the best pillar width, which is critical in terms of the recovery.

The results and discussions presented in Chapter 4 and 5 highlight the significant findings of this research. Parameters such as the pillar size, depth, and rock mass properties, were observed to strongly influence the stability of pillars in underground coal mining. The machine learning scheme can be promising to improve the interpretation of the numerical results and may provide a practical tool for inexperienced mine design operators.

Overall, the findings appear consistent in demonstrating the influence of factors like pillar width, material characteristics, coal seam dip, and depth on stability. Weaker material properties and inclined coal seam dips tend to reduce stability, while wider pillars and shallower depths enhance stability. Below are the summarized and analyzed versions of the results.

1. Pillar Width and Stability: Increasing pillar width provides greater stability and horizontal displacements reduce. Beyond 12 meters, differences in the horizontal displacement due to material type become less noticeable. This suggests a correlation between stability and the pillar width.

2. Material Characteristics: Decreasing geomechanical characteristics from MP_1 to MP_5 leads to an increase in horizontal displacement. This indicates that weaker material properties result in less stability.
3. Coal Seam Dip: Pillars in a coal seam with a 5°, 10°, or 15° dip angle exhibit more horizontal displacements compared to those with a horizontal seam. This suggests that a steeper seam dip can reduce the stability.
4. Depth of Seam: Increasing the depth of the seam leads to higher horizontal displacements. This implies that deeper seams may pose additional stability challenges.
5. Comparison of Pillars: Horizontal displacement remains constant when pillars are at the same depth and the pillar width is fixed, regardless of the dip of the coal seam. This suggests that certain factors, such as depth and width, may have a more significant impact on stability than seam dip.
6. Yielded Span: The yielded span expands as rock mass quality decreases and as the coal seam dip increases. However, increasing pillar width leads to a decrease in the yielded span, indicating that wider pillars are more stable.
7. Principal Stresses: The major principal stress increases with an increase in coal seam dip and with weakening material properties. Peak stress points also move closer to the abutment as rock strength diminishes.
8. Stability and Depth: Deeper abutments, especially in inclined models, tend to have higher measurements, suggesting that depth can impact stability.
9. Effect of Field Stress Ratio: As the k value increases, horizontal displacement increases, too and stability of pillars decreases.
10. Rock Mass Quality: As rock mass quality decreases, the risk of pillar instability increases. MP_5 is the weakest rock mass and is most likely to cause instability. A greater extent of the peak stress value on the abutment indicates greater stability.

Further research could focus on refining and expanding the ANN model, incorporating additional variables, expanding the database by more numerical

models, and conducting field scale measurements to increase the reliability and applicability of the proposed methods.

In conclusion, this dissertation contributes to the advancement of underground coal mining practice by integrating the numerical simulations and machine learning. The findings presented here have potential to enhance the safety and efficiency of coal mining industry.

REFERENCES

Alamri, A. H. (2022). Application of machine learning to stress corrosion cracking risk assessment. *Egyptian Journal of Petroleum*, *31*(4), 11–21. https://doi.org/10.1016/J.EJPE.2022.09.001

Aydan, Ö., Tokashiki, N., & Ulusa, R. (2015). Rock Mass Quality Rating (RMQR) for Rock Engineering. *International Journal of the JCRM*, *11*(1).

Aydan, Ö., Ulusay, R., & Tokashiki, N. (2014). A new rock mass quality rating system: Rock Mass Quality Rating (RMQR) and its application to the estimation of geomechanical characteristics of rock masses. *Rock Mechanics and Rock Engineering*, *47*(4), 1255–1276. https://doi.org/10.1007/s00603-013-0462-z

Azarafza, M., Nanehkaran, Y. A., Rajabion, L., Akgün, H., Rahnamarad, J., Derakhshani, R., & Raoof, A. (2020). Application of the modified Q-slope classification system for sedimentary rock slope stability assessment in Iran. *Engineering Geology*, *264*, 105349. https://doi.org/10.1016/J.ENGGEO.2019.105349

Barbero, M., & Barla, G. (2010). Stability analysis of a rock column in seismic conditions. *Rock Mechanics and Rock Engineering*, *43*(6). https://doi.org/10.1007/s00603-010-0097-2

Barton, F. E., Amos, H. E., Albrecht, W. J., & Burdick, D. (1974). *Treating peanut hulls to improve digestibility for ruminants. J. Anim. S*. *38*(4), 860–864.

Bieniawski, Z. T. (1977). A review of coal pillar strength formulas by W. A. Hustrulid. *Rock Mechanics Felsmechanik Mécanique Des Roches*, *10*(1–2). https://doi.org/10.1007/BF01261805

Bieniawski, Z. T. (1978). Determining rock mass deformability: experience from case histories. *International Journal of Rock Mechanics and Mining Sciences And*, *15*(5). https://doi.org/10.1016/0148-9062(78)90956-7

Bieniawski, Z. T. (1984). Rock Mechanics Design in Mining and Tunneling. In *Rock Mech Des in Min and Tunneling*. https://doi.org/10.1016/0148-9062(85)93235-8

Bieniawski, Z. T. (1989). Engineering rock mass classifications: a complete manual for engineers and geologists in mining, civil, and petroleum engineering. *Engineering Rock Mass Classifications: A Complete Manual for Engineers and Geologists in Mining, Civil, and Petroleum Engineering*.

Brady, B. H. G., & Brown, E. T. (2004). *Rock Mechanics for underground mining* (3rd ed.). Springer.

Brown, E. T., & Hoek, E. (1988). Determination of shear failure envelope in rock masses. *Journal of Geotechnical Engineering*, *114*(3), 71–73.

Cahill-Webb, F. (2018). The Implementation of the Paris Agreement on Climate Change: The adoption of the “Pledge and Review” governance approach. *The Implementation of the Paris Agreement on Climate Change*.

Chen, R., & Stimpson, B. (1997). Simulation of deformation and fracturing in potash yield pillars, Vanscoy, Saskatchewan. *Can. Geotech. J.*, *34*, 283–292.

Coal Mining. (2015, July 25). *Images Coal Mining Methods*.

Cui, L., Sheng, Q., Zhang, J., Dong, Y. kou, & Guo, Z. shan. (2022). Evaluation of input geological parameters and tunnel strain for strain-softening rock mass based on GSI. *Scientific Reports*, *12*(1). https://doi.org/10.1038/s41598-022-23587-x

Das, A. J., Mandal, P. K., Ghosh, N., Singh, A. P., Kumar, R., Tewari, S., & Bhattacharjee, R. (2023). Evaluation of energy accumulation, strain burst potential and stability of rock mass during underground extraction of a highly

stressed coal seam under massive strata-a field study. *Engineering Geology*, *322*. https://doi.org/10.1016/j.enggeo.2023.107178

Deshpande, V., Modi, P., & Sant, A. V. (2022). Analysis of Levenberg Marquardt - ANN based reference current generation for control of shunt active power filter. *Materials Today: Proceedings*, *62*(P13), 7104–7108. https://doi.org/10.1016/j.matpr.2022.02.030

Eberhardt, E., Stead, D., & Coggan, J. S. (2004). Numerical analysis of initiation and progressive failure in natural rock slopes—the 1991 Randa rockslide. *International Journal of Rock Mechanics and Mining Sciences*, *41*(1), 69–87. https://doi.org/10.1016/S1365-1609(03)00076-5

Energy Information Administration. (1995). *Longwall Mining*.

Energy Information Administration. (2021). Key World Energy Statistics 2021 – Statistics Report. *IEA Publications*.

Erdogan, H. H., Duzgun, H. S., & Selcuk-Kestel, A. S. (2019). Quantitative hazard assessment for Zonguldak Coal Basin underground mines. *International Journal of Mining Science and Technology*, *29*(3), 453–467. https://doi.org/10.1016/J.IJMST.2018.11.004

Frank, I. C. (2002). Miracle of the miners: The quecreek rescue from an ED perspective. In *Journal of Emergency Nursing* (Vol. 28, Issue 6). https://doi.org/10.1067/men.2002.129927

Frith, R., & Reed, G. (2018). Coal pillar design when considered a reinforcement problem rather than a suspension problem. *International Journal of Mining Science and Technology*, *28*(1), 11–19. https://doi.org/10.1016/J.IJMST.2017.11.013

Frith, R., & Reed, G. (2019). Limitations and potential design risks when applying empirically derived coal pillar strength equations to real-life mine stability

problems. *International Journal of Mining Science and Technology*, *29*(1), 17–25. https://doi.org/10.1016/j.ijmst.2018.11.024

Galvin, J. M. (2016). Ground engineering - principles and practices for underground coal mining. In *Ground Engineering - Principles and Practices for Underground Coal Mining*. https://doi.org/10.1007/978-3-319-25005-2

Ghasemi, E., & Shahriar, K. (2012). A new coal pillars design method in order to enhance safety of the retreat mining in room and pillar mines. *Safety Science*, *50*(3), 579–585. https://doi.org/10.1016/J.SSCI.2011.11.005

Goh, A. T. C., & Zhang, W. (2012). Reliability assessment of stability of underground rock caverns. *International Journal of Rock Mechanics and Mining Sciences*, *55*, 157–163. https://doi.org/10.1016/j.ijrmms.2012.07.012

Griffith, A. A. (1921). The phenomena of rupture and flow in solids. *VI. Philosophical Transactions of the Royal Society of Londo. Series A, Containing Papers of a Mathematical or Physical Character*, *221(582–593)*, 163–198.

Havaej, M., Stead, D., Eberhardt, E., & Fisher, B. R. (2014). Characterization of bi-planar and ploughing failure mechanisms in footwall slopes using numerical modelling. *Engineering Geology*, *178*, 109–120. https://doi.org/10.1016/J.ENGGEO.2014.06.003

Hoek, E., & Brown, E. T. (1997). Practical Estimates of Rock Mass Strength. *Int. J. Rock Mech. Min. Sci*, *34*(8), 1165–1186.

Hoek, E., & Brown, E. T. (2019). The Hoek–Brown failure criterion and GSI – 2018 edition. *Journal of Rock Mechanics and Geotechnical Engineering*, *11*(3), 445–463. https://doi.org/10.1016/j.jrmge.2018.08.001

Hoek, E., Carranza-Torres, C., & Corkum, B. (2002). *Hoek-Brown Failure Criterion-2002 Edition*.

Hoek, E., & Diederichs, M. S. (2006). Empirical estimation of rock mass modulus. *International Journal of Rock Mechanics and Mining Sciences*, *43*(2). https://doi.org/10.1016/j.ijrmms.2005.06.005

Hoek, E., Kaiser, P. K., & Bawden, W. F. (2000). *Support of underground excavations in hard rock* (4th ed.). A.A. Balkema, .

IEA. (2021). Coal 2021. *Coal*.

International Energy Agency, I. (2022). *Coal 2022*. www.iea.org

Ivanova, S., Vesnina, A., Fotina, N., & Prosekov, A. (2022). An Overview of Carbon Footprint of Coal Mining to Curtail Greenhouse Gas Emissions. In *Sustainability (Switzerland)* (Vol. 14, Issue 22). https://doi.org/10.3390/su142215135

Jaiswal, A., & Shrivastva, B. K. (2009). Proposed hybrid method of partial extraction. *Journal of Scientific and Industrial Research*, *68*(4), 307–311.

Javed, S., Satyanarayana Murthy, Y. V. V., Baig, R. U., & Prasada Rao, D. (2015). Development of ANN model for prediction of performance and emission characteristics of hydrogen dual fueled diesel engine with Jatropha Methyl Ester biodiesel blends. *Journal of Natural Gas Science and Engineering*, *26*, 549–557. https://doi.org/10.1016/j.jngse.2015.06.041

Kang, H., Gao, F., Xu, G., & Ren, H. (2023). Mechanical behaviors of coal measures and ground control technologies for China's deep coal mines – A review. *Journal of Rock Mechanics and Geotechnical Engineering*, *15*(1), 37–65. https://doi.org/10.1016/J.JRMGE.2022.11.004

Karacan, C. Ö. (2009). Reconciling longwall gob gas reservoirs and venthole production performances using multiple rate drawdown well test analysis. *International Journal of Coal Geology*, *80*(3–4). https://doi.org/10.1016/j.coal.2009.09.006

Kucuker, H. (2006). Occupational fatalities among coal mine workers in Zonguldak, Turkey, 1994-2003. *Occupational Medicine*, *56*(2). https://doi.org/10.1093/occmed/kqj023

Laginha Serafim, J., & Paulino Pereira, J. (1983). *CONSIDERATIONS ON THE GEOMECHANICAL CLASSIFICATION OF BIENIAWSKI. 1*. https://doi.org/10.1016/0148-9062(84)90053-6

Le, Q. P., & Dao, V. C. (2023). Roof Condition Characteristics Affecting the Stability of Coal Pillars and Retained Roadway. *Environmental Science and Engineering*, 463–477. https://doi.org/10.1007/978-3-031-20463-0_29

Le, T. D., Oh, J., Hebblewhite, B., Zhang, C., & Mitra, R. (2018). A discontinuum modelling approach for investigation of Longwall Top Coal Caving mechanisms. *International Journal of Rock Mechanics and Mining Sciences*, *106*. https://doi.org/10.1016/j.ijrmms.2018.04.025

Li, C., Zhao, Y., & He, Y. (2021). OpenFOAM solver of the methane behaviour near the coal mine tunnelling face and its application. *Journal of Geophysics and Engineering*, *18*(3). https://doi.org/10.1093/jge/gxab027

Li, J. X., Tsang, M., Zhong, R., Esterle, J., Pirona, C., Rajabi, M., & Chen, Z. (2023). Automatic coal mine roof rating calculation using machine learning. *International Journal of Coal Geology*, *274*, 104292. https://doi.org/10.1016/J.COAL.2023.104292

Li, X., & Chai, Y. (2019). Determination of pillar width to improve mining safety in a deep burst-prone coal mine. *Safety Science*, *113*, 244–256. https://doi.org/10.1016/j.ssci.2018.12.003

Liu, S., Yang, K., Zhang, T., & Tang, C. (2020). Rib Spalling 3D Model for Soft Coal Seam Faces with Large Mining Height in Protective Seam Mining: Theoretical and Numerical Analyses. *Geofluids*, *2020*. https://doi.org/10.1155/2020/8828844

Mark, C. (2006). *The evolution of intelligent coal pillar design: 1981–2006.* https://www.researchgate.net/publication/292413023

Mark, C., & Agioutantis, Z. (2019). Analysis of coal pillar stability (ACPS): A new generation of pillar design software. *International Journal of Mining Science and Technology*, *29*(1), 87–91. https://doi.org/10.1016/J.IJMST.2018.11.007

Mark, C., & Chase, F. (1997). *Analysis of Retreat Mining Pillar Stability (ARMPS). Paper in New Technology for Ground Control in Retreat Mining, NIOSH IC 9446*.

Matlab. (2023). *MathWorks*.

McArdle, B. (2016). *An Assessment of Multiple Seam Mine Stress Conditions Using A Numerical Modelling Approach*. The University of Queensland Faculty of Engineering, Architecture and Information Technology.

Ministry of Energy and Natural Resources. (2023). *Energy and Natural Resources*.

Nguyen, V. N., Pham, T. N., Osinski, P., Nguyen, T. C., & Trinh, L. H. (2022). Substantiation of pillar parameters in mining of inclined coal seams in Quang Ninh Province, Vietnam. *Mining Science and Technology (Russian Federation)*, *7*(2). https://doi.org/10.17073/2500-0632-2022-2-93-99

Noraishah Ismail, S., Ramli, A., & Abdul Aziz, H. (2021). Research trends in mining accidents study: A systematic literature review. *Safety Science*, *143*, 105438. https://doi.org/10.1016/J.SSCI.2021.105438

Osgoui, R. R. (2007). *Development of An Elasto-Plastic Analytical Model For Design of Grouted Rock Bolts in Tunnels With Particular Reference to Poor Rock Masses*. Middle East Technical University.

Peng, S. S. (1978). *Coal Mine Ground Control*. John Wiley & Sons, Inc..

Peng, S. S. , & Chiang, H. S. (1984). *Longwall Mining*. John Wiley & Sons.

Pohl, W. L. (2011). Economic Geology Principles and Practice. In *Economic Geology Principles and Practice*. https://doi.org/10.1002/9781444394870

Putri, R. H. K. (2020). Coal Pillar Strength Formula in Indonesian coal mines. *Journal of Earth and Marine Technology (JEMT), 1*(1). https://doi.org/10.31284/j.jemt.2020.v1i1.1147

Ram, S., Waclawik, P., Nemcik, J., Kukutsch, R., Kumar, A., Singh, A. K., & Gong, L. (2022). Mechanical behaviors of deep pillar sandwiched between strong and weak layers. *Journal of Rock Mechanics and Geotechnical Engineering*. https://doi.org/10.1016/j.jrmge.2022.11.006

Read, S. A. L., Richards, L. R., & Perrin, N. D. (1999). Application of the Hoek-Brown failure criterion to New Zealand greywacke rocks. . *In Proceeding of the 9th International Congress on Rock Mechanics* , 655–660.

Salmi, E. F., & Sellers, E. J. (2022). A Rock Engineering System Based Abandoned Mine Instability Assessment Index with Case Studies for Waihi Gold Mine. *Engineering Geology, 310*. https://doi.org/10.1016/j.enggeo.2022.106869

Saroglou, C., Qi, S., Guo, S., & Wu, F. (2019). ARMR, a new classification system for the rating of anisotropic rock masses. *Bulletin of Engineering Geology and the Environment*, *78*(5). https://doi.org/10.1007/s10064-018-1369-4

Shabanimashcool, M., & Li, C. C. (2013). A numerical study of stress changes in barrier pillars and a border area in a longwall coal mine. *International Journal of Coal Geology*, *106*, 39–47. https://doi.org/10.1016/J.COAL.2012.12.008

Shan, P., Sun, H., Lai, X., Dai, J., Gao, J., Yang, P., Li, W., Li, C., & Yan, C. (2022). Numerical Method for Predicting and Evaluating the Stability of Section Coal Pillars in Underground Longwall Mining. *Frontiers in Earth Science, 10*. https://doi.org/10.3389/feart.2022.894118

Sheng, D., Yu, J., Tan, F., Tong, D., Yan, T., & Lv, J. (2022a). Rock mass quality classification based on deep learning: A feasibility study for stacked autoencoders. *Journal of Rock Mechanics and Geotechnical Engineering*. https://doi.org/10.1016/J.JRMGE.2022.08.006

Sheng, D., Yu, J., Tan, F., Tong, D., Yan, T., & Lv, J. (2022b). Rock mass quality classification based on deep learning: A feasibility study for stacked autoencoders. *Journal of Rock Mechanics and Geotechnical Engineering*. https://doi.org/10.1016/J.JRMGE.2022.08.006

Sidorenko, A. A., Sidorenko, S. A., & Ivanov, V. V. (2021). NUMERICAL MODELLING OF MULTIPLE-SEAM COAL MINING AT THE TALDINSKAYA-ZAPADNAYA-2 MINE. *ARPN Journal of Engineering and Applied Sciences*, *16*(5), 568–574.

Simeons, C. (1978). Coal: its Role in Tomorrow's Technology. In *Coal: its Role in Tomorrow's Technology*. William Clowes & Sons Limited. https://doi.org/10.1016/c2013-0-03018-6

Soomro, A. H., & Jilani, M. T. (2020). Application of IoT and Artificial Neural Networks (ANN) for Monitoring of Underground Coal Mines. *International Conference on Information Science and Communication Technology*.

Spada, M., & Burgherr, P. (2016). An aftermath analysis of the 2014 coal mine accident in Soma, Turkey: Use of risk performance indicators based on historical experience. *Accident Analysis & Prevention*, *87*, 134–140. https://doi.org/10.1016/J.AAP.2015.11.020

Stefanko, R. (1983). *Coal Mining Technology Theory and Practice*. New York: Society of Mining Engineers of The American Institute of Mining, Metallurgical, and Petroleum Engineers, Inc.

Sun, Z., Wu, Y., Lu, Z., Feng, Y., Chu, X., & Yi, K. (2020). Stability analysis and derived control measures for rock surrounding a roadway in a lower coal seam

under concentrated stress of a coal pillar. *Shock and Vibration, 2020*. https://doi.org/10.1155/2020/6624983

Tewari, S., Kushwaha, A., Bhattacharjee, R., & Porathur, J. L. (2018). Crown pillar design in highly dipping coal seam. *International Journal of Rock Mechanics and Mining Sciences*, *103*, 12–19. https://doi.org/10.1016/J.IJRMMS.2018.01.012

Van der Merwe, J. N. (2006). *Beyond Coalbrook: what did we really learn? Mining history*. https://doi.org/https://doi.org/10.10520/AJA0038223X_3128

Vlachopoulos, N., & Vazaios, I. (2018). The Numerical Simulation of Hard Rocks for Tunnelling Purposes at Great Depths: A Comparison between the Hybrid FDEM Method and Continuous Techniques. *Advances in Civil Engineering, 2018*. https://doi.org/10.1155/2018/3868716

Waclawik, P., Ptacek, J., Konicek, P., Kukutsch, R., & Nemcik, J. (2016). Stress-state monitoring of coal pillars during room and pillar extraction. *Journal of Sustainable Mining, 15*(2). https://doi.org/10.1016/j.jsm.2016.06.002

Wojtecki, Ł., Iwaszenko, S., Apel, D. B., Bukowska, M., & Makówka, J. (2022). Use of machine learning algorithms to assess the state of rockburst hazard in underground coal mine openings. *Journal of Rock Mechanics and Geotechnical Engineering*, *14*(3), 703–713. https://doi.org/10.1016/J.JRMGE.2021.10.011

Wojtecki, Ł., Iwaszenko, S., Apel, D. B., & Cichy, T. (2021). An attempt to use machine learning algorithms to estimate the rockburst hazard in underground excavations of hard coal mine. *Energies, 14*(21). https://doi.org/10.3390/en14216928

Yardimci, A. G., & Karpuz, C. (2017). Fuzzy Rock Mass Rating: Soft-Computing-Aided preliminary stability analysis of weak rock slopes. In *Handbook of Research on Trends and Digital Advances in Engineering Geology*. https://doi.org/10.4018/978-1-5225-2709-1.ch003

Yılmaz, R., & Koyuncu, D. T. (2020). BİR DÖNÜŞÜMÜN BAŞLANGIÇ HİKÂYESİ: KARA ELMAS VE ENDÜSTRİ DEVRİM. *Trakya Üniversitesi Sosyal Bilimler Dergisi*. https://doi.org/10.26468/trakyasobed.757598

Zhang, W., Zhang, R., Wu, C., Goh, A. T. C., Lacasse, S., Liu, Z., & Liu, H. (2020). State-of-the-art review of soft computing applications in underground excavations. *Geoscience Frontiers*, *11*(4), 1095–1106. https://doi.org/10.1016/J.GSF.2019.12.003

Zhou, Z., Zang, H., Cao, W., Du, X., Chen, L., & Ke, C. (2019). Risk assessment for the cascading failure of underground pillar sections considering interaction between pillars. *International Journal of Rock Mechanics and Mining Sciences*, *124*, 104142. https://doi.org/10.1016/J.IJRMMS.2019.104142

Zhu, C., Wang, L., & Li, S. (2022). The Investigation of Strata Control for Ultrasoft Coal Seam Mining. *Geofluids*, *2022*. https://doi.org/10.1155/2022/8130555

APPENDICES

A. FEM Results for the Center Pillar and Right Pillar When Depth=100 m and k=0.5

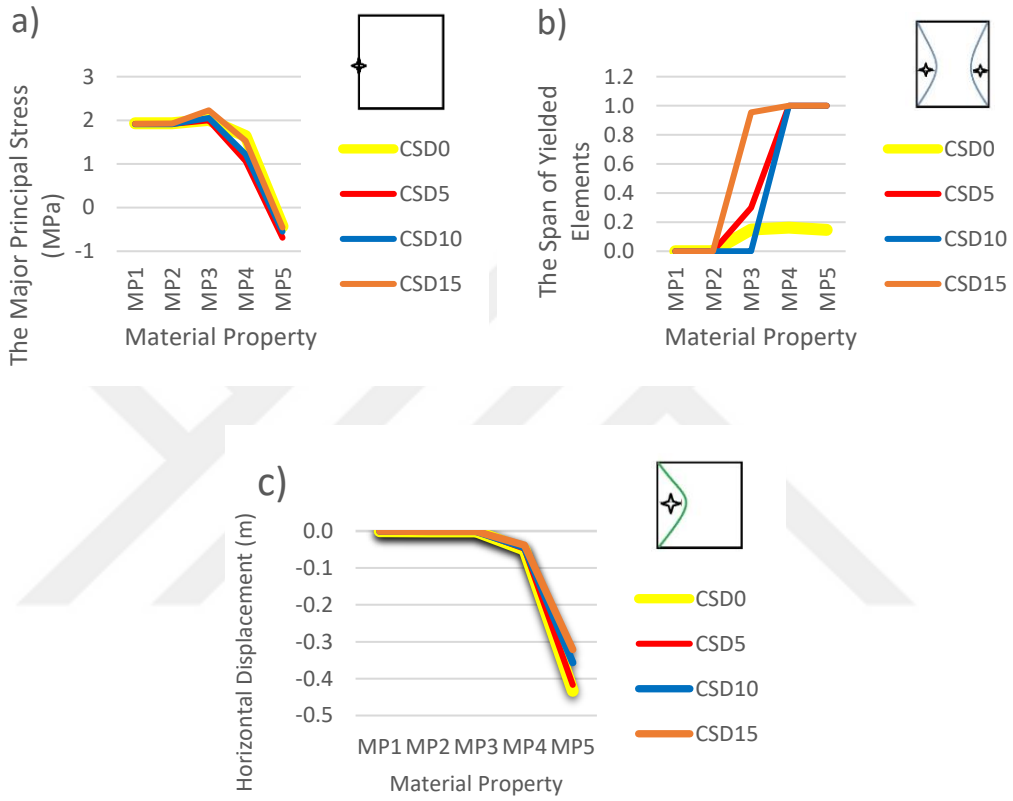

Figure A. 1 a) Major Principal Stress, b) Yielded Span, c) Horizontal Displacement vs. Material Properties for the Center Pillar

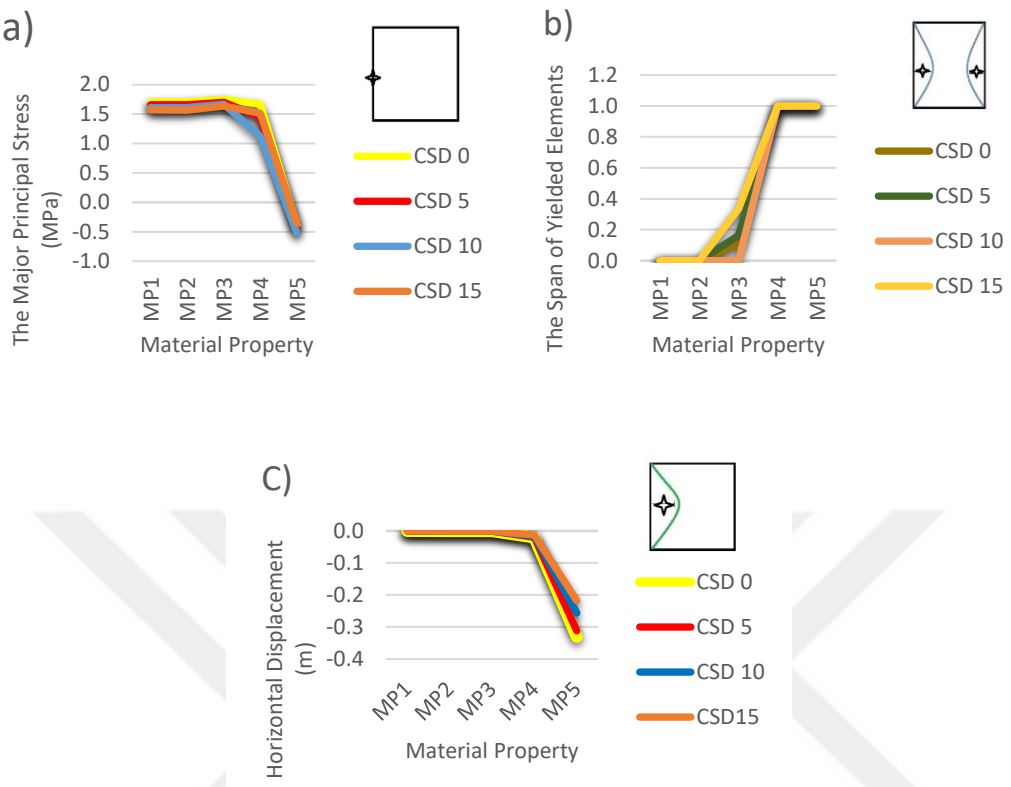

Figure A. 2 a) Major Principal Stress, b) Yielded Span, c) Horizontal Displacement vs. Material Properties for the Right Pillar

B. FEM Results for the Center Pillar, Right Pillar, and Right Abutment When Depth=100 m and k=1

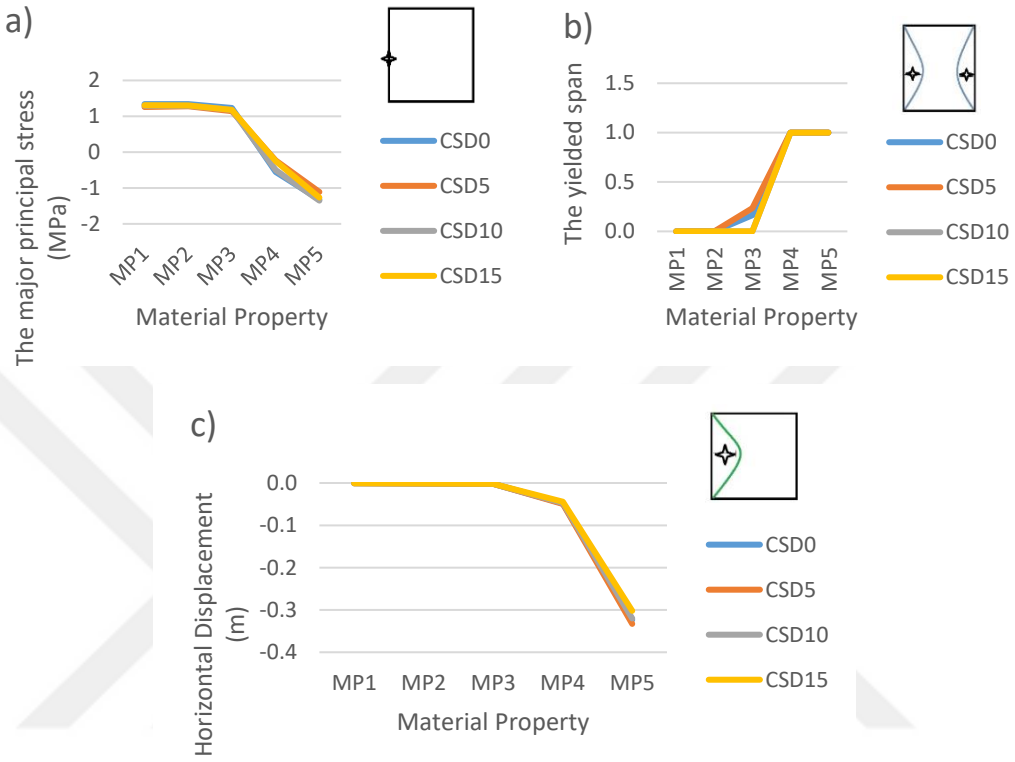

Figure B. 1 a) Major Principal Stress, b) Yielded Span, c) Horizontal Displacement vs. Material Properties for Center Pillar

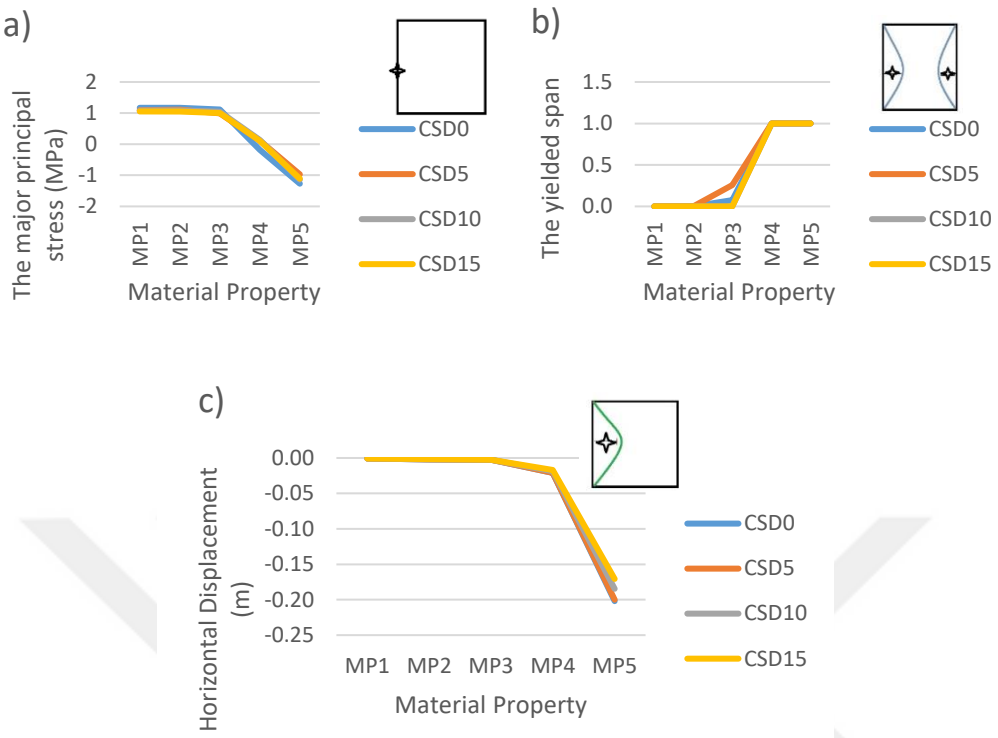

Figure B. 2 a) Major Principal Stress, b) Yielded Span, c) Horizontal Displacement vs. Material Properties for Right Pillar

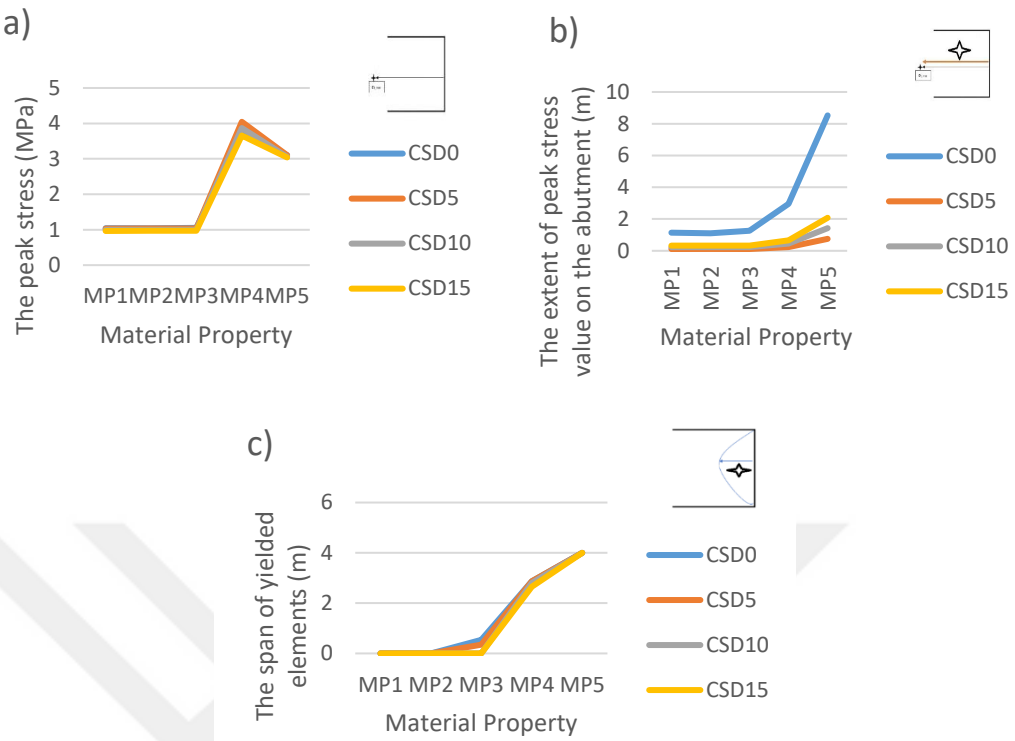

Figure B. 3 a) Peak Stress, b) The Extent of Peak Stress Value on The Abutment, c) The Span of the Yielded Elements vs. Material Properties for Right Abutment

C. FEM Results for the Center Pillar, Right Pillar, and Right Abutment When Depth=100 m and k=1.5

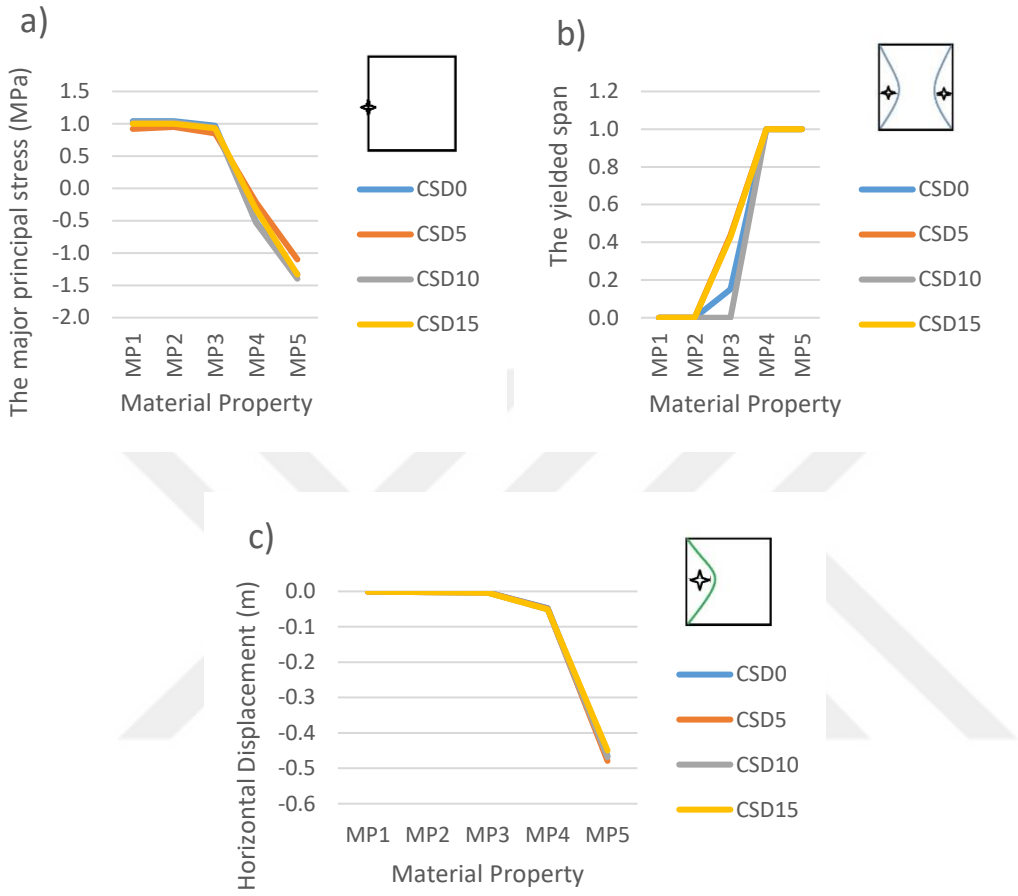

Figure C. 1 a) Major Principal Stress, b) Yielded Span, c) Horizontal Displacement vs. Material Properties for Center Pillar

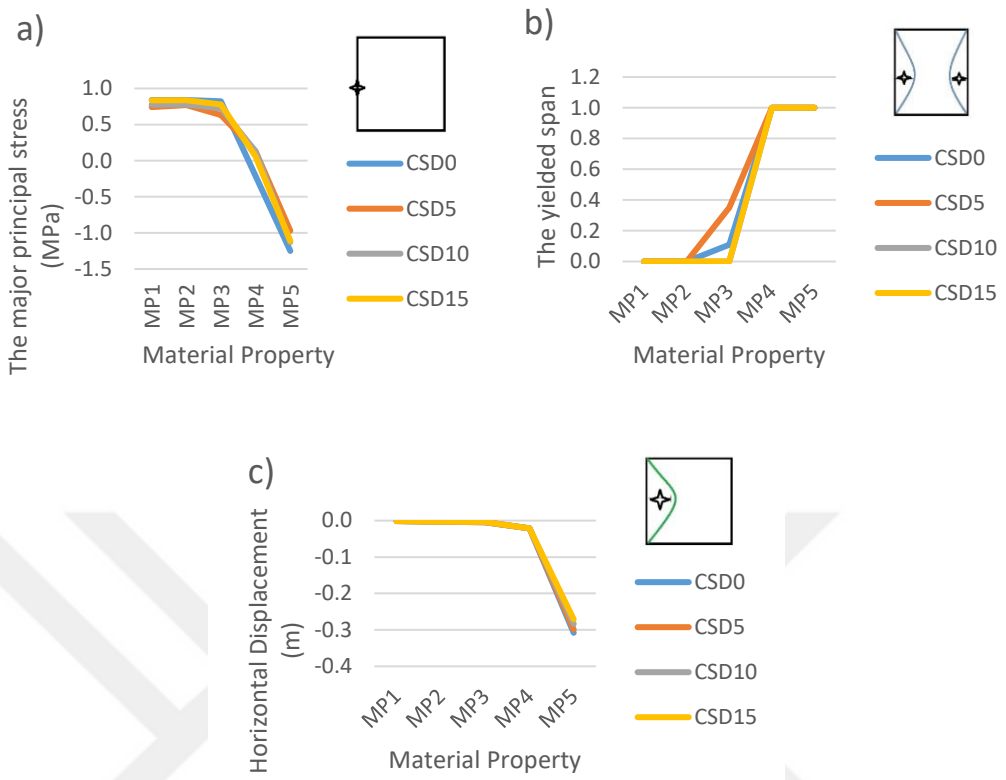

Figure C. 2 a) Major Principal Stress, b) Yielded Span, c) Horizontal Displacement vs. Material Properties for Right Pillar

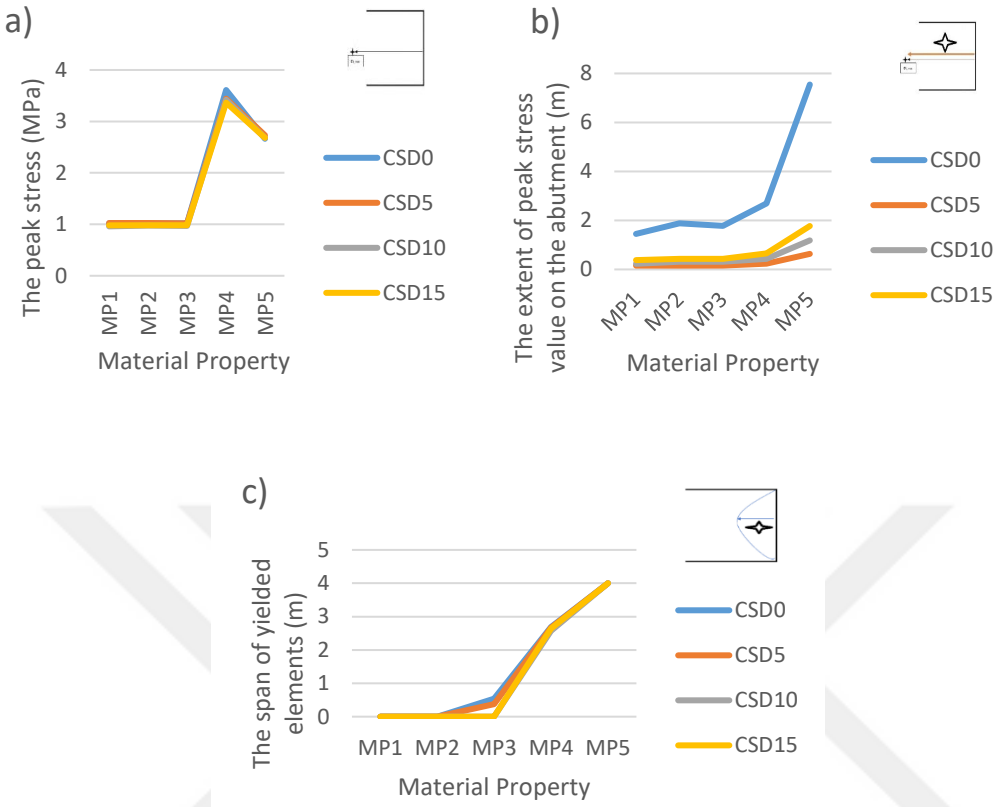

Figure C. 3 a) Peak Stress, b) The Extent of Peak Stress Value on The Abutment, c) The Span of the Yielded Elements vs. Material Properties for Right Abutment

D. FEM Results for the Left, Center, and Right Pillar, and Left and Right Abutment When Depth=200 m and k=1

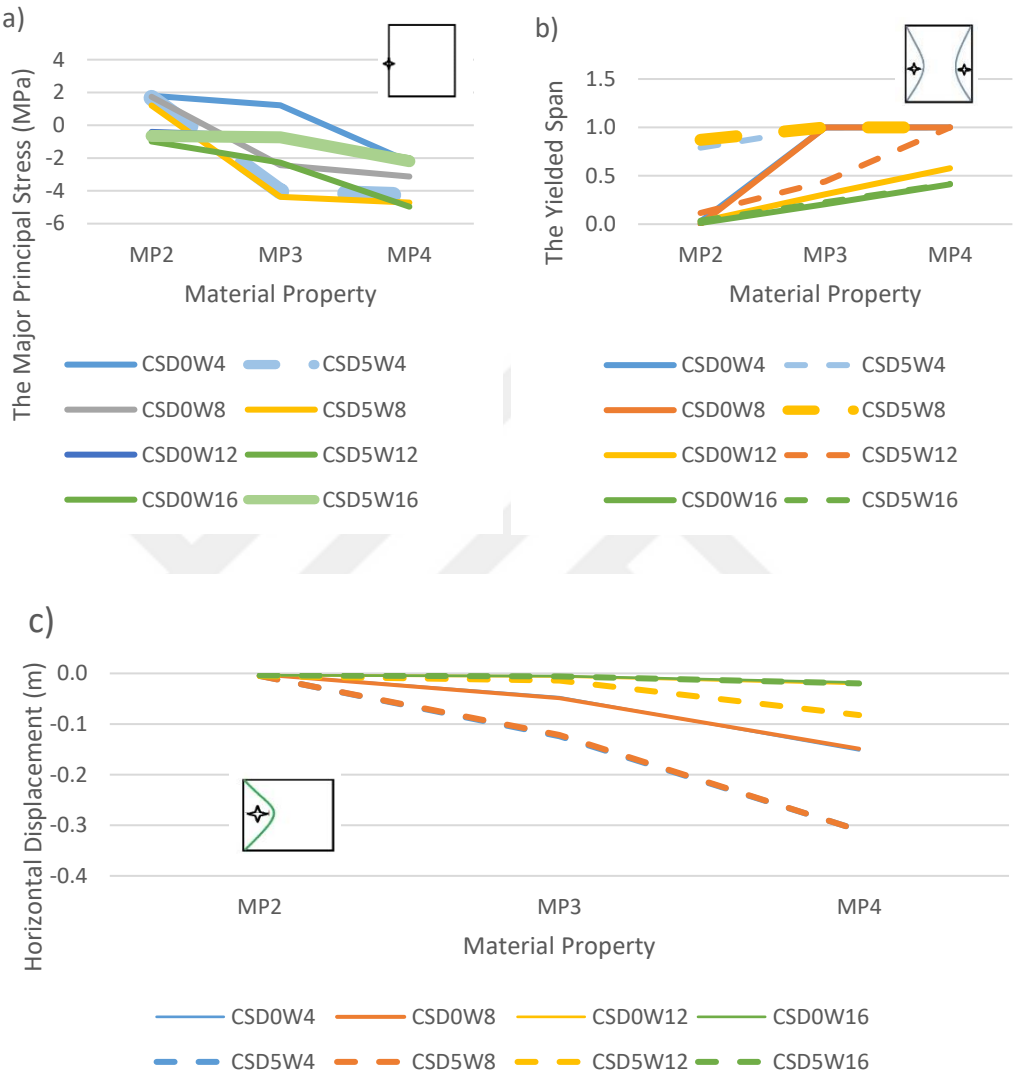

Figure D. 1 a) Major Principal Stress, b) Yielded Span, c) Horizontal Displacement vs. Material Properties for Left Pillar

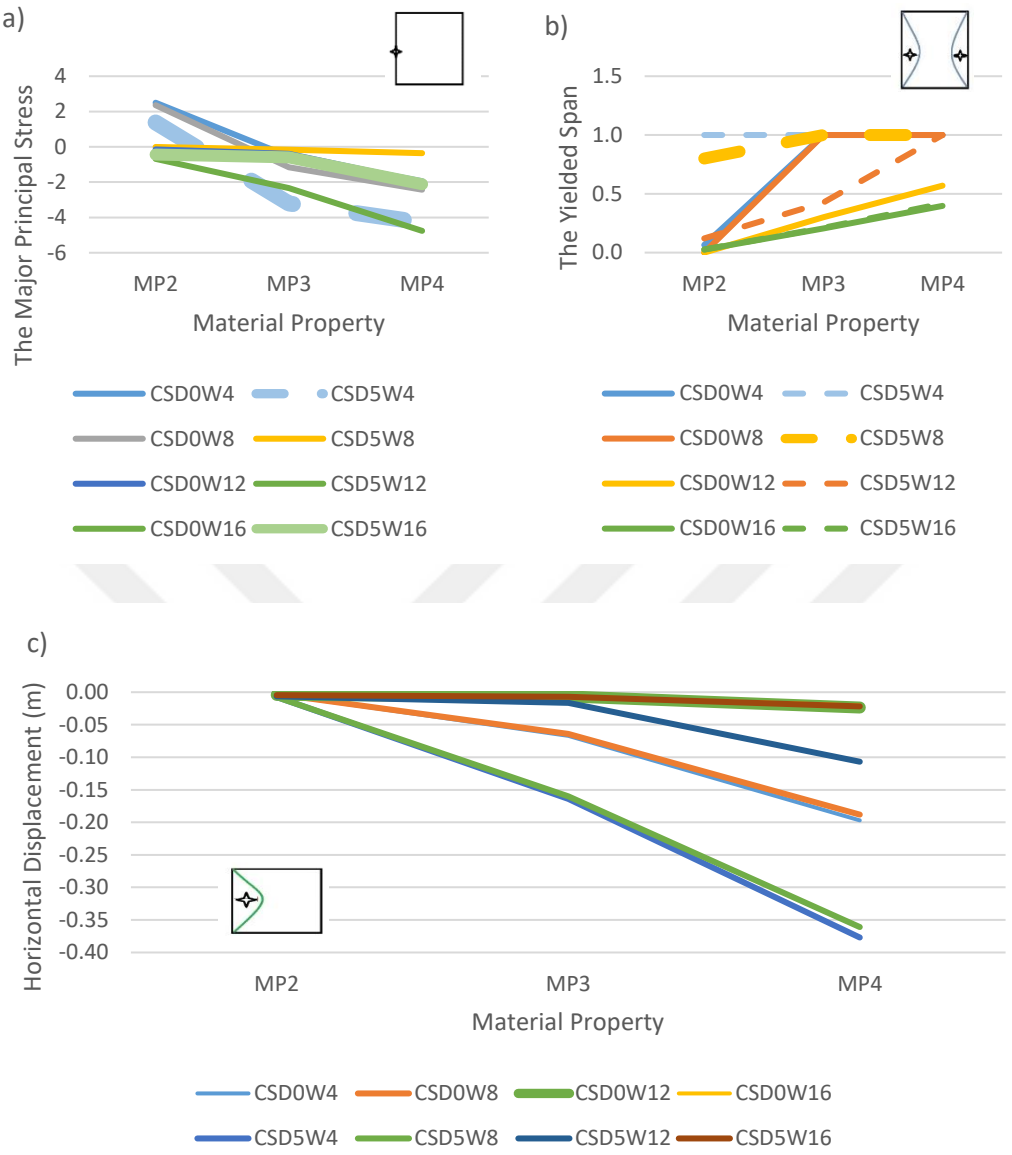

Figure D. 2 a) Major Principal Stress, b) Yielded Span, c) Horizontal Displacement vs. Material Properties for Center Pillar

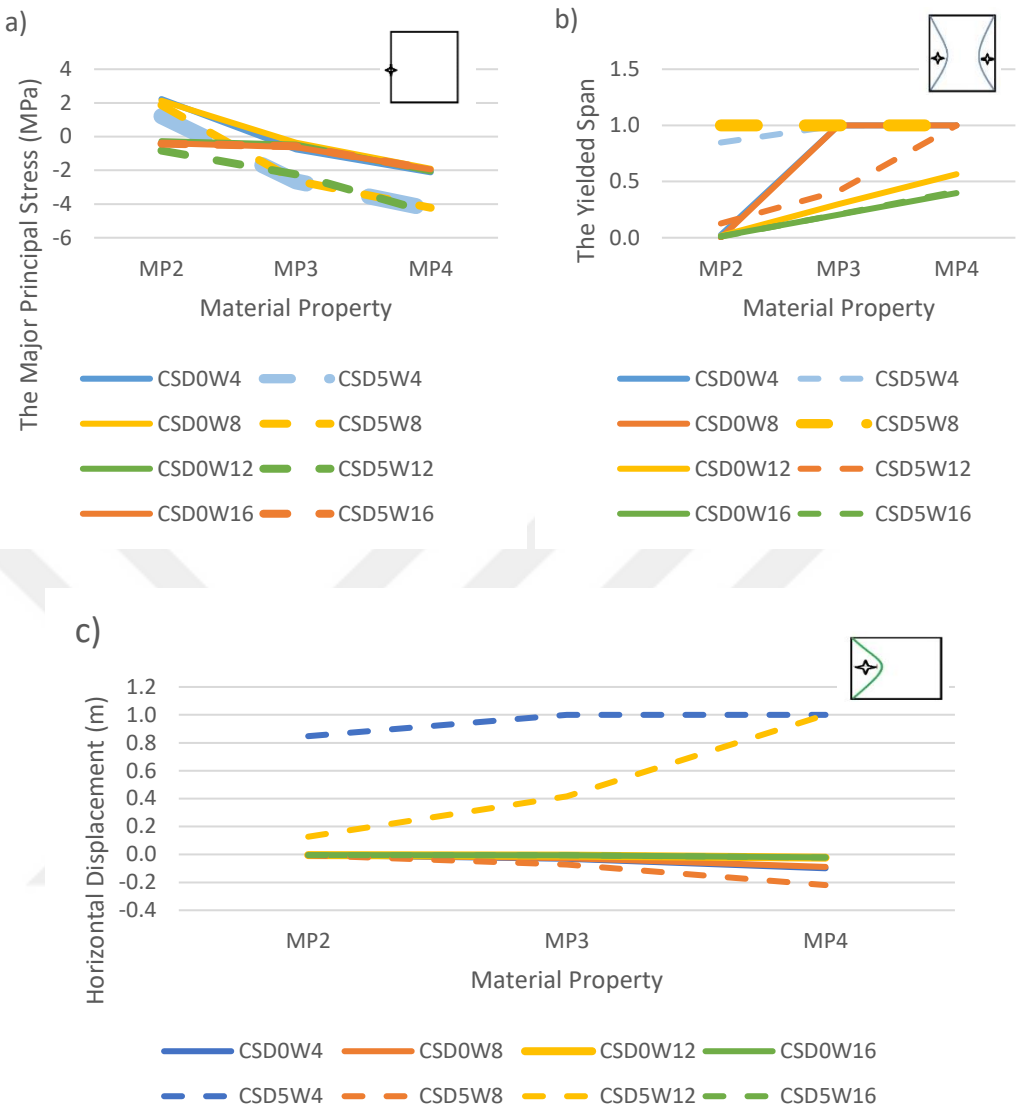

Figure D. 3 a) Major Principal Stress, b) Yielded Span, c) Horizontal Displacement vs. Material Properties for Right Pillar

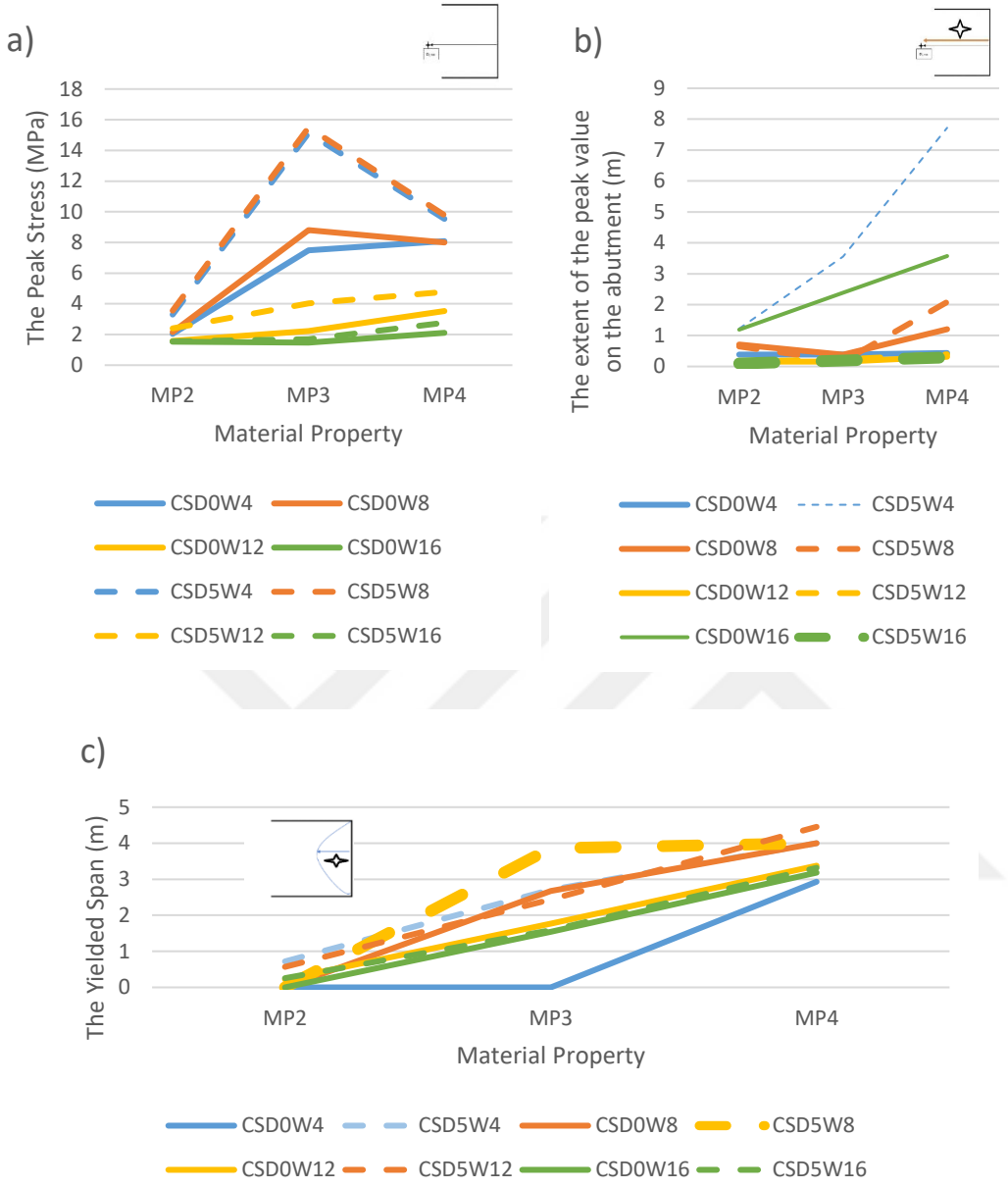

Figure D. 4 a) Peak Stress, b) The Extent of Peak Stress Value on The Abutment, c) The Span of the Yielded Elements vs. Material Properties for Left Abutment

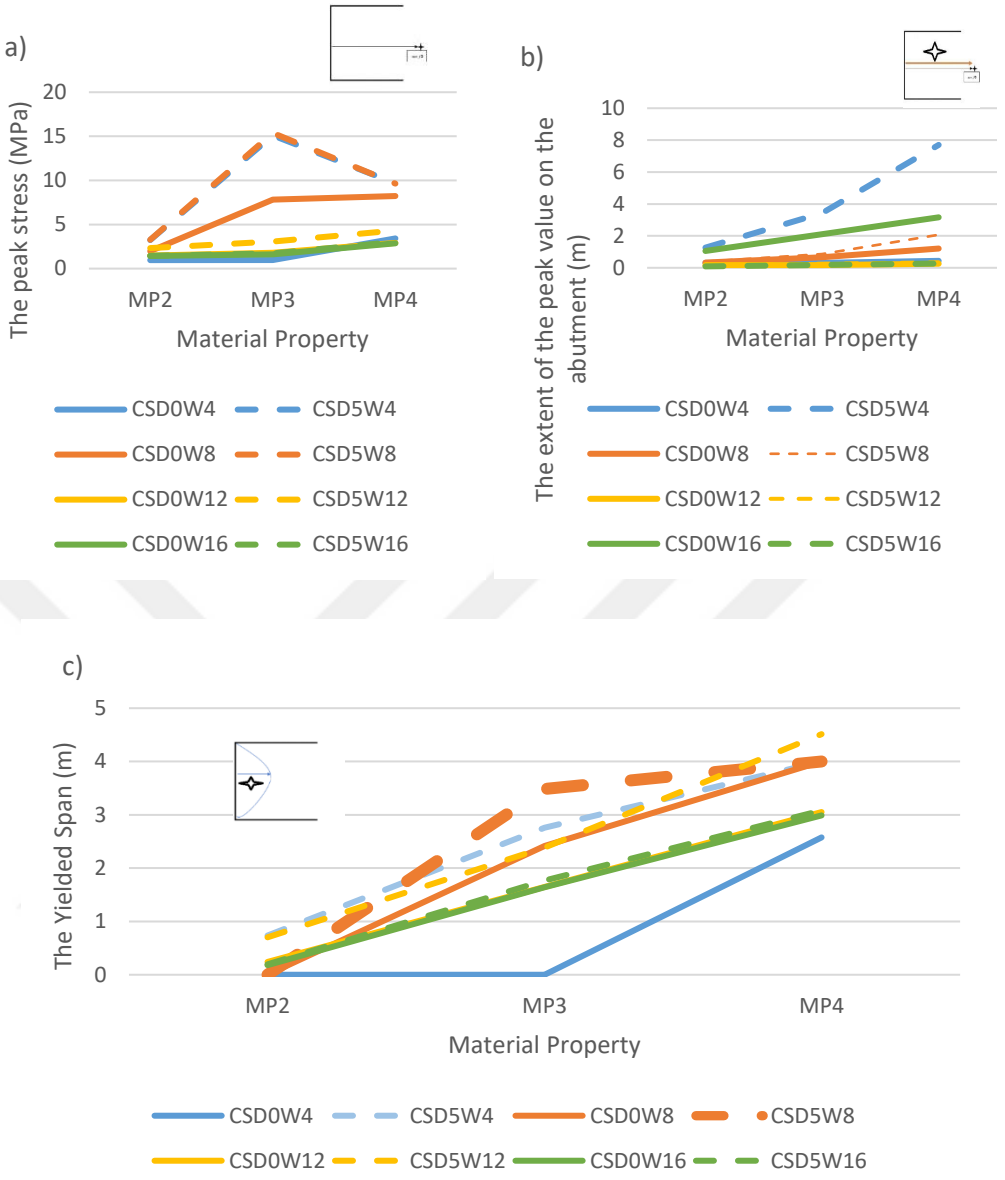

Figure D. 5 a) Peak Stress, b) The Extent of Peak Stress Value on The Abutment, c) The Span of the Yielded Elements vs. Material Properties for Right Abutment

E. FEM Results for the Left, Center, and Right Pillar, and Left and Right Abutment When Depth=300 m and k=1

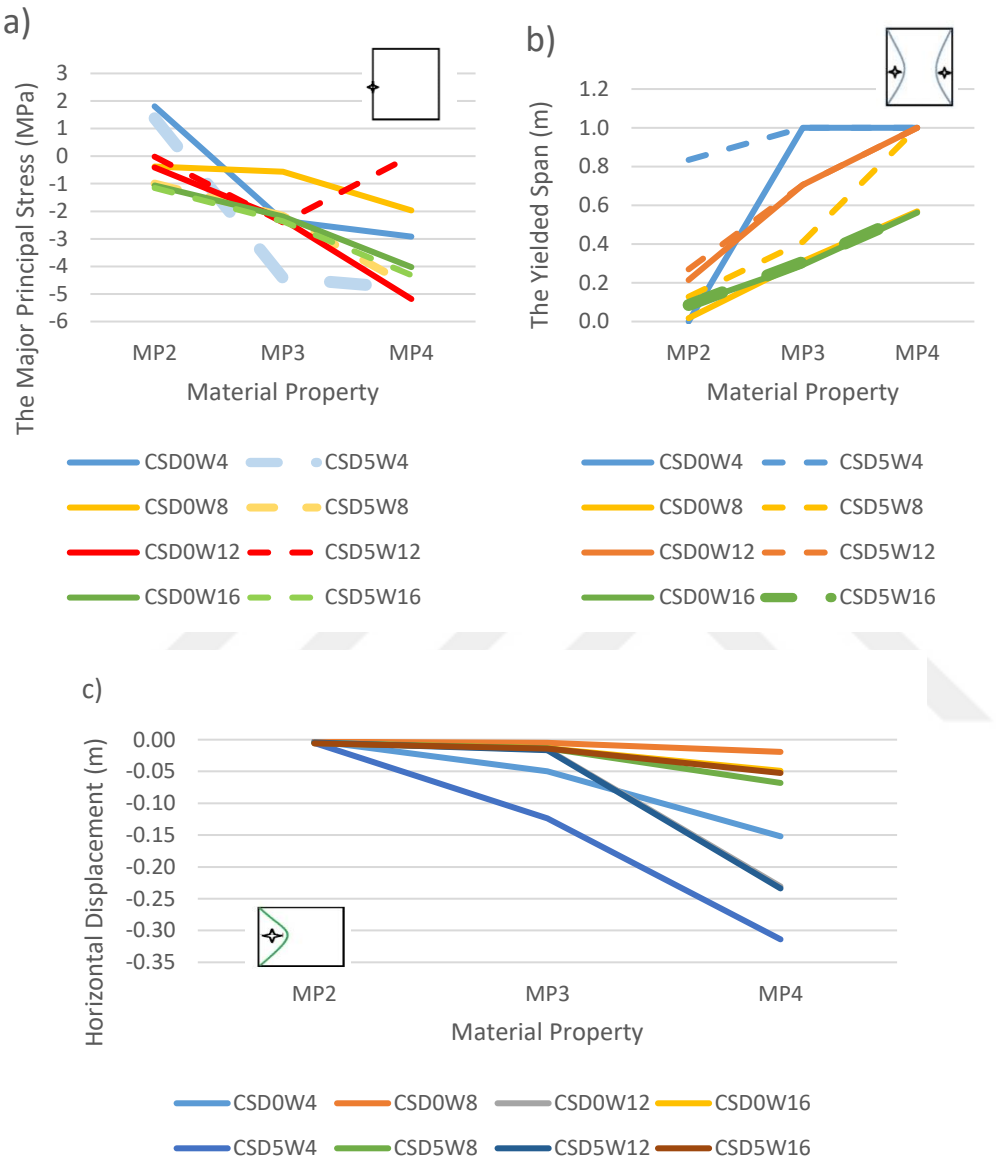

Figure E. 1 a) Major Principal Stress, b) Yielded Span, c) Horizontal Displacement vs. Material Properties for Left Pillar

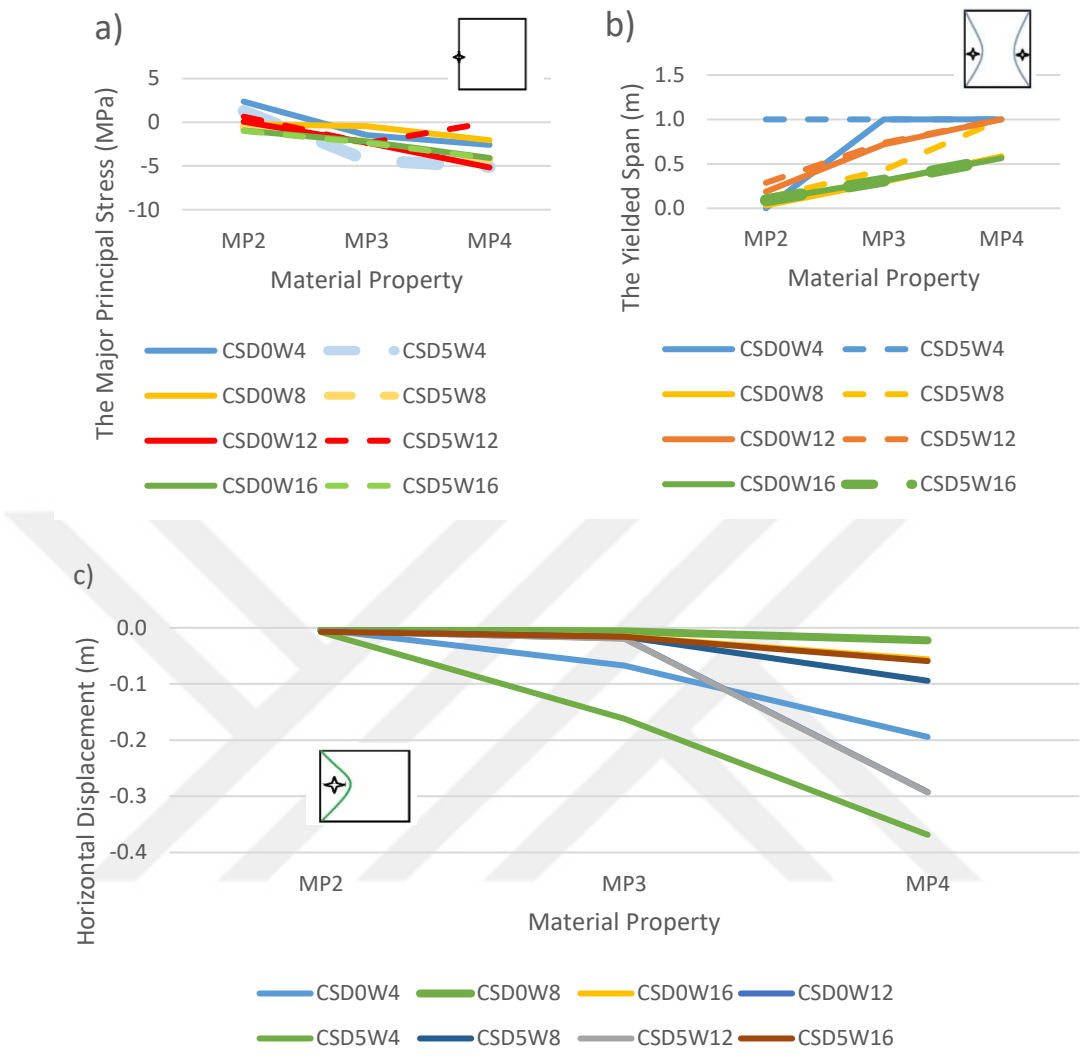

Figure E. 2 a) Major Principal Stress, b) Yielded Span, c) Horizontal Displacement vs. Material Properties for Center Pillar

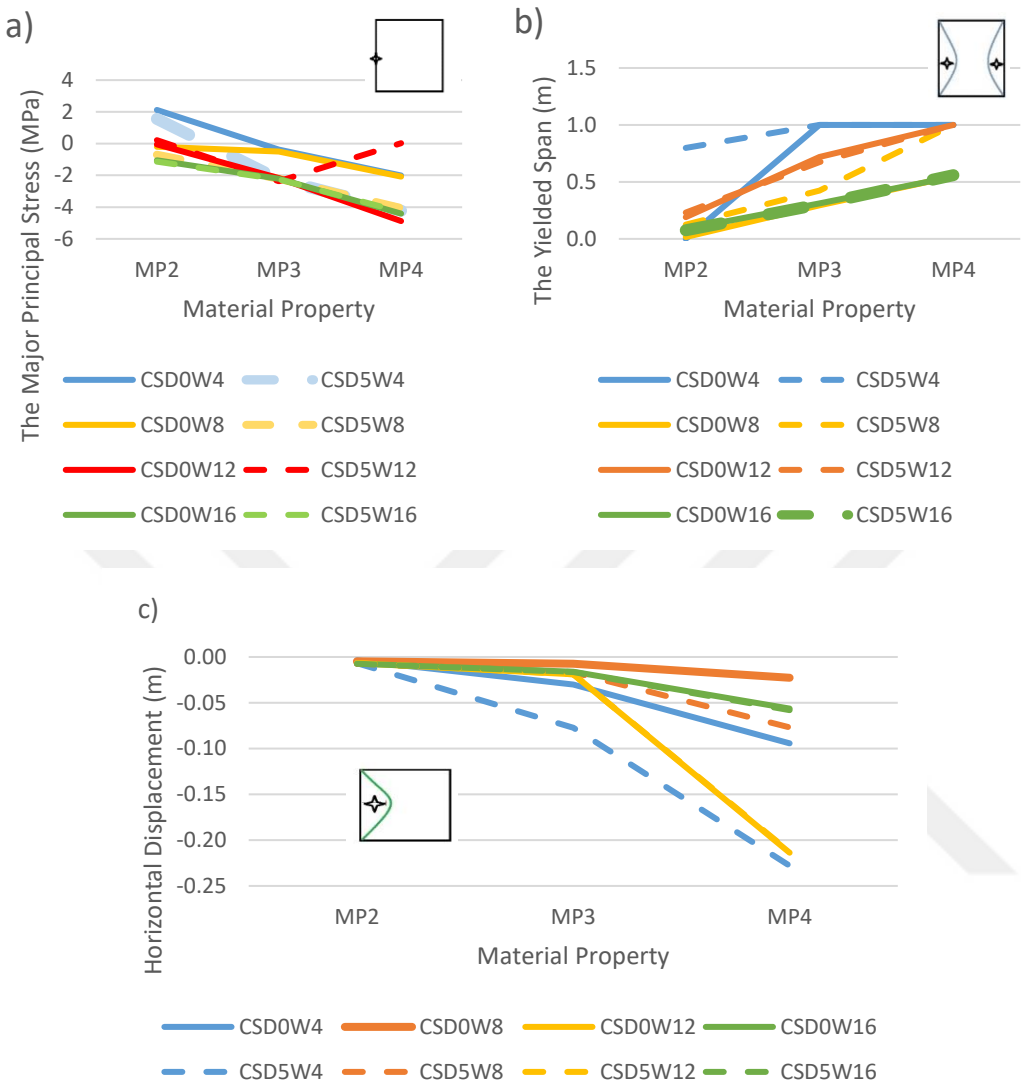

Figure E. 3 a) Major Principal Stress, b) Yielded Span, c) Horizontal Displacement vs. Material Properties for Right Pillar

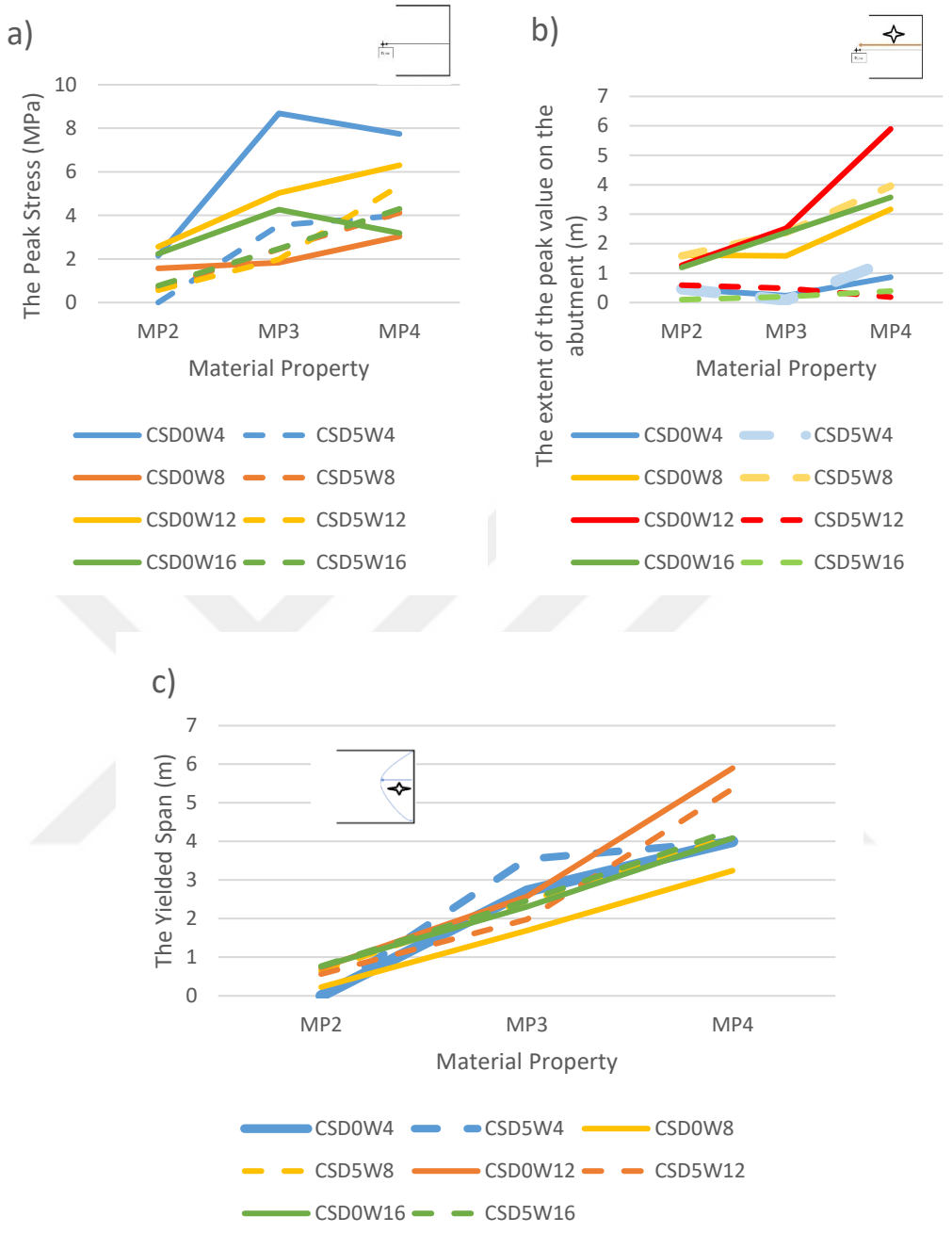

Figure E. 4 a) Peak Stress, b) The Extent of Peak Stress Value on The Abutment, c) The Span of the Yielded Elements vs. Material Properties for Left Abutment

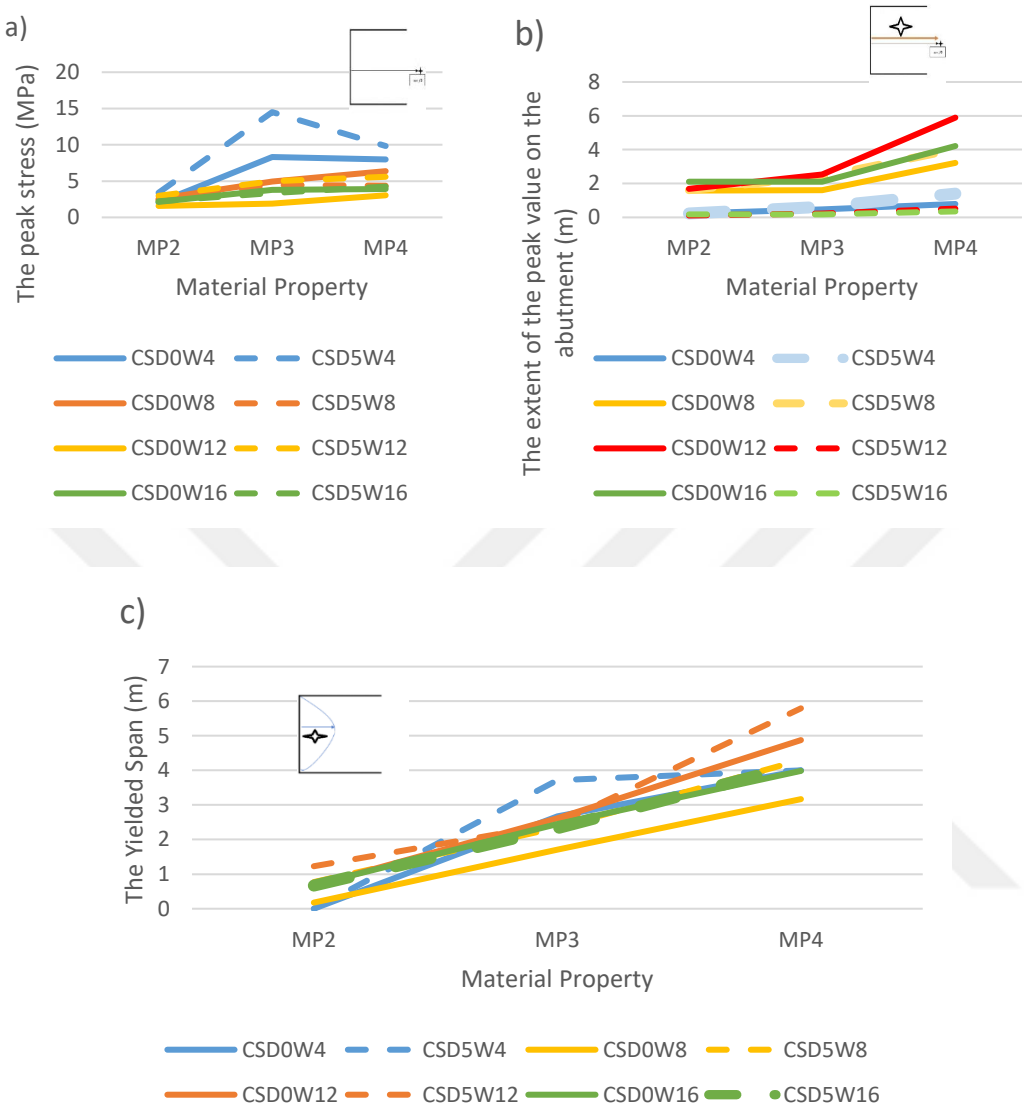

Figure E. 5 a) Peak Stress, b) The Extent of Peak Stress Value on The Abutment, c) The Span of the Yielded Elements vs. Material Properties for Right Abutment

F. FEM Results for the Left, Center, and Right Pillar, and Left and Right Abutment When Depth=400 m and k=0.5

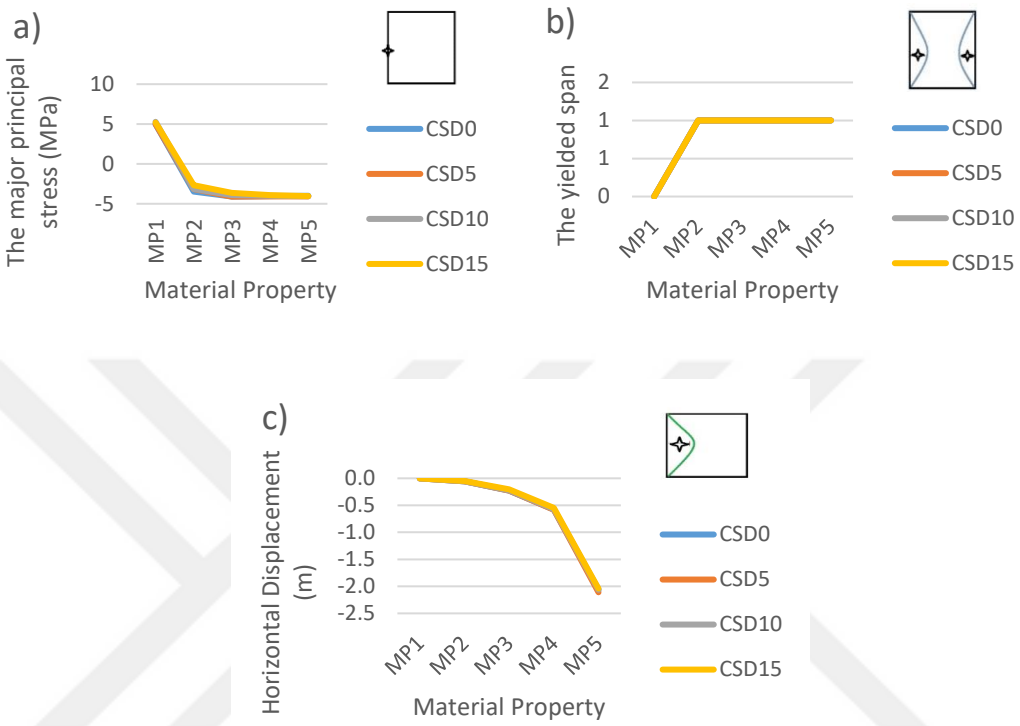

Figure F. 1 a) Major Principal Stress, b) Yielded Span, c) Horizontal Displacement vs. Material Properties for Left Pillar

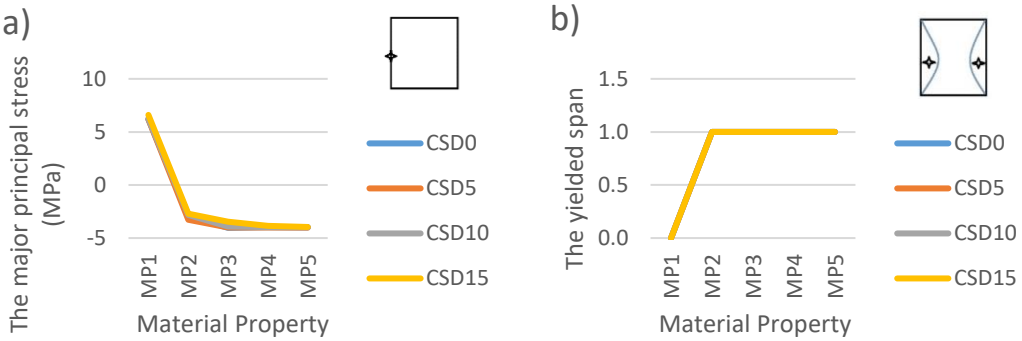

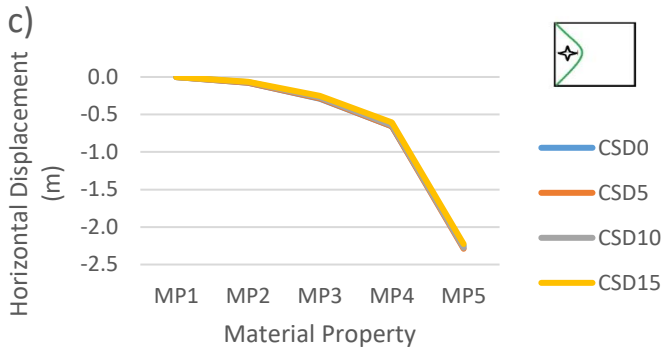

Figure F. 2 a) Major Principal Stress, b) Yielded Span, c) Horizontal Displacement vs. Material Properties for Center Pillar

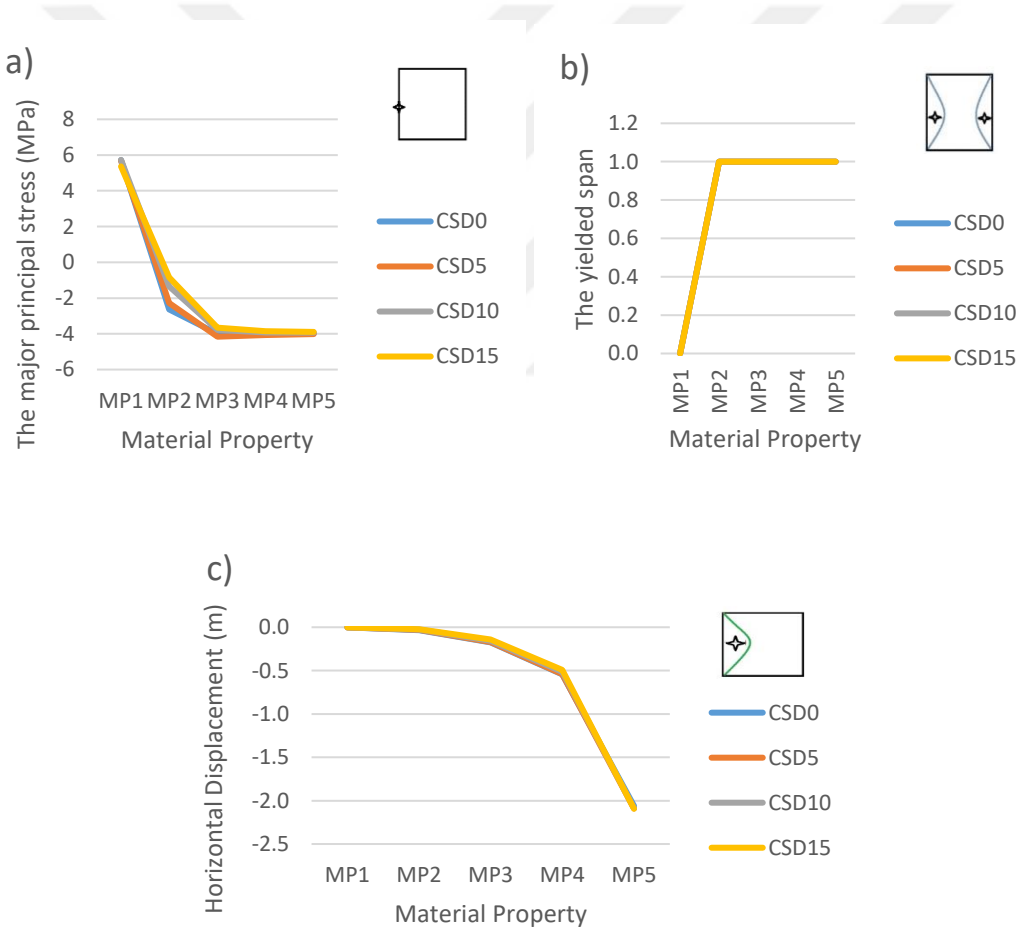

Figure F. 3 a) Major Principal Stress, b) Yielded Span, c) Horizontal Displacement vs. Material Properties for Right Pillar

Figure F. 4 a) Peak Stress, b) The Extent of Peak Stress Value on The Abutment, c) The Span of the Yielded Elements vs. Material Properties for Left Abutment

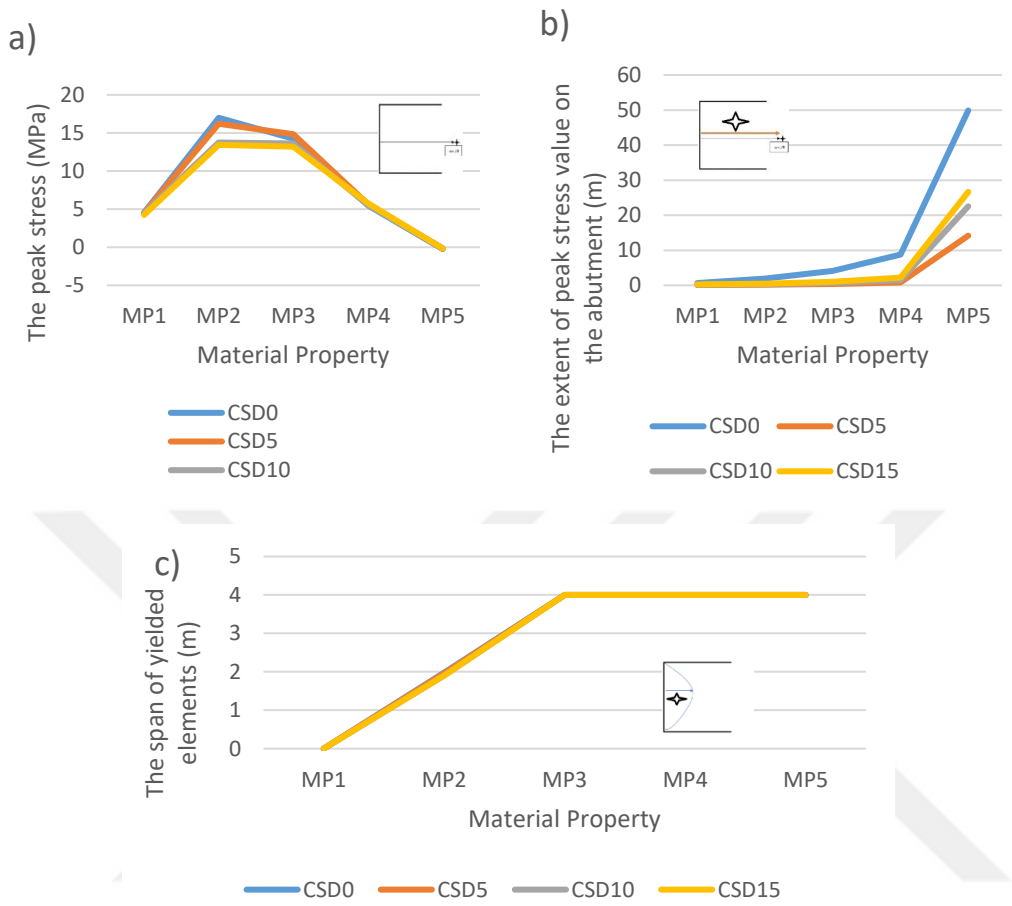

Figure F. 5 a) Peak Stress, b) The Extent of Peak Stress Value on The Abutment, c) The Span of the Yielded Elements vs. Material Properties for Right Abutment

G. FEM Results for the Left, Center, and Right Pillar, and Left and Right Abutment When Depth=400 m and k=1

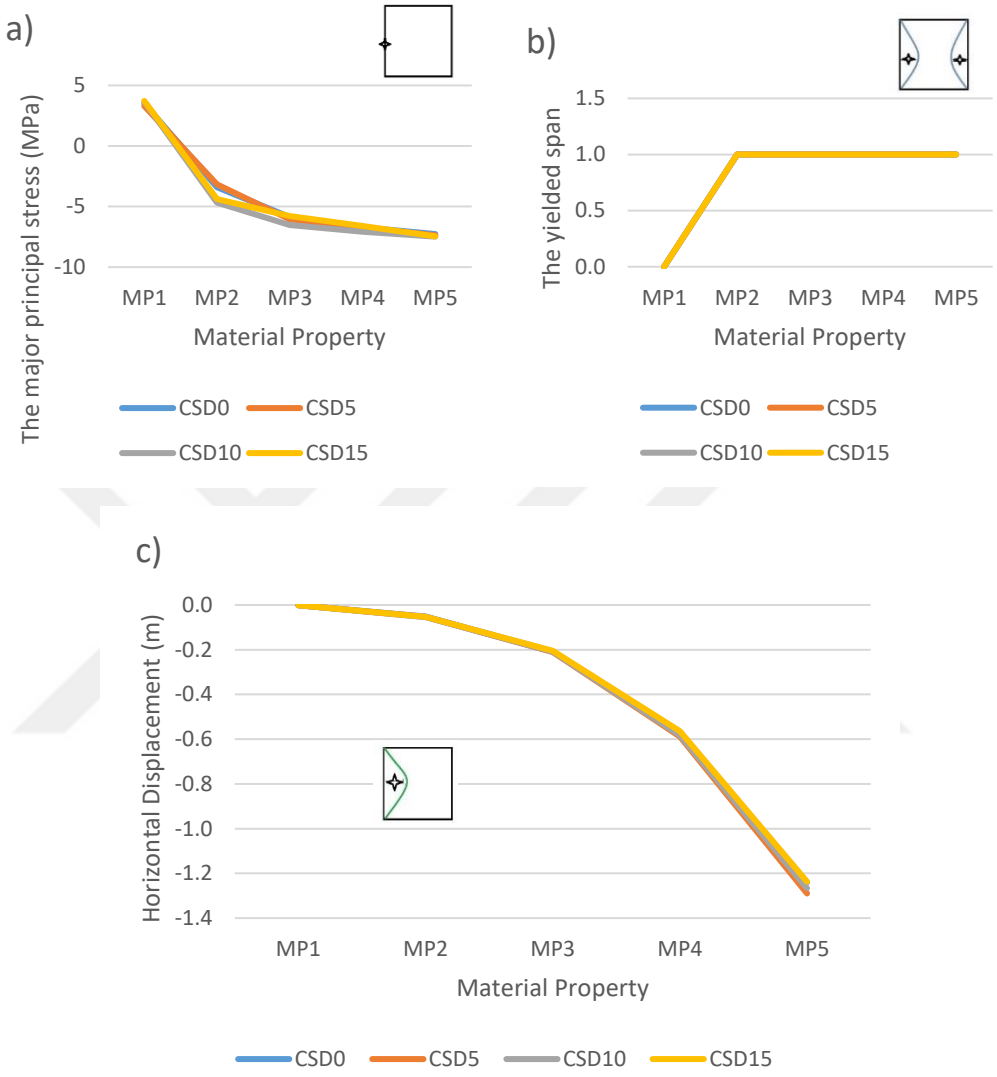

Figure G. 1 a) Major Principal Stress, b) Yielded Span, c) Horizontal Displacement vs. Material Properties for Left Pillar

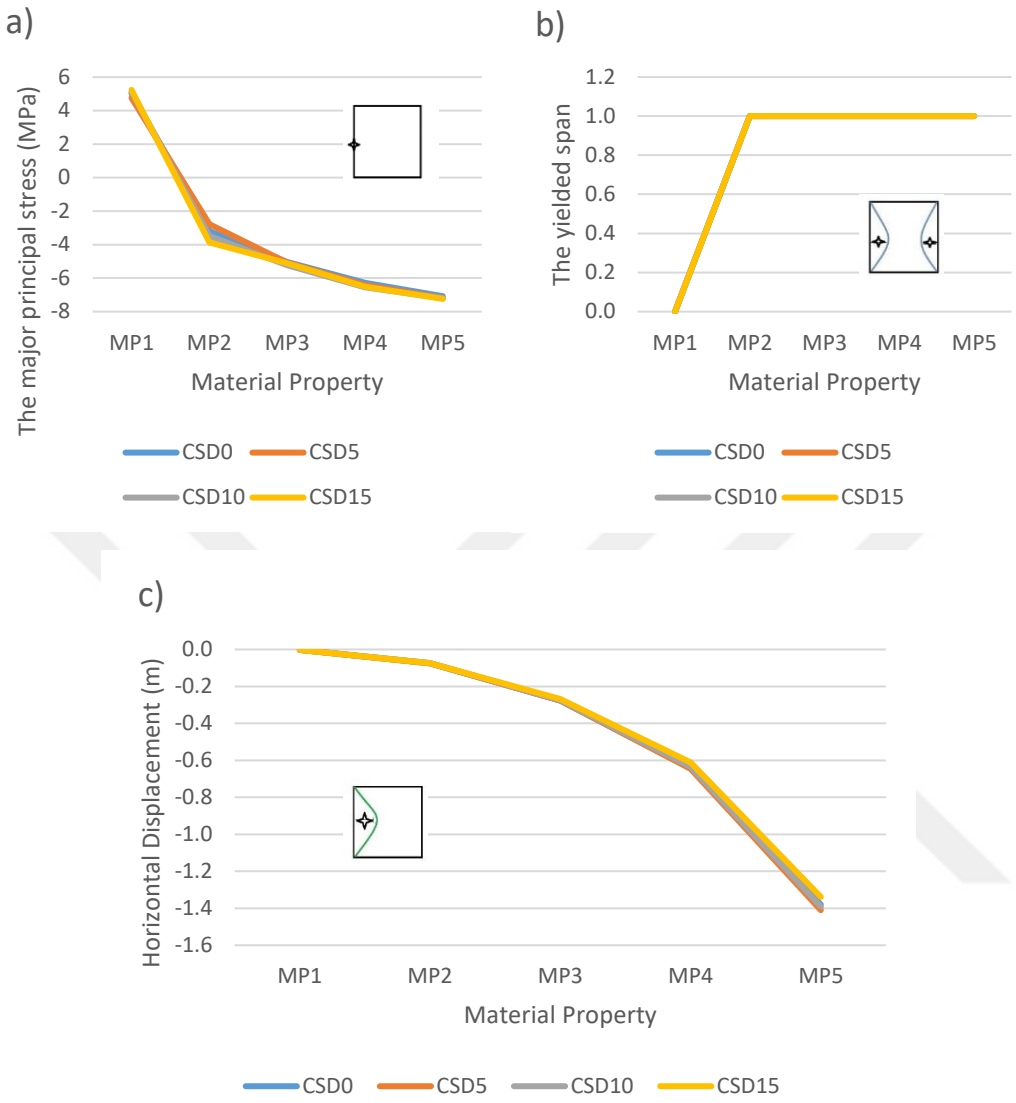

Figure G. 2 a) Major Principal Stress, b) Yielded Span, c) Horizontal Displacement vs. Material Properties for Center Pillar

Figure G. 3 a) Major Principal Stress, b) Yielded Span, c) Horizontal Displacement vs. Material Properties for Right Pillar

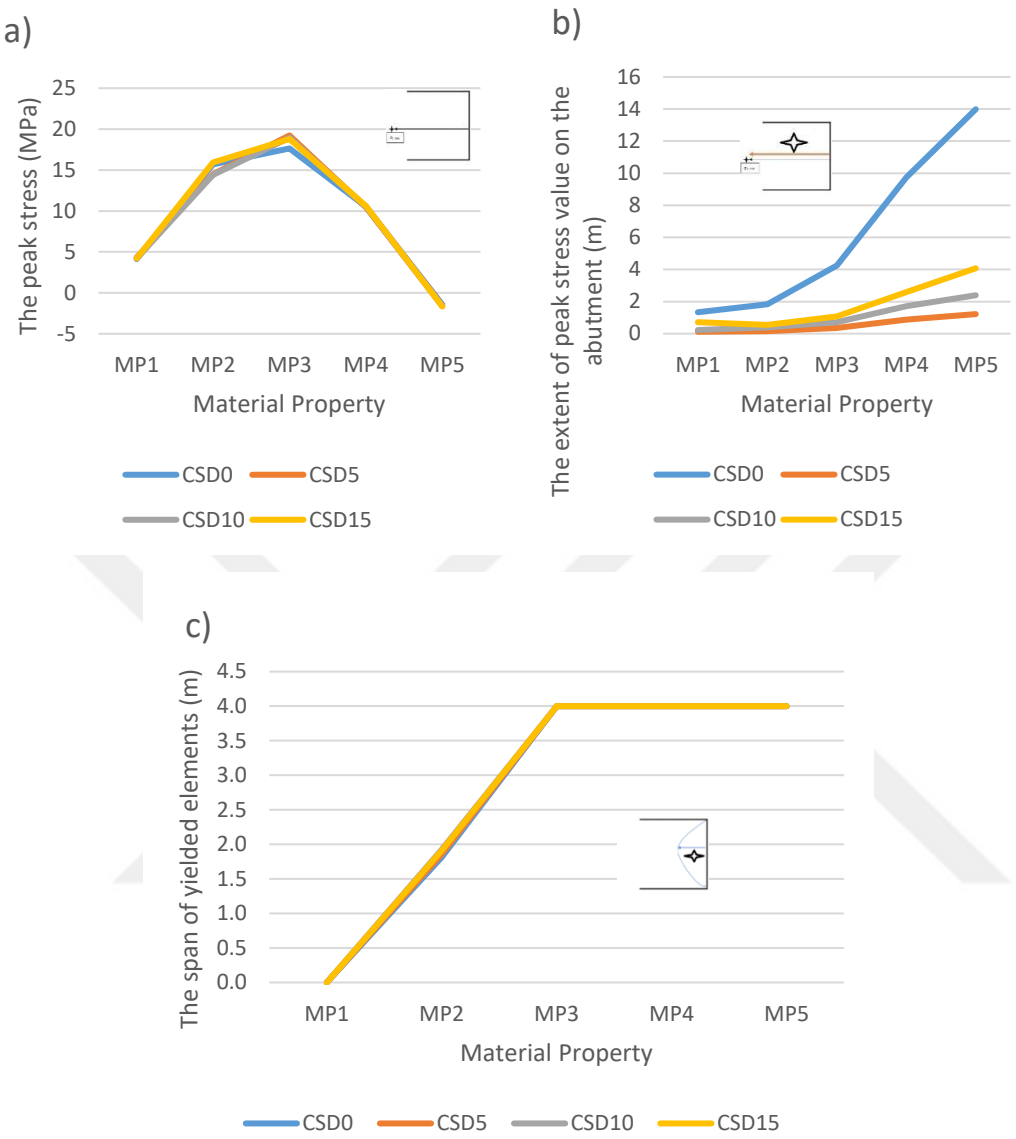

Figure G. 4 a) Peak Stress, b) The Extent of Peak Stress Value on The Abutment, c) The Span of the Yielded Elements vs. Material Properties for Left Abutment

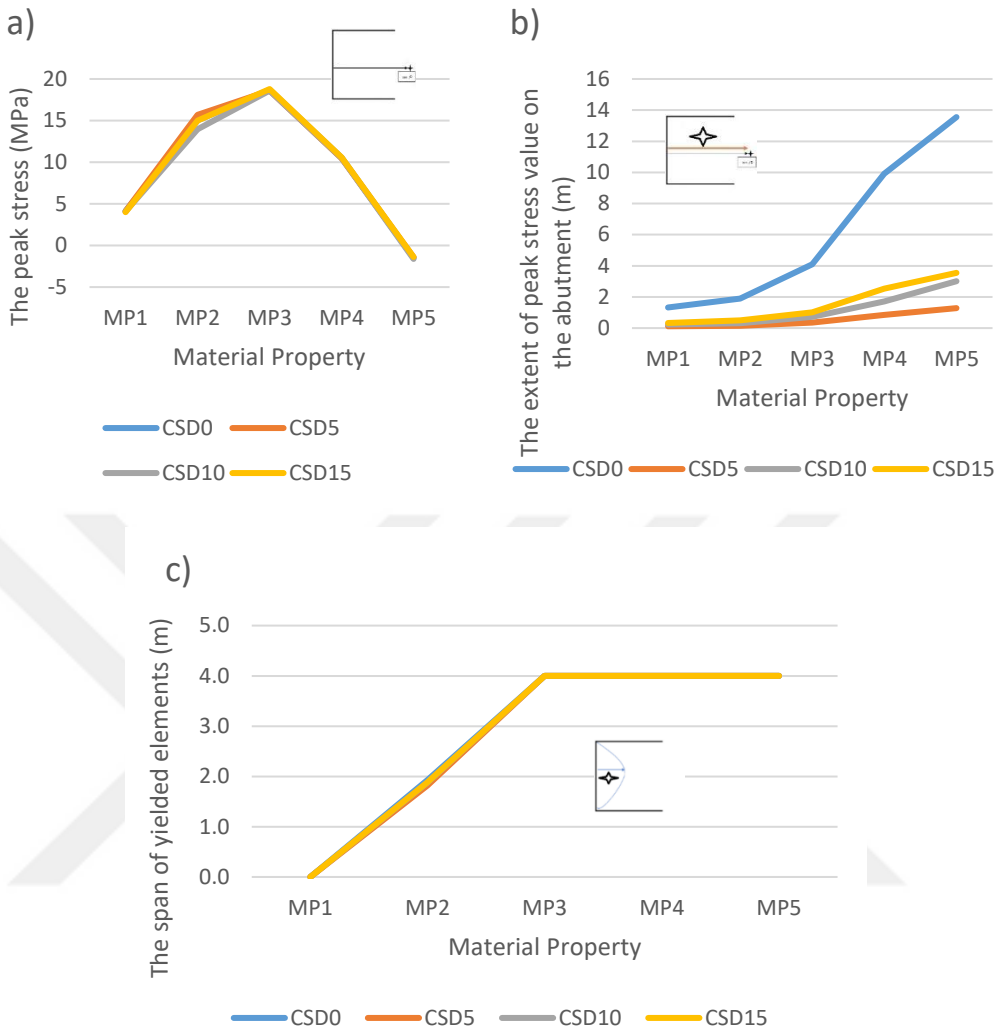

Figure G. 5 a) Peak Stress, b) The Extent of Peak Stress Value on The Abutment, c) The Span of the Yielded Elements vs. Material Properties for Right Abutment

H. FEM Results for the Left, Center, and Right Pillar, and Left and Right Abutment When Depth=400 m and k=1.5

Figure H. 1 a) Major Principal Stress, b) Yielded Span, c) Horizontal Displacement vs. Material Properties for Left Pillar

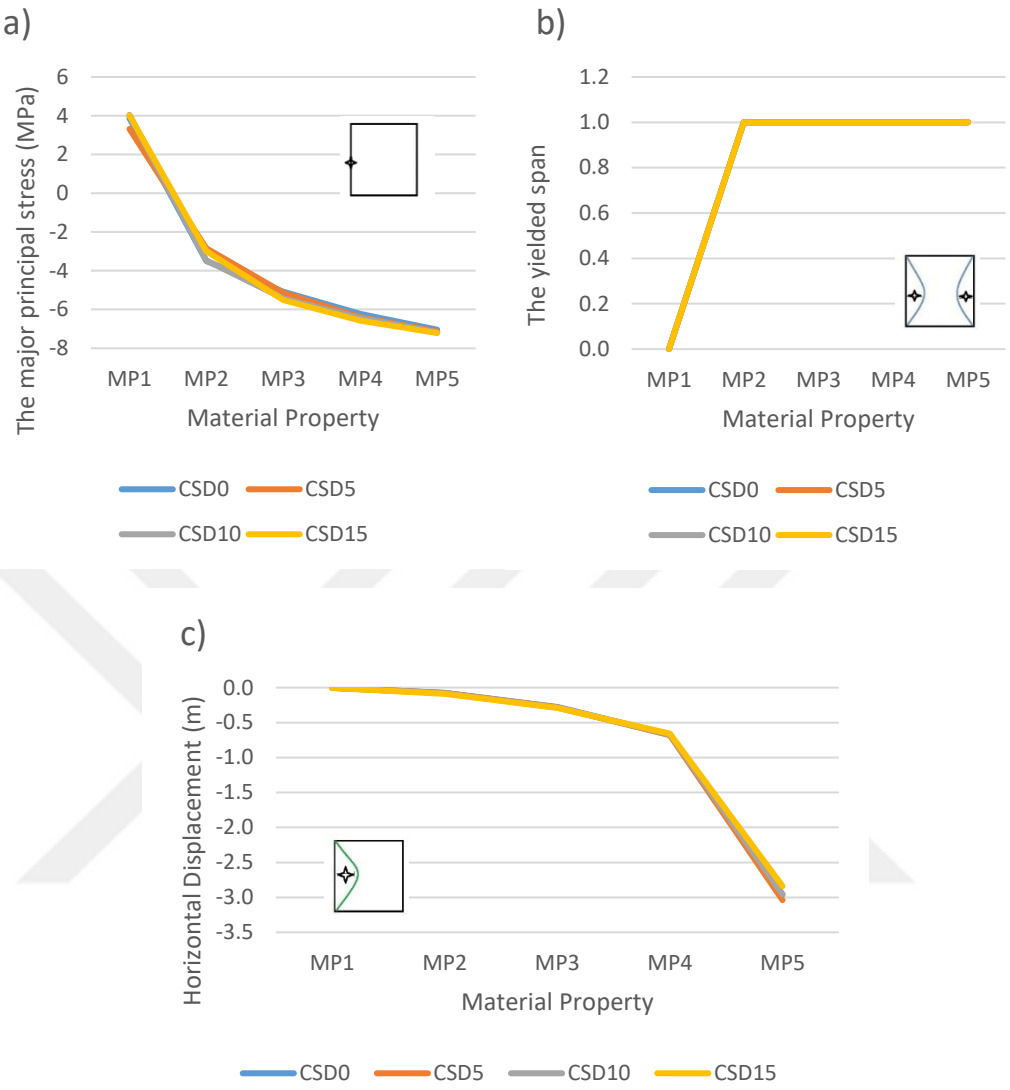

Figure H. 2 a) Major Principal Stress, b) Yielded Span, c) Horizontal Displacement vs. Material Properties for Center Pillar

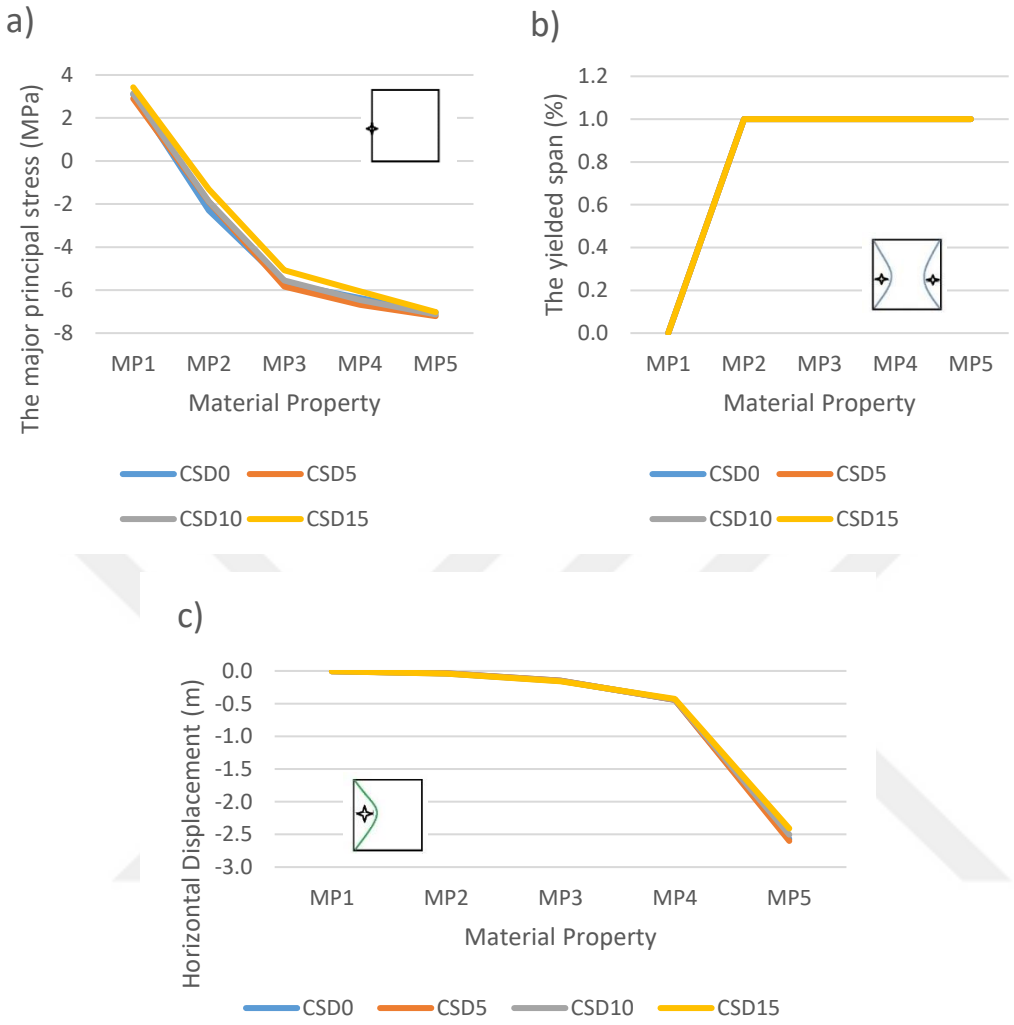

Figure H. 3 a) Major Principal Stress, b) Yielded Span, c) Horizontal Displacement vs. Material Properties for Right Pillar

Figure H. 4 a) Peak Stress, b) The Extent of Peak Stress Value on The Abutment, c) The Span of the Yielded Elements vs. Material Properties for Left Abutment

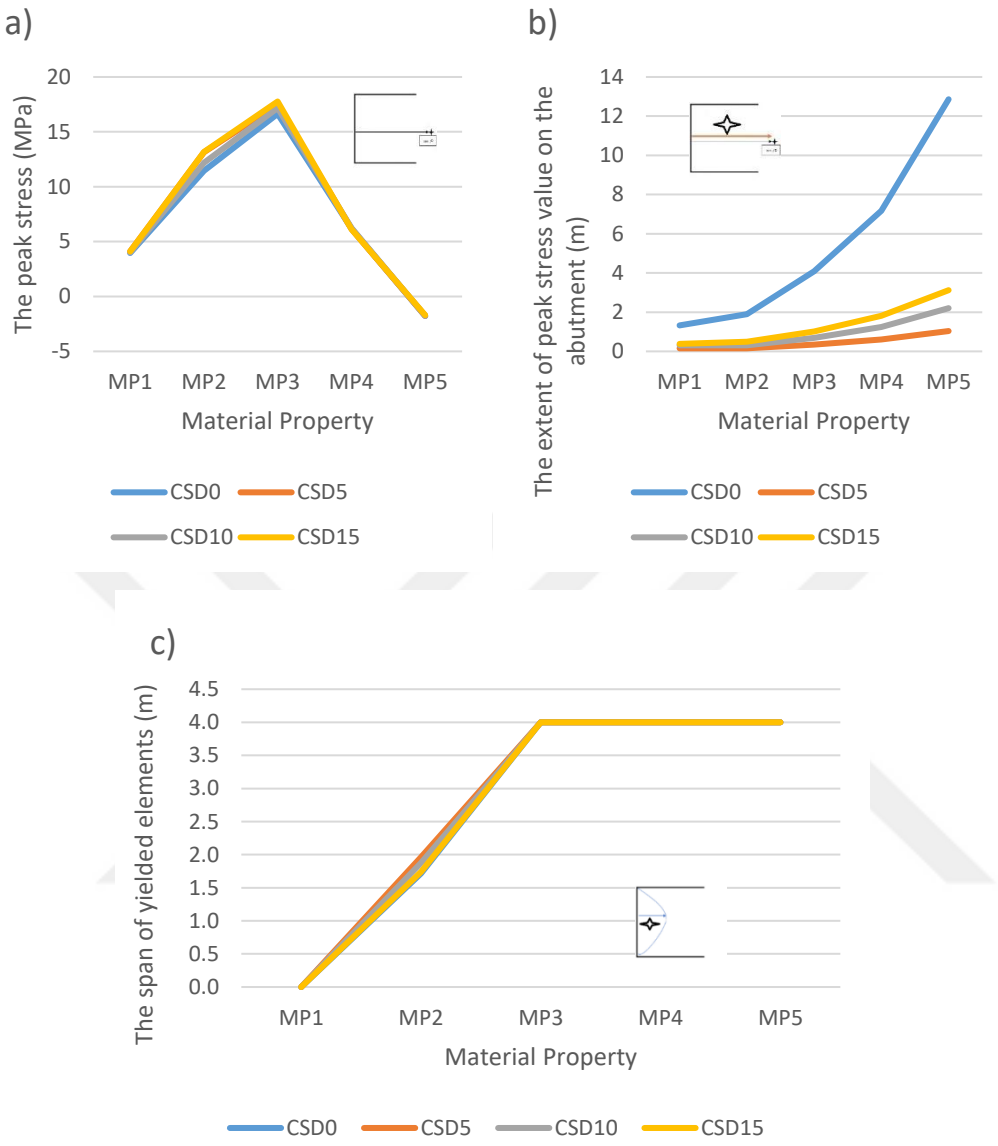

Figure H. 5 a) Peak Stress, b) The Extent of Peak Stress Value on The Abutment, c) The Span of the Yielded Elements vs. Material Properties for Right Abutment